Development of a new technique for objective assessment of gestures in mini-invasive surgery

Jenny Alexandra Cifuentes Quintero

INSTITUT NATIONAL DES SCIENCES APPLIQUÉES LYON

UNIVERSIDAD NACIONAL DE COLOMBIA

Development of a new technique for objective assessment of gestures in mini-invasive surgery

Jenny Alexandra Cifuentes Quintero

Thèse soutenue le: 3 juillet 2015

N°d'ordre: 2015ISAL0056

Jury :

Jean Louis VERCHER, Directeur de Recherche CNRS Institut des Sciences du Mouvement
Jesús Francisco VARGAS BONILLA, Professeur Universidad de Antioquia
Jan BACCA RODRIGUEZ , Professeur Universidad Nacional de Colombia
Pierre Boulanger, Professeur University of Alberta
Flavio Prieto, Professeur Universidad Nacional de Colombia
Hervé Tanneguy REDARCE, Professeur Laboratoire Ampère INSA de Lyon
Minh Tu PHAM, Maître de Conférences Laboratoire Ampère INSA de Lyon
Richard MOREAU , Maître de Conférences Laboratoire Ampère INSA de Lyon
Carlos Alberto PARRA, Professeur Universidad Javeriana

Institut National des Sciences Appliquées de Lyon - Universidad Nacional de Colombia
Laboratoire Ampère, UMR CNRS 5005, Département Génie Mécanique Conception
Laboratorio de Mecatrónica, Departamento de Ingeniería Mecánica y Mecatrónica

2015

Development of a new technique for objective assessment of gestures in mini-invasive surgery

Jenny Alexandra Cifuentes Quintero

A dissertation presented in partial fulfillment of the requirements for the degree of:
Doctor en Ingeniería - Ingeniería Mecánica y Mecatrónica

Supervisor:
Ph.D Tanneguy Redarce
Ph.D Flavio Prieto

Line of Research:
Hand Gesture Recognition
Research Groups
Grupo de Automática GAUNAL

Institut National des Sciences Appliquées de Lyon - Universidad Nacional de Colombia
Laboratoire Ampère, UMR CNRS 5005, Département Génie Mécanique Conception
Laboratorio de Mecatrónica, Departamento de Ingeniería Mecánica y Mecatrónica
2015

INSA Direction de la Recherche - Ecoles Doctorales – Quinquennal 2011-2015

SIGLE	ECOLE DOCTORALE	NOM ET COORDONNEES DU RESPONSABLE
CHIMIE	**CHIMIE DE LYON** **http://www.edchimie-lyon.fr** Sec : Renée EL MELHEM Bat Blaise Pascal 3e etage 04 72 43 80 46 Insa : R. GOURDON secretariat@edchimie-lyon.fr	M. Jean Marc LANCELIN Université de Lyon – Collège Doctoral Bât ESCPE 43 bd du 11 novembre 1918 69622 VILLEURBANNE Cedex Tél : 04.72.43 13 95 directeur@edchimie-lyon.fr
E.E.A.	**ELECTRONIQUE, ELECTROTECHNIQUE, AUTOMATIQUE** **http://edeea.ec-lyon.fr** Sec : M.C. HAVGOUDOUKIAN Ecole-doctorale.eea@ec-lyon.fr	M. Gérard SCORLETTI Ecole Centrale de Lyon 36 avenue Guy de Collongue 69134 ECULLY Tél : 04.72.18 60.97 Fax : 04 78 43 37 17 Gerard.scorletti@ec-lyon.fr
E2M2	**EVOLUTION, ECOSYSTEME, MICROBIOLOGIE, MODELISATION** **http://e2m2.universite-lyon.fr** Sec : Safia AIT CHALAL Bat Atrium- UCB Lyon 1 04.72.44.83.62 Insa : S. REVERCHON Safia.ait-chalal@univ-lyon1.fr	M. Fabrice CORDEY Laboratoire de Géologie de Lyon Université Claude Bernard Lyon 1 Bât Géode – Bureau 225 43 bd du 11 novembre 1918 69622 VILLEURBANNE Cédex Tél : 04.72.44.83.74 Sylvie.reverchon-pescheux@insa-lyon.fr fabrice.cordey@ univ-lyon1.fr
EDISS	**INTERDISCIPLINAIRE SCIENCES-SANTE** **http://www.ediss-lyon.fr** Sec : Safia AIT CHALAL Bat Atrium – UCB Lyon 1 04 72 44 83 62 Insa : Safia.ait-chalal@univ-lyon1.fr	Mme Emmanuelle CANET-SOULAS INSERM U1060, CarMeN lab, Univ. Lyon 1 Bâtiment IMBL 11 avenue Jean Capelle INSA de Lyon 696621 Villeurbanne Tél : 04.72.11.90.13 Emmanuelle.canet@univ-lyon1.fr
INFOMATHS	**INFORMATIQUE ET MATHEMATIQUES** **http://infomaths.univ-lyon1.fr** Sec :Renée EL MELHEM Bat Blaise Pascal 3e etage infomaths@univ-lyon1.fr	Mme Sylvie CALABRETTO LIRIS – INSA de Lyon Bat Blaise Pascal 7 avenue Jean Capelle 69622 VILLEURBANNE Cedex Tél : 04.72. 43. 80. 46 Fax 04 72 43 16 87 Sylvie.calabretto@insa-lyon.fr
Matériaux	**MATERIAUX DE LYON** **http://ed34.universite-lyon.fr** Sec : M. LABOUNE PM : 71.70 –Fax : 87.12 Bat. Saint Exupéry Ed.materiaux@insa-lyon.fr	M. Jean-Yves BUFFIERE INSA de Lyon MATEIS Bâtiment Saint Exupéry 7 avenue Jean Capelle 69621 VILLEURBANNE Cedex Tél : 04.72.43 71.70 Fax 04 72 43 85 28 Ed.materiaux@insa-lyon.fr
MEGA	**MECANIQUE, ENERGETIQUE, GENIE CIVIL, ACOUSTIQUE** **http://mega.universite-lyon.fr** Sec : M. LABOUNE PM : 71.70 –Fax : 87.12 Bat. Saint Exupéry mega@insa-lyon.fr	M. Philippe BOISSE INSA de Lyon Laboratoire LAMCOS Bâtiment Jacquard 25 bis avenue Jean Capelle 69621 VILLEURBANNE Cedex Tél : 04.72 .43.71.70 Fax : 04 72 43 72 37 Philippe.boisse@insa-lyon.fr
ScSo	**ScSo*** **http://recherche.univ-lyon2.fr/scso/** Sec : Viviane POLSINELLI Brigitte DUBOIS Insa : J.Y. TOUSSAINT viviane.polsinelli@univ-lyon2.fr	Mme Isabelle VON BUELTZINGLOEWEN Université Lyon 2 86 rue Pasteur 69365 LYON Cedex 07 Tél : 04.78.77.23.86 Fax : 04.37.28.04.48 isavonb@dbmail.com

*ScSo : Histoire, Géographie, Aménagement, Urbanisme, Archéologie, Science politique, Sociologie, Anthropologie

This thesis is dedicated to my parents and aunt Eilsa who have supported me all the way since the beginning of my studies. Also, this thesis is dedicated to my fiancé who has been a great source of motivation and inspiration. Finally, this thesis is dedicated to all those who believe in the richness of learning.

You can teach a student a lesson for a day; but if you can teach him to learn by creating curiosity, he will continue the learning process as long as he lives.

Clay P. Bedford

Abstract

One of the most difficult tasks in surgical education is to teach students what is the optimal magnitude of forces and torques to guide the instrument during operation. This problem becomes even more relevant in the field of Mini Invasive Surgery (MIS), where the depth perception is lost and visual field is reduced. In this way, the evaluation of surgical skills involved in this field becomes in a critical point in the learning process. Nowadays, this assessment is performed by expert surgeons observation in different operating rooms, making evident subjectivity issues in the results depending on the trainer in charge of the task.

Research works around the world have focused on the development of the automated evaluation techniques, that provide an objective feedback during the learning process. Therefore, first part of this thesis describe a new method of classification of 3D medical gestures based on biomechanical models (kinematics). This new approach analyses medical gestures based on the smoothness and quality of movements related to the tasks performed during the medical training. Thus, gesture classification is accomplished using an arc length parametrization to compute the curvature for each trajectory. The advantages of this approach are mainly oriented towards time and location independence and problem simplification. The study included several gestures that were performed repeatedly by different subjects; these data sets were acquired, also, with three different devices.

Second part of this work is focused in a classification technique based on kinematic and dynamic data. In first place, an empirical expression between movement geometry and kinematic data is used to compute a different variable called the affine velocity. Experiments carried out in this work show the constant nature of this feature in basic medical gestures. In the same way, results proved an adequate classification based on this computation. Parameters found in previous experiments were taken into account to study movements more complex. Likewise, affine velocity was used to perform a segmentation of pick and release tasks, and the classification stage was completed using an energy computation, based on dynamic data, for each segment. Final experiments were performed using six video cameras and an instrumented laparoscope. The 3-D position of the end effector was recorded, for each participant, using the OptiTrack Motive Software and reflective markers mounted on the laparoscope. Force and torque measurements, on the other hand, were acquired using force and torque sensors attached to the instrument and located between the tool tip and the handle of the tool in order to capture the interaction between participant and the manipulated material. Results associated to these experiments present a correlation between the energy values and the surgical skills of the participants involved in these experiments.

Keywords: Affine Velocity; Curvature Analysis; Dynamic Arc Length Warping; Energy; Gesture Classification; Hand Motion Tracking; One-Sixth Power Law; Segmentation.

Resumen

Una de las tareas más complicadas durante la enseñanza en cirugía consiste en explicarles a los estudiantes cuáles son las magnitudes óptimas de las fuerzas y los torques, al momento de guiar el instrumento durante la operación. Este problema obtiene mayor trascendencia en el campo de la cirugía mini-invasiva (MIS), donde se pierde la percepción de profundidad y se reduce el campo visual. Debido a esto, la evaluación de habilidades quirúrgicas, asociadas a este campo, se convierte en un punto crítico en el proceso de aprendizaje. Hoy en dia, esta evaluación se realiza mediante la observación de cirujanos expertos en diferentes salas de operación, haciendo evidente los problemas de subjetividad en los resultados, dependiendo del entrenador a cargo de la tarea.

Investigaciones alrededor del mundo se han enfocado en el desarrollo de nuevas técnicas de evaluación automáticas, con el fin de brindar una realimentación objetiva durante el proceso de aprendizaje. De esta manera, la primera parte de este trabajo de tesis describe un nuevo método de clasificación de gestos médicos 3D basado en modelos biomecánicos (cinemáticos). Este nuevo enfoque permite analizar los gestos médicos, en relación con la suavidad y calidad de los movimientos, asociados a las tareas realizadas durante el entrenamiento médico. La clasificación de gestos, es entonces, lograda usando una parametrización de longitud de arco con el fin de calcular la curvatura para cada trayectoria. Las ventajas del método están orientadas principalmente a la independencia del tiempo y de la localización espacial y a la simplificación del problema estudiado. Este estudio involucra diversos gestos realizados repetidamente por diferentes participantes, cuyos datos fueron adquiridos por 3 dispositivos diferentes.

La segunda parte de este trabajo se enfoca en una técnica de clasificación basada tanto en datos cinemáticos como dinámicos. En primer lugar, se implementó una expresión empírica entre la geometría del movimiento y los datos cinemáticos con el fin de calcular una variable diferente llamada Velocidad Afín. Los experimentos desarrollados en este trabajo muestran la naturaleza constante de esta característica en gestos médicos básicos. De la misma forma, los resultados muestran que una adecuada clasificación es lograda con base en esta implementación. Finalmente, los parámetros encontrados en los experimentos previos fueron tomados en cuenta para estudiar movimientos más complejos. Así, la velocidad afín fue usada para realizar la segmentación de tareas de tomar y soltar y la etapa de clasificación se implementó usando el cálculo de la energía para cada segmento. Los últimos experimentos de este trabajo fueron desarrollados usando seis camaras de video y un instrumento laparoscópico. La posición 3D del efector final fue registrada, para cada participante, usando el software Motive OptiTrack y se utilizaron marcadores reflectivos instalados sobre el laparóscopo. Por otra parte, las medidas de fuerza y torque fueron adquiridas usando sensores de fuerza y torque

atados al instrumento y localizados entre la punta del instrumento y la manija de la herramienta con el fin de capturar la interacción entre el participante y el material manipulado. Los resultados asociados a estos experimentos muestran una correlación entre los valores de energía y las habilidades quirúrgicas de los participantes involucrados en los experimentos.

Palabras Claves: Análisis de Curvatura; Clasificación de Gestos; Dynamic Arc Length Warping; Energía; Ley de Potencia Un-Sexto; Segmentación; Seguimiento del Movimiento de la Mano; Velocidad Afín

Résumé

L'une des tâches les plus difficiles de l'enseignement en chirurgie, consiste à expliquer aux étudiants quelles sont les amplitudes des forces et des couples à appliquer pour guider les instruments au cours d'une opération. Ce problème devient plus important dans le domaine de la chirurgie mini-invasive (MIS) où la perception de profondeur est perdue et le champ visuel est réduit. Pour cette raison, l'évaluation de l'habileté chirurgicale associée est devenue un point capital dans le processus d'apprentissage en médecine. Aujourd'hui cette évaluation est faite de manière empirique en salle d'opérations par l'observation des chirurgiens, de sorte que des problèmes évidents de subjectivité apparaissent dans la formation des médecins, selon l'instructeur en charge de l'enseignement.

De nombreuses études et rapports de recherches dans le monde entier concernent le développement de techniques automatisées d'évaluation du geste et permettent de fournir un retour d'expérience objectif pendant le processus d'apprentissage. La première partie du travail présenté dans cette thèse introduit une nouvelle méthode de classification de gestes médicaux 3D reposant sur des modèles cinématiques et biomécaniques. Cette nouvelle approche analyse de manière qualitative mais aussi quantitative les mouvements associ'es aux tâches effectuées au cours de la formation médicale. La classification du geste est réalisée en utilisant un paramétrage reposant sur la longueur d'arc pour calculer la courbure pour chaque trajectoire. Les avantages de cette approche sont principalement motivés par l'indépendance du temps, d'un système de repérage absolu et la réduction du nombre de données à traiter. L'étude inclus l'analyse expérimentale de plusieurs gestes, obtenus avec plusieurs types de capteurs et réalisés par différents sujets.

La deuxième partie de ce travail se concentre dans une technique de classification reposant sur les données cinématiques et dynamiques. En premier lieu, une expression empirique, entre la géométrie du mouvement et les données cinématiques, est utilisée pour calculer une nouvelle variable appelée vitesse affine. Les expériences conduites dans ce travail de thèse montrent la nature constante de cette grandeur lorsque les gestes médicaux sont simples et identiques. De la même façon, les résultats expérimentaux montrent que l'utilisation de la vitesse affine conduit à une classification adéquate des gestes. Les paramètres associés au modèle de vitesse affine trouvé ont été pris en compte, par la suite, pour étudier des mouvements plus complexes et effectuer une segmentation des tâches de préhension et de dépôt. Finalement, une dernière technique de classification a été implémentée en utilisant un calcul de l'énergie utilisée au cours de chaque segment du geste. Cette méthode a été validée expérimentalement en utilisant six caméras et un laparoscope instrumenté. La position 3-D de l'extrémité de l'effecteur a été enregistrée, pour plusieurs participants, en utilisant le logiciel OptiTrack Motive et des marqueurs réfléchissants montés sur le laparoscope. Les

mesures de force et de couple, d'autre part, ont été acquises à l'aide des capteurs fixés sur l'outil et situés entre la pointe et la poignée de l'outil afin de capturer l'interaction entre le participant et le matériau manipulé. Les résultats expérimentaux présentent une bonne corrélation entre les valeurs de l'énergie et les compétences chirurgicales des participants impliqués dans ces expériences.

Mots-clés: Analyse de Courbure; Classification des gestes; Dynamic Arc Length Warping; Énergie; Loi de Puissance Un-Sixième; Segmentation; Suivi du Mouvement de la Main; Vítesse Affine

Contents

List of Figures

List of Tables

1 Introduction

Minimally Invasive Surgery (MIS) is becoming more and more common practice in medicine. Using this technology, surgeries previously performed through large incisions that required long recovery times can now be performed with a much shorter recovery time and with reduced risk to the patient. Although on one hand MIS ensure many advantages to patients, on the other hand it requires surgeons to perform a much longer and difficult training process which create numerous new challenges for surgical training. Indeed, MIS requires to acquire new hand-eye coordination and visualization skills because of the displaced of haptic perception produced by laparoscopes and the loss of stereo and the reduced of the field of view created by the use of endoscopic camera([42, 60, 47]).

Therefore, the assessment of technical skills during training is critical for quality insurance and safety. Typically, surgical learning is based on an apprenticeship model. In this approach, students are taught on the job, starting with the least difficult tasks and progressing towards more advanced skills, while the trainer controls the overall course of the procedure and evaluate the trainee performance. This process, especially, in MIS, makes it much harder for the trainer to keep track of the trainee progress. Traditional skills assessments are mainly knowledge based and the analysis of the actual performance is mainly subjective, with measurements that show poor accuracy, repeatability, and reliability ([5, 78, 115]).

For that reason, a new approach of surgical assessment is required to ensure that surgeons have adequate skills level to be allowed to operate freely on patients. Being able to perform accurate evaluation not only provides an objective evaluation of performance but also can be used in research to examine what factors affect surgical proficiency. For instance, what is the effect of drugs, lack of sleep, stress or time away from the operating room on surgical proficiency. In some countries, a periodic evaluation, that includes visual memory and psychomotor performance, is required to recertify doctors in a specific health field [14].

1.1. Subjective Surgical Skill Assessment

Some efforts have been made to obtain a reliable assessment method. Among these works the Objective Structured Assessment of Technical Skills (OSATS) rating system [80] was developed. Using this evaluation method, the trainees perform standardized surgical tasks while an expert surgeon evaluates their performance. The assessment includes a task-specific

checklist that identifies all important steps in a procedure. Using OSATS, a score is assigned for every step the trainee completes adequately (0 or 1). In addition, a Global Assessment Score (GAS) is used to assess the overall performance using seven levels. This approach has subjective elements which create large variations in the scores assigned by different trainers.

A similar scoring system has been developed for MIS, the Global Assessment of Laparoscopy Skills (GOALS) [47]. This approach evaluates five categories (depth perception, bimanual dexterity, efficiency, tissue handling and autonomy), where each category proficiency is score between 1 to 5. Although, this system evaluates different aspects of MIS, it is still subjective as it requires an evaluator to provide a score.

On the whole, assessment of psychomotor skills commonly used in the surgical training, such as analysis of operative case logs, evaluation reports of training, and direct observation with or without the use of rating scales assigned by different experts are not objective and reliable [131, 29, 39]. The need to measure technical skill level and proficiency in surgeons, as part of formal competence assessment and revalidation, has become increasingly recognized [28, 27, 97, 23], especially when previous work has shown that academic achievement do not correlate, or even correlate negatively, with surgical skill measured subjectively [113, 112].

1.2. Automated Objective Surgical Skill Evaluation

These measures have been quite useful in the surgical skill assessment for many years. However, they require different expert surgeons to provide the assesment, which can lead to subjective results in the training process. For this reason, an automated objective surgical skill evaluation approach has been the topic of research for the last 20 years. The main idea is to digitize the surgeon movements (gestures), using video images or any sensing devices, and to process this information in order to obtain objective assesment.

In particular, machine vision solutions has been explored by many researchers around the world. Important issues include: placement and numbers of tracking cameras, targets visibility, and feature selection and extraction. The optimal placement and the determination of the number of cameras are critical to obtain robust recognition to deal with the visibility issues of hand tracking.

The use of one [81] or multiple cameras [67] has been studied for hand gesture recognition with accurate results. In particular, in [105], a hand tracking system using two cameras is described showing results capable of measuring a 27 DOF hand model. In order to deal with hands visibility, some researchers have used simple markers located on key points to facilitate the tracking and recognition of hand movements. In this way, gloves [36] and reflective markers [55] located on the instrument have been used to improve the recognition process.

The objective assessment of surgical skills has also been explored using the position values of instruments tracking based on endoscopic image sequences [122]. Another contributions for endoscopic images analysis include image enhancement methods such as: temporal filtering, distortion correction, and color normalization [129]. In many vision-based systems occlusion is a critical issue and has been dealt with redundant tracking devices, robust filtering, and better detection algorithms [70].

Automated objective surgical skill evaluation has not yet been developed because of a number of issues such as: visibility issues with motion capture devices, reliable algorithms, and proper similarity metrics. Some trainers offer an assessment of surgical skills based on simple features such as task completion time [32, 43, 109]. A skill evaluation surveys in MIS [123] suggest that the learning curve for operator is a coarse measure of performance [123]. Time alone is not an adequate measure of the precision of task performance [118]. Several researchers have proposed different metrics for hand gesture classification.

In many prototype systems, the raw data obtained from the acquisition system is processed and analyzed in order to obtain reliable and accurate assessment results. The most common analysis algorithms are based on global features. In this approach, the whole surgical procedure data set is reduced to a set of simple features that are then used to evaluate performance relative to some pre-defined standards. Although, in some surveys [84, 37], this method has been successful in differentiating some skill levels, it cannot be used to distinguish gestures quantitatively well.

Global Features

Most research in objective surgical skill assessment has been focusing entirely on **Global Features** because these measures are usually simple to calculate, to analyze, and to compare between groups. The operation time, for instance, has been widely used in this field, however as mentioned previously, it has been proved that this measure alone is not an adequate proficiency measure [117]. For this reason, several features have been proposed to obtain some estimate of proficiency level [18, 17, 25, 48]. Among these are the following:

- **Path Length :** Length of the instrument tip trajectory;
- **Depth Perception :** Distance of the instrument tip traveled along its own axis;
- **Motion Smoothness :** Feature based on the third derivative of position;

- **Angular Area:** Parameter based on the area covered by the farthest positions of the instrument tip;
- **Volume:** Parameter based on the volume generated by the farthest positions of the instrument tip;
- **Movement Economy:** Relation among the ideal and the real path length;
- **Deviation from the ideal path:** Cumulative sum of the differences between the ideal and the real path;
- **Accuracy:** Parameter computed to measure the accurateness of placing the instrument tip in different places in 3D;
- **Rotational Orientation or Response Orientation:** Rotation of the instrument measured around its own axis;
- **Number of movements:** Parameter based on the velocity changes along the trajectory.

Using global features good results have been achieved for simple tasks, but they have not been very good for more complex tasks.

Local Analysis

A more detailed comparison between surgical gestures can be obtained using a local trajectory analysis. This approach consider each element and the patterns of the trajectory. This level of analysis can be implemented to distinguish between different skill levels and gestures and provide more detailed assessment about the performance. Some approaches based on this idea include movement segmentation, hidden Markov modeling, and non-linear similarity measures.

- **Movement Segmentation:** This approach is based on the idea that every single surgical procedure can be segmented and recognized at low level using elementary units. In this case, the whole trajectory could be decomposed into steps, sub-steps, tasks, sub-tasks and tool motions depending on its complexity. The main advantage of this method is that it is based on the fact that after segmentation, the analysis of each segment becomes simpler. In [106], the smallest motion used in surgery called surgemes is detected and based on this unit, the whole procedure is segmented. MacKenzi and Cao, on the other hand, segmented MIS tasks into smaller subtasks and examine durations and relative timing at each hierarchical level (tasks and subtasks) [77].

This method have been used successfully not only for MIS procedures but also for other procedures such as ophthalmological surgeries [69]. However, the main research topic in this field remains the adequate and effective segmentation technique.

- **Hidden Markov Modeling:** Surgical process modeling involves the correlation between a feature vector and each trajectory. The most known modeling tool includes the use of Hidden Markov Models (HMMs) with satisfactory results in the speech recognition field [58]. HMMs have been defined as a set of states that include an initial state, a set of outputs, and a set of state transitions. In particular, in gesture recognition, each state represents a set of possible surgical gestures [91, 72]. The methodology developed in [107, 108] is based on Markov Modeling and a subset of HMMs. The force/torque measures of each trajectory were used to define force/torque signatures associated with 14 different types of tool/tissue interactions and the result was a surgical performance index which represented a ratio of statistical similarity between different surgeons. In [82] they processed the kinematic data acquired from different surgical gestures to define an expert model using HMMs. In general HMMs have been useful to perform hand gesture recognition with a good accuracy for a large gesture set. However, the hidden nature of this approach makes it difficult to examine the internal behavior. In addition, the extensive training necessary for HMMs is time consuming and do not guarantee good results [70].

- **Non-linear Similarity Measures:** There are some problems to perform the comparison using sensor data (position, speed, acceleration) related with data synchronization when one of the signals has a larger stream of data than the others. Several methods were proposed to deal with this issue using a nonlinear approach where data is shrunk or expanded along the time axis. In this case, each path is modeled as a sequence of consecutive points in a multidimensional (2D or 3D) Euclidean space. In this approach, a time series similarity measure is used to obtain a distance metric. Different algorithms have been implemented, such as Dynamic Time Warping (DTW) [57, 124], Derivative Dynamic Time Warping (DDTW) [61] or Longest Common Subsequence (LCSS) to find the optimal alignment of two signals [8]. Several advances have been made in the field of objective assessment of surgical skills using these algorithms. Dermitzakis *et al.* [31] explore the viability of DTW as a classification method for upper−limb prosthetics. In particular, in surgical gestures classification, [96] the trajectory curvature values was used to match and compare each gesture to a template using the DTW method. Blum [13] use Canonical Correlation Analysis (CCA) to extract the information from the video and various statistical models. Although DTW strongly depends on the temporal order, the best results were obtained with this method.

1.3. Contributions and Organization

1.3.1. Contributions

This thesis makes several contributions to the gesture recognition field:

1. A new approach that includes data parametrization of the position and orientation trajectories, based on cumulative arc-length is presented. The conversion to cumulative arc-length parametrization does not remove information compared to the time-domain representation of a signal, since this conversion is similar to a time normalization operation. The main advantages of such an approach are the possibility of comparing similar trajectories performed at different speeds and of analysing trajectories independently from a sensor coordinate system. In this scheme, a curvature computation is carried out in order to perform the analysis and classification of the gestures which is also invariant to the sensor coordinate systems. The advantages include the reduction of the problem dimensionality from 3D to 1D simplifying the classification problem and its implementation. The experimental results shows that gesture comparison can be performed for three different sensing devices.

2. Using this new approach, a survey is performed based on quaternions theory. The benefits of using quaternion alongside with Dynamic Arc Length Warping is presented and compared to other classic technique. The proposed approach can be used with quaternion data to distinguish similar and different gestures. An experimental validation is carried out to classify a series of simple human gestures.

3. A new analysis based on affine velocity of surgical gestures, is presented. We demonstrate that constant equi-affine velocity in hand human gestures can be observed and can be used to segment gesture trajectories. Based on these results, some modifications of the one-sixth power law's exponents across different gestures are described. Experimental proofs include the analysis of obstetrical and navigation gestures acquired during medical training. The results show that averaging over all subjects and gestures, the power law exponents are in accordance with constant spatial equi-affine velocity.

4. Finally, based on the previous results, complex trajectories were analysed using a segmentation algorithm that use affine velocity. Gesture classification is obtained based on the energy calculated from each segment. For these experiments, six cameras, an instrumented laparoscope and a complete minimally invasive training system were used. The position values for each gesture were obtained based on OptiTrack Motive Software and the laparoscope was identified using reflective markers. In addition, dynamic data were acquired by the instrumentation of each laparoscope using a force and torque sensor located between the tool tip and the handle of the tool to capture the interaction between participant and the manipulated material.

During this thesis several papers have been submitted and published in peer reviewed conferences and journals:

1. **Objective Assessment of Surgical Skills.** *Jenny A. Cifuentes, Minh Tu Pham, Richard Moreau, Flavio Prieto and Pierre Boulanger.* **ASME 2012 11th Biennial Conference on Engineering Systems Design and Analysis** Volume 4: Advanced Manufacturing Processes; Biomedical Engineering; Multiscale Mechanics of Biological Tissues; Sciences, Engineering and Education; Multiphysics; Emerging Technologies for Inspection and Reverse Engineering; Advanced Materials and Tribology. Nantes, France, July 2â“4, 2012. Conference Sponsors: International. ISBN: 978-0-7918-4487-8.

2. **An arc-length warping algorithm for gesture recognition using quaternion representation.** *Jenny A. Cifuentes, Minh Tu Pham, Richard Moreau, Flavio Prieto and Pierre Boulanger.* In Engineering in Medicine and Biology Society (EMBC), 2013, **35th Annual International Conference of the IEEE.** (pp. 6248-6251). Conference 07/2013; 2013:6248-6251. DOI: 10.1109/EMBC.2013.6610981.

3. **Why and how to objectively evaluate medical gestures?.** *Jenny Cifuentes, Richard Moreau, Flavio Prieto, Minh Tu Pham and Tanneguy Redarce.* **IRBM**, Elsevier, 2013, 34 (1), pp.74-78. DOI:10.1016/j.irbm.2012.12.001.

4. **Automatic gesture analysis using constant affine velocity.** *Jenny Cifuentes, Pierre Boulanger, Minh Tu Pham, Richard Moreau, and Flavio Prieto.* (2014, August). In Engineering in Medicine and Biology Society (EMBC), 2014, **36th Annual International Conference of the IEEE** (pp. 1826-1829). IEEE. DOI: 10.1109/EMBC.2014.6943964.

5. **Surgical Gesture Classification and Skill Evaluation using Affine Velocity.** *Jenny Cifuentes, Pierre Boulanger, Minh Tu Pham, Richard Moreau, and Flavio Prieto.* (2015, March). IEEE Transactions on Human-Machine Systems **Submitted**.

6. **Medical Gesture Recognition Using Dynamic Arc-Length Warping.** *Jenny Cifuentes, Pierre Boulanger., Minh Tu Pham, Richard Moreau, and Flavio Prieto.* (2015, March). IEEE Transactions on Human-Machine Systems **Submitted**.

1.3.2. Thesis Organization

Chapter 2 introduces the existing algorithms to obtain time series similarity measures. Metric and non metric distances are taken into account and a simulation analysis, that includes the techniques with more accurate results, is developed to show the main advantages. Chapter 3 describes the algorithm that was developed and implemented. The simulation analysis as well as the experimental results are presented. In this way, a survey based on quaternions theory is also given. Chapter 4 includes the affine velocity description and its corresponding

analysis on obstetrical and surgical gestures. Conclusion and proposed future directions are discussed in Chapter 5.

2 Time Series Similarity Measures: A review

Multi-dimensional time series are sets of data in which multiple measurements are made simultaneously. These kind of series contain a vector of feature values for each occurrence of the series. Most time-series research focus on providing solutions to calculate similarity measures among different sequences with results in a broad range of applications. Several techniques have been proposed in order to provide algorithms for efficient processing in the case of static time series with the same or different lengths. These approaches could be classified into three categories: feature based, model based, and sequence distance based [136] :

2.1. Feature Based Approach

In this category, time series dimensionality is reduced using suitable feature selection algorithms.The resulting feature vector is then used to carry out the final classification. Many researcher have worked on this particular strategy based using different techniques:

- **Time Series Shapelets:** Feature extraction can be performed using time series that can be, in some way, the most representative of a class. In a two-classe case, a shapelet can be used to divide the time series into two parts, based on a given threshold. The training process is performed to maximize the extracted information and the resulting algorithm is integrated with the construction of the decision tree [138]. In [76], the shapelets calculation and the classification algorithm are not related. In this case, authors extracted the k best shapelets and calculated the distances between the time series and the shapelets. Results allow to obtain a transformation of data in a new space in order to improve the accuracy of the method. Authors proved that this approach can be more accurate and significantly faster in the classification field. However it has been proved, even if shapelets are computed off-line, that this approach is significant time consuming [75].

- **Spectral Methods:** Another techniques widely used are based on spectral methods such as Wavelet decomposition and Fourier Analysis. These approaches take into account global and local features of sequences in order to perform the classification. In

this way, Aggarwal et al. [3] take advantage of the multi-resolution property of wavelet decomposition, in order to develop an algorithm which extract the features for the classification, at different levels of granularity. In addition, Wavelet Transformations allows a dimensionality reduction improving the efficiency in the classification process. A detailed study of wavelets used to analyse the performance of similarity searching, in time series, is presented in [102]. However, studies have shown that Discrete Wavelet Transform does not decrease the relative matching error and its computational complexity is quite high [134]. One way to solve these problems is using the Discrete Fourier Transform (DFT), which has a lower complexity. In [4], this approach is implemented as an efficient indexing method by mapping time series to the frequency domain. Their experiments results show that a good performance is obtained by analysing the first low-frequency harmonics (1 to 3). The main disadvantage of this technique is related to the assumption that both sequences have the same length. This issue can be solved using a sliding window to perform the mapping and taking only the first coefficients [40]. A variation of this approach has been proposed in [103], where authors improve the efficiency to compute the similarity distance by using the last Fourier coefficients.

- **Eigenvalue Techniques:** Feature extraction can be efficiently achieved using an eigenvalue analysis such as Singular Value Decomposition (SVD) or Principal Component Analysis (PCA). In [133], dimension reduction of feature vectors is obtained using SVD. Their results show that this approach can improve the efficiency as it provides the best linear least squares error to data. On the other hand, Yang and Shahabi [137] compute the similarity measures using PCA to generate and compare the principal components and associated eigenvalues for multidimensional time series. Experimental results show an improvement in the precision of calculations. In general, eigenvalue techniques handle discontinuities much better than spectral methods. This fact can be visualized in the low performance of spectral techniques obtained with signals that have several spikes or abrupt jumps, are used as inputs [64]. Although eigenvalue methods give optimal linear dimensionality reduction, they seems to be untenable for large data sets [35].

2.2. Model Based Approach

Model based classification techniques are based on generative models which are represented using probability distributions. During the training process, parameters involved in the model are learned and classification is carried out based on the highest likelihood of the class [136].

- **Statistical Model:** In this category, models such as Gaussian mixture models, Markov and hidden Markov models are used. Specifically, Smyth [121] describe a probabilistic model to cluster time series using HMMs. They propose a methodology to compute an adequate hidden cluster structure in data sets of sequences. Some variations have been proposed in order to improve the precision of this method. In [6], authors suggest to use the Bayesian framework as a stop criterion during the HMM training or as a distance measure when clustering HMMs, obtaining a very accurate classification. However, this approach has a high complexity and requires an extensive training step which is time consuming [70].

- **Neural Network Models:** A multi - layer perceptron (MLP) neural networks consist of one or more layers of neurons between the input and output layers. Each neuron in a layer is connected by weighted links and the output of each unit is the sum of its inputs through an activation function. In [93], several first and second-order statistical features are used to perform the classification, based on a MLP neural network. Results present a faster and better classification for larger time series. Advantages are directly related to the fact that this approach involves a learning process, allowing to the user does not need to have so much knowledge about the problem. Different structures for the neural networks have been propose. Among them, Pham and Oztemel [94] have proposed to use the length of each time series as the number of neurons in the input layer. In [95], a procedure based on Learning Vector Quantization (LVQ) network, with a similar structure, is suggested in order to increase the classification accuracy and decrease the learning time. The disadvantages associated to this approach are the noise and time series length sensitivity. Likewise, the length of the sequences analysed should be the same and any change in this parameter requires retraining the entire network [70].

2.3. Sequence Distance Based Approach

Distance based techniques are based on similarity measures calculated between different sequences $\mathbf{x}_1[k]$ and $\mathbf{x}_2[l]$ of dimension n and m respectively defined as:

$$\begin{aligned} \mathbf{x}_1[k] &= \{x_1(1;k), x_1(2;k), x_1(3;k), .., x_1(n;k)\}, \\ \mathbf{x}_2[l] &= \{x_2(1;l), x_2(2;l), x_2(3;l), .., x_2(m;l)\}. \end{aligned} \tag{2-1}$$

This approach is determinant to obtain an adequate classification, specially when the sequences have different lengths or local time variations. Based on this advantages, survey presented in this work is focused on this category. Similarity measures could be classified into two categories: elastic and non-elastic metrics.

2.3.1. Non Elastic Metrics

This classification includes a huge set of metrics. For this reason, just 20 of the best known metrics that have a good performance in classification problems and pattern recognition, will be presented in this section [19, 101, 12, 34]. Taking into account that each time series of length of m could be represented as a vector in the p-dimensional space, then the simplest approach to define the distance between two multi-dimensional series of equal dimension n is to use the notion of p-norm. The p-norm distance, noted $L_p(\mathbf{x}_1[k], \mathbf{x}_2)[l]$ is defined as:

$$L_p(\mathbf{x}_1[k], \mathbf{x}_2[l]) = \left(\sum_{i=1}^{n} |x_1(i;k) - x_2[i;l]|^p \right)^{\frac{1}{p}}. \tag{2-2}$$

The Euclidean distance, in particular, has been widely used as a similarity metric in time series research because of its simplicity [40, 63]. In this case, the distance value $d_{(Eucl)}$ between two n-dimensional sequences ($\mathbf{x}_1[k]$, $\mathbf{x}_2[l]$) is computed by:

$$d_{(Eucl)}(\mathbf{x}_1[k], \mathbf{x}_2[l]) = \sqrt{\sum_{i=1}^{n} |x_1(i;k) - x_2(i;l)|^2}. \tag{2-3}$$

The Manhattan distance $d_{(Manh)}$, on the other hand, computes the sum of the distances between each pair of points $\mathbf{x}_1[k], \mathbf{x}_2[l]$ along axes at right angles, like the paths described by a car moving in a city laid out in square blocks [54]:

$$d_{(Manh)}(\mathbf{x}_1[k], \mathbf{x}_2[l]) = \sum_{i=1}^{n} |x_1(i;k) - x_2(i;l)|. \tag{2-4}$$

Other metrics assume that one axis is more important than the others. This is the case of the Chebyshev distance or maximum metric $d_{(Cheb)}$. It is a metric defined on a vector space where the distance between two sequences ($\mathbf{x}_1$[k],$\mathbf{x}_2[l]$) is the sum of the greatest of their differences along any coordinate dimension:

$$d_{(Cheb)}(\mathbf{x}_1[k], \mathbf{x}_2[l]) = \sum_{i=1}^{n} \max|x_1(i;k) - x_2(i;l)|. \tag{2-5}$$

The binary similarity metrics, meanwhile, play a critical role in pattern analysis problems such as classification, clustering, etc. in fields like image retrieval [119], biometrics [16] and handwritten character recognition [15]. 2-6 is known as Gower distance $d_{(Gower)}$ [45]:

$$d_{(Gower)}(\mathbf{x}_1[k], \mathbf{x}_2[l]) = \frac{1}{m}\sum_{i=1}^{n} |x_1(i;k) - x_2(i;l)|. \tag{2-6}$$

It has been a method widely used in ecology because it can handle continuous and categorical variables with an accurate results. Bray Curtis distance, sometimes called as Sorensen distance $d_{(BCurtis)}$, is a normalization method that takes the space as a grid similar to the Manhattan distance (2-4):

$$d_{(BCurtis)}(\mathbf{x}_1[k], \mathbf{x}_2[l]) = \frac{\sum_{i=1}^{n} |x_1(i;k) - x_2(i;l)|}{\sum_{i=1}^{m} |x_1(i;k) + x_2(i;l)|}. \tag{2-7}$$

Similar metrics as the Soergel and Kulczynski distances can be used :

$$d_{(Soergel)}(\mathbf{x}_1[k], \mathbf{x}_2[l]) = \frac{\sum_{i=1}^{n} |x_1(i;k) - x2(i;l)|}{\sum_{i=1}^{n} \max(x_1(i;k), x_2(i;l))}. \tag{2-8}$$

$$d_{(Kulczy)}(\mathbf{x}_1[k], \mathbf{x}_2[l]) = \frac{\sum_{i=1}^{n} |x_1(i;k) - x_2(i;l)|}{\sum_{i=1}^{n} \min(x_1(i;k), x_2(i;l))}. \tag{2-9}$$

These coefficients were used as they were originally formulated for presence/absence data. They do not place the assumption on the data that differences between high data values are considered more significant than the same difference between low data values. Dot product, by itself, is used as a similarity metric in a wide range of applications:

$$d_{(dot)}(\mathbf{x}_1[k], \mathbf{x}_2[l]) = \sum_{i=1}^{n} (x_1(i;k) \bullet x_2(i;l)). \tag{2-10}$$

This distance d_{dot} is based in the sum of the products of each pair of points of the two sequences. Moreover, Cosine similarity distance d_{cos}, which is a normalized inner product, measures the angular difference between two sequences $\mathbf{x}_1[k]$ and $\mathbf{x}_2[l]$:

$$d_{(cos)}(\mathbf{x}_1[k], \mathbf{x}_2[l]) = \sum_{i=1}^{n} \frac{(x_1(i;k) \bullet x_2(i;l))}{\sqrt{\sum_{i=1}^{n} x_1(i;k)^2} \bullet \sqrt{\sum_{i=1}^{n} x_2(i;l)^2}}. \tag{2-11}$$

In [66], authors measure the correlation between filters using the Peak-to-Correlation energy :

$$d_{(poc)}(\mathbf{x}_1[k], \mathbf{x}_2[l]) = \frac{\sum_{i=1}^{n}(x_1(i;) \bullet x_2(i;l))}{\sum_{i=1}^{n} x_1(i;k)^2 + \sum_{i=1}^{n} x_2(i;l)^2 + \sum_{i=1}^{n} x_1(i;k) \bullet x_2(i;l)}. \tag{2-12}$$

This feature provides precise results in the presence of noise. The numerator of Motyka distance is normalized using the sum of feature vectors at each dimension increasing the robustness:

$$d_{(mot)}(\mathbf{x}_1, \mathbf{x}_2) = \frac{\sum_{i=1}^{m}(\min(\mathbf{x}_1(i), \mathbf{x}_2(i)))}{\sum_{i=1}^{m}(x_1(i) + x_2(i))}. \tag{2-13}$$

Its applications include fingerprint recognition and DNA repeats detection [101]. Ruzicka metric, for its part, calculates the relation between the sum of the minimum shared attributes and the sum of the maximum attributes values:

$$d_{(Ruz)}(\mathbf{x}_1[k], \mathbf{x}_2[l]) = \frac{\sum_{i=1}^{n}(\min(x_1(i;k), x_2(i;l)))}{\sum_{i=1}^{n}(\max(x_1(i;k), x_2(i;l)))}. \tag{2-14}$$

Although this similarity distance is more affected to the large differences, it has been used in applications that include the analysis of Internet traffic [83]. Tanimoto metric, on the other hand, has been widely used in both fingerprint [132] and image pattern recognition [44] and some researches have been published in the text document clustering field [56]:

$$d_{(tan)}(\mathbf{x}_1[k],\mathbf{x}_2[l]) = \frac{\sum_{i=1}^{n} x_1(i;k) + \sum_{i=1}^{n} x_2(i;l) - 2\sum_{i=1}^{n} \min(x_1(i;k), x_2(i;l))}{\sum_{i=1}^{n} (\max(x_1(i;k), x_2(i;l)))}. \tag{2-15}$$

Matusita (2-16) and Squared Chord (2-17) metrics have shown to provide a reliable criteria in applications like the image and video retrieval using the energy values as the feature space [62, 52, 51]:

$$d_{(Mat)}(\mathbf{x}_1[k],\mathbf{x}_2[l]) = \sqrt{\sum_{i=1}^{n} (\sqrt{x_1(i;k)} - \sqrt{x_2(i;l)})^2}, \tag{2-16}$$

$$d_{(SChord)}(\mathbf{x}_1[k],\mathbf{x}_2[l]) = \sum_{i=1}^{n} (\sqrt{x_1(i;k)} - \sqrt{x_2(i;l)})^2. \tag{2-17}$$

Squared Euclidean metric calculates the sum squared difference at each dimension of feature vector:

$$d_{(SEc)}(\mathbf{x}_1[k],\mathbf{x}_2[l]) = \sum_{i=1}^{n} (x_1(i;k) - x_2(i;l))^2. \tag{2-18}$$

This factor is included in other similarity distances such as Squared χ^2:

$$d_{(Sx)}(\mathbf{x}_1[k],\mathbf{x}_2[l]) = \sum_{i=1}^{n} \frac{(x_1(i;k) - x_2(i;l))^2}{x_1(i;k) + x_2(i;l)}, \tag{2-19}$$

Pearson:

$$d_{(Pearson)}(\mathbf{x}_1[k],\mathbf{x}_2[l]) = \sum_{i=1}^{n} \frac{(x_1(i;k) - x_2(i;l))^2}{x_2(i;l)}, \tag{2-20}$$

and symmetric χ^2 divergence:

$$d_{(SxD)}(\mathbf{x}_1[k],\mathbf{x}_2[l]) = \sum_{i=1}^{n} \frac{(x_1(i;k) - x_2(i;l))^2 (x_1(i;k) + x_2(i;l))}{x_1(i;k) \bullet x_2(i;l)}. \tag{2-21}$$

These distances have been used successfully in pattern recognition field [71, 44]. Although these metrics have had accurate results in specific applications in engineering, Euclidean norm remains being the most used in several fields, such as least squares, Eigen-problems, mainly in statistics, etc. [85]. The main reason lies in its simplicity, ease of implementation, time and space efficiency, and its accurate results [104]. Experimental results have proved that where there is no distortion and assuming gaussian noise in data, Euclidean distance is known to be the optimal metric [40].

2.3.2. Elastic Metrics

Non-lastic metrics are an efficient and easy way to calculate the similarity between time series. Specifically, time series data objects allow the use of many traditional norms as well as more specialized measures based on the application [10]. However, for practical data sets, distortions start to appear as soon as the two sequences do not have the same size. In order to overcome these pitfalls, researchers have suggested more flexible metrics to compute the similarity between time series.

Practical problems can raise in practice when noise and outliers appear in the measurements. For this reason, the required distance functions that can address the following issues [128] are:

- **Different sampling rates or different speeds:** Measurements acquired by specific devices are not necessarily the result of sampling at fixed time intervals. Moreover, the sensors involved could generate outliers or inconsistent sampling frequencies during some time instants.
- **Outliers:** Noise or some outliers could be introduced by a human failure or because sensor damages when the data are being acquired.
- **Different Lengths:** Using non-elastic metrics, when the time series have different size, it is necessary to decide if it is required to truncate the longer sequence or pad with zeros the shorter, which introduces distortion to the similarity measure.
- **Efficiency:** The distance function should express the user's notion of similarity and also provide an efficient computation.

Longest Common Subsequence

Longest Common Subsequence Algorithm (LCSS) finds the subsequence of two different sequences that best corresponds to each-other. The similarity distance is based on the ratio between the length of the longest common subsequence and the length of the whole sequence. The subsequence is not necessarily composed of consecutive points, the order of points is not

arranged and some points can remain unmatched. LCSS has been implemented successfully to compare text strings [92]. When this approach is applied to series of numerical values, a threshold is required to determine when values of corresponding points are treated as equal.

Consider two sequences of feature vectors (position, velocity, orientation, etc) defined in 2-1. For $\mathbf{x}_1[k]$ let $\text{Head}(\mathbf{x}_1)[k] = \{x_1(1;k), x_1(2;k), x_1(3;k), .., x_1(n-1;k)\}$ be the sequence $\mathbf{x}_1[k]$ removing its last element and similarly for $\mathbf{x}_2[l]$. In this way, the LCSS distance between $\mathbf{x}_1$ and $\mathbf{x}_2$ is defined as:

$$LCSS(\mathbf{x}_1[k], \mathbf{x}_2[l]) = \begin{cases} 0, & \text{if } \mathbf{x}_1[k] \text{ or } \mathbf{x}_2[l] \text{ empty.} \\ 1 + \text{LCSS}(\text{Head}(\mathbf{x}_1[k]),\mathbf{x}_2[l]), & \text{if } \mathbf{x}_1[k] = \mathbf{x}_2[l]. \\ \max(\text{LCSS}(\text{Head}(\mathbf{x}_1[k]),\mathbf{x}_2[l]),\text{LCSS}(\mathbf{x}_1[k],\text{Head}(\mathbf{x}_2[l]))) & \text{otherwise.} \end{cases} \tag{2-22}$$

The solution for this problem involves to compute the distance for smaller instances with a few amount of points and then continues by adding new ones to the sequence. This equation:

$$LCSS[k,l] = \begin{cases} 0, & \text{if } i = 0. \\ 0, & \text{if } j = 0. \\ 1 + \text{LCSS}[i-1, j-1] & \text{if } \mathbf{x}_1[k] = \mathbf{x}_2[l]. \\ \max(\text{LCSS}[k-1, l],\ \text{LCSS}[i, j-1]) & \text{otherwise.} \end{cases} \tag{2-23}$$

can be solved using dynamic programming (2-23).

Where $LCSS[i,j]$ denotes the longest common subsequence between the first i elements of sequence x_1 and the first j elements of sequence x_2. Although, the LCSS model described in 2-23 matches exact values, it necessary allows more flexible matching between two time series including certain range in the values. Given an integer δ and a real positive number ϵ, $\text{LCSS}(x_1, x_2)$ is defined in 2-24.

$$\text{LCSS}_{\delta,\epsilon} = \begin{cases} 0, & \text{if } \mathbf{x}_1[k] \text{ or } \mathbf{x}_2[l] \text{ is empty .} \\ 1 + \text{LCSS}_{\delta,\epsilon}(\text{Head}(\mathbf{x}_1),\ \text{Head}(\mathbf{x}_2)) & \text{if } |x_1(n) - x_2(n)| < \epsilon. \\ & \text{and} |n - m| \leq \delta. \\ \max(\text{LCSS}_{\delta,\epsilon}(\text{Head}(\mathbf{x}_1),\mathbf{x}_2),\ \text{LCSS}_{\delta,\epsilon}(x_1,\text{Head}(\mathbf{x}_2))) & \text{otherwise.} \end{cases} \tag{2-24}$$

The constant δ controls how far in time is possible go in order to match a given point from one time series to a point in another time series. On the other hand, ϵ describes the matching

threshold. The similarity function D_{LCSS} between two sequences $\mathbf{x}_1$ and $\mathbf{x}_2$, given δ and ϵ, is defined in 2-25. LCSS algorithm to compute the LCSS similarity distance is summarized in the Algorithm 1.

$$D_{LCSS}(\delta, \epsilon, \mathbf{x}_1[k], \mathbf{x}_2[l]) = \frac{\mathrm{LCSS}_{\delta,\epsilon}(\mathbf{x}_1[k], \mathbf{x}_2[l])}{\max(n, m)}. \tag{2-25}$$

The alignment between two time series, computed with this algorithm, could be seen in the Figure **2-1**. Where $\mathbf{x}_1$ and $\mathbf{x}_2$ are the blue and red trajectories, the gray zone represents the matching area defined by ϵ and δ and the alignment is shown by lines between each pair of points chosen for the matching and subsequent calculation of similarity measure. The matching threshold and the similarity value in this example are presented in the title.

Data: $\mathbf{x}_1[k], \mathbf{x}_2[l]$
Result: LCSS Similarity Distance
initialization;
for *k=1* **to** m **do**
  for $i \leftarrow (k - \delta)$ **to** $k + \delta$ **do**
    if $l <= 0$ ***or*** $l > m$ **then** $\mathbf{x}_2[l] + \epsilon >= \mathbf{x}_1[k]$ **and** $\mathbf{x}_2[l] - \epsilon <= \mathbf{x}_1[k]$
    LCSS[k+1,l+1]=LCSS[k,l]+1;
    $LCSS[k, l+1] > LCSS[k+1, l]$ LCSS[k+1,l+1]=LCSS[k,l+1];
    else
      LCSS[k+1,l+1]=LCSS[k+1,l];
    end
  end
end
LCS_ Distance=**max**[LCSS[n,:]]/**max**[n,m];

Algorithm 1: LCSS Algorithm.

The best results for this algorithm have been obtained with planar trajectories, because the configuration of variables δ and ϵ in multidimensional spaces makes it less accurate finding wrong alignments and more time consuming. In addition, if the movements are recorded with different update frequencies, LCSS does nor work appropriately and the similarity measure calculated is not accurate [116]. An example of this behaviour is shown in Figure **2-2**, where each trajectory has a different update frequency causing that earlier points of sequence 1 are matched with every point of sequence 2 that is included in range ϵ. Due to this algorithm does not take into account how the points are assigned, it is not possible to find a better alignment with this approach.

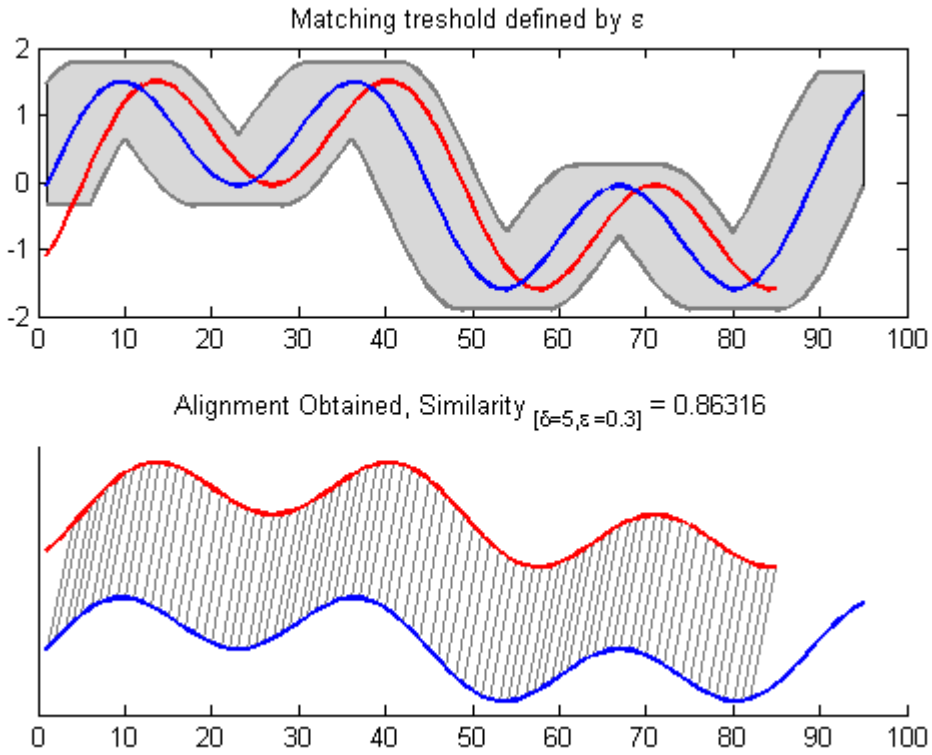

Figure 2-1: Similarity distance based in the LCSS alignment.

Dynamic Time Warping

Dynamic Time Warping (DTW) is a time series alignment algorithm. It aims at aligning two sequences by warping the time axis iteratively until an optimal match between the two sequences is found. In [59], authors show the benefits of DTW among other gesture recognition algorithms such as Hidden Markov Models. Specifically, they summarize and compare some important features (developer cost, time, complexity, recognition accuracies) between these recognition methods (Table **2-1**).

Consider two sequences of feature vectors as in 2-1. To align two sequences using DTW, an n-by-m matrix is constructed, where the (i^{th},j^{th}) element of the matrix contains the distance $d(\mathbf{x}_1[k], \mathbf{x}_2[l])$ between the two points $\mathbf{x}_1[k], \mathbf{x}_2[l]$. The distance computed for each pair of points, is non-elastic and is usually chosen by the author. In this work, based on conclusions of Section 2.3.1, the Euclidean distance is calculated between the feature values of each combination of points. These distances are used to calculate cumulative distance matrix. Each matrix element (k, l) corresponds to the alignment between the points $\mathbf{x}_1[k]$ and $\mathbf{x}_2[l]$ (Figure **2-3**) and a warping path (green path) is a continuous set of matrix elements

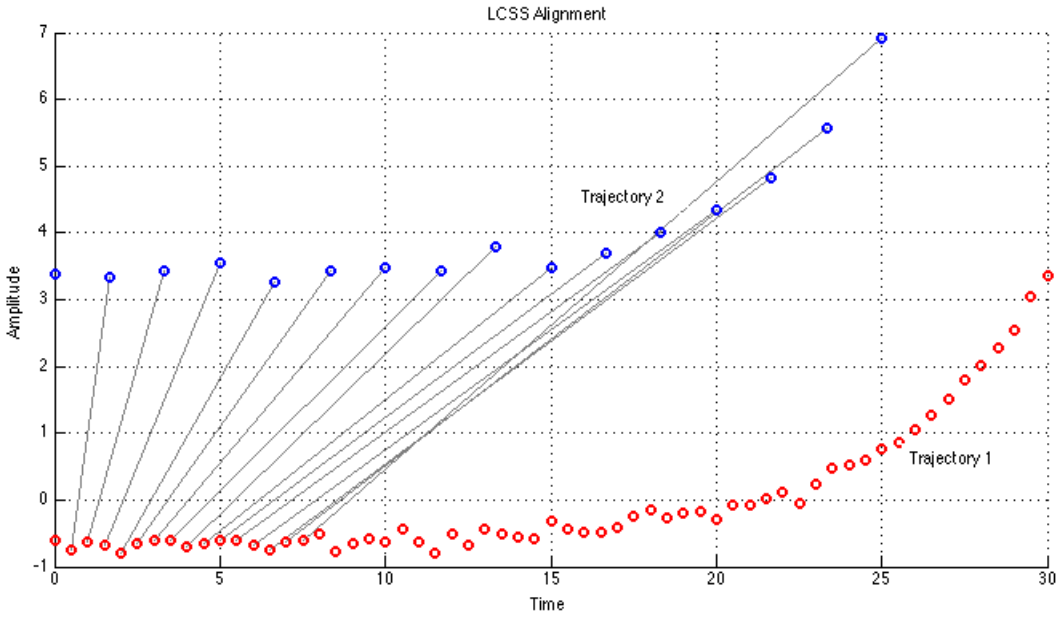

Figure 2-2: LCSS alignment for trajectories with different update frequencies.

that defines a mapping between x_1 and x_2. To find the best match or alignment between these two sequences it is necessary to find a path through the grid which minimizes the total distances between them. The basic method for finding the optimal warping matrix requires the evaluation of an exponential number of warping paths. For this reason, dynamic programming is used to find the optimal warping path. 1D-DTW algorithm to find the DTW similarity distance is summarized in the Algorithm 2.

Method	Developer Cost	Time Complexity	Recognition, Accuracy (Single-Path)	Recognition, Accuracy, Equal Coding Condition (Multi-Path)	Recognition, Accuracy, Minimal Coding Condition (Multi-Path)
Hidden Markov Model	High	Cubic	Good	Great	Good
Dynamic Time Warping	Moderate	Cubic	Excellent	Excellent	Great

Table 2-1: Comparison between Dynamic Time Warping and Hidden Markov Models [59].

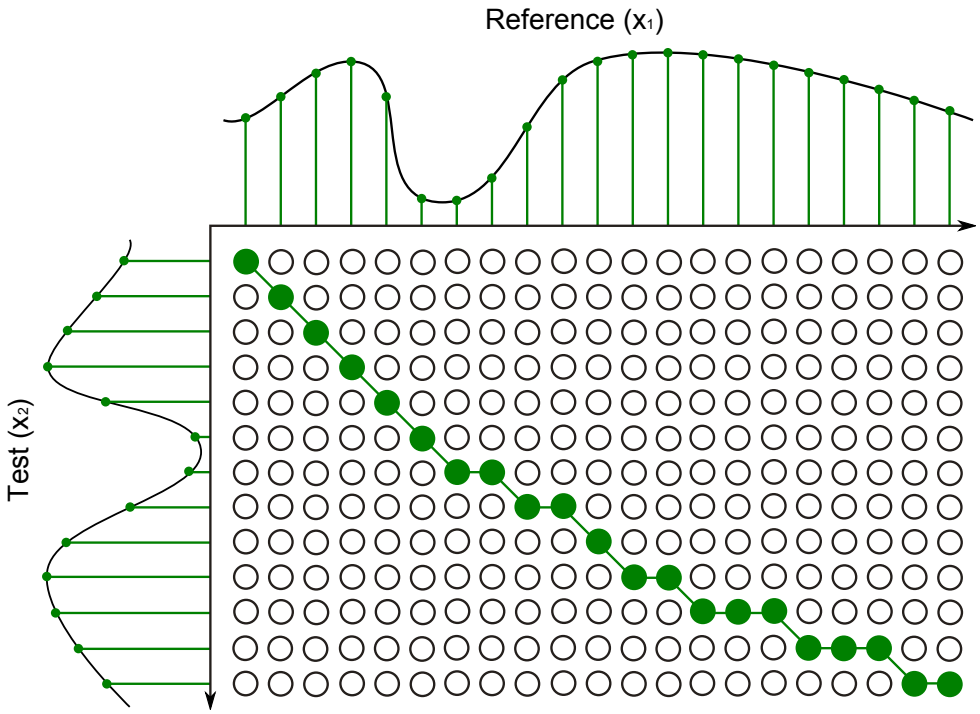

Figure 2-3: Cumulated Distance Matrix.

Data: $\mathbf{x}_1[k], \mathbf{x}_2[l]$
Result: DTW Similarity Distance
initialization;
for *k=1* **to** n **do**
  for *l=1* **to** m **do**
    distance=NonElasticMetric($x_1[i], x_2[j]$);
    DTW[i,j]= distance + min(DTW [i-1,j], DTW [i,j-1], DTW [i-1, j-1]);
  end
end

Algorithm 2: 1D-DTW Algorithm.

In Figure **2-4**, the alignment for two planar trajectories, obtained using DTW, is presented. The results show that a natural alignment for trajectories with different size and scale (magnitude and time) is possible using DTW.

From this calculation, in Figure **2-5**, each gray line matchs a point in one sequence to its correspondingly similar point in the other sequence. Both trajectories have similar amplitude values but they have been separated in such a way that the alignment can be observed easiest.

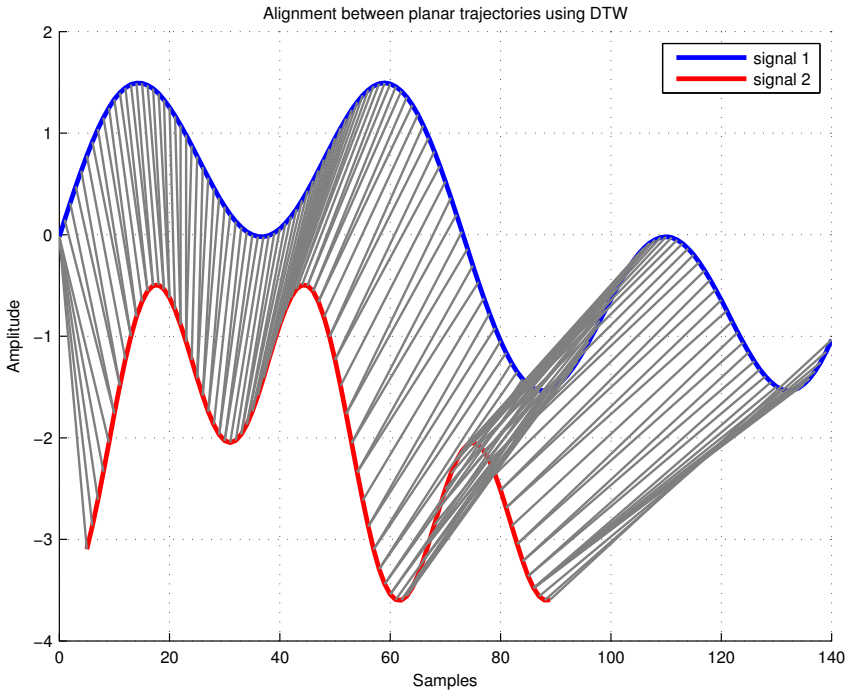

Figure 2-4: DTW Alignment.

If both of trajectories were equal, every line would be straight because no warping would be necessary to match both sequences.

Multidimensional Dynamic Time Warping

Sequences acquired from surgical gestures are multidimensional time series. In order to analyze them, some authors like [124] have suggested some variations of the classical DTW algorithm called Multidimensional Dynamic Time Warping (MD-DTW). This approach includes the addition of the distances in all dimensions to find the best synchronization. To analyze the different dimensions with this method, it is necessary to normalize each dimension to a zero mean and unit variance. The advantages of MD-DTW can be seen when multidimensional series have synchronization information distributed over different dimensions, then applying 1D-DTW for only one dimension could result in wrong alignments. MD-DTW algorithm to calculate the similarity distance is summarized in the Algorithm 3. In Figure **2-5**, a MD-DTW alignment is shown for three dimensional trajectories with different size, scale and location.

Data: $\mathbf{x}_1[n1], \mathbf{x}_2[n2]$
Result: MD-DTW Similarity Distance
initialization;
x1=mean($x_1[1...n1]$) $\mathbf{x}2 = mean(\mathbf{x}_2[1...n2])$ $\mathbf{x}1 =$
$\mathbf{x}1/StandardDeviation(\mathbf{x}_1[1...n1])$ $\mathbf{x}2 =$
$\mathbf{x}2/StandardDeviation(\mathbf{x}_2[1...n2])$ **for** K=*1* **to** *n1* **do**
  for *l*=*1* **to** *n2* **do**
    distance=distance+NonElasticMetric($\mathbf{x}_1[k], \mathbf{x}_2[l]$);
  end
  MDDTW[i,j]= distance + min(MDDTW [i-1,j], MDDTW [i,j-1], MDDTW [i-1, j-1]);
end

Algorithm 3: MD-DTW Algorithm

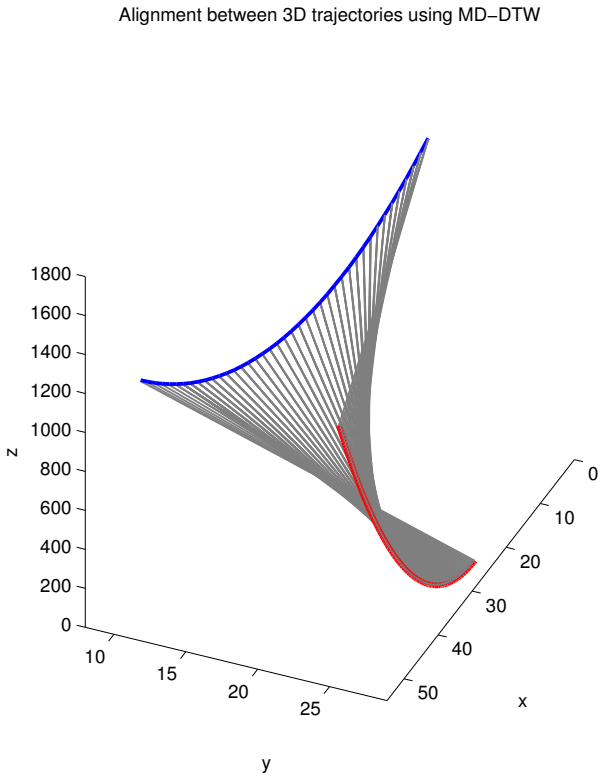

Figure 2-5: MD-DTW Alignment.

Multidimensional Derivative Dynamic Time Warping

According to [61] and [140] DTW attempts to align two vectors that are similar except for local accelerations and decelerations in time axis, the algorithm is likely to be successful. However, the classical DTW algorithm has problems when the two sequences have great variations in their feature data. Figure 2.6(a) shows that this variations resulting in poor alignments located on the first maximum and minimum of the blue trajectory. To prevent this problem, the latter authors have suggested to consider the first derivative of the sequences rather the raw data.

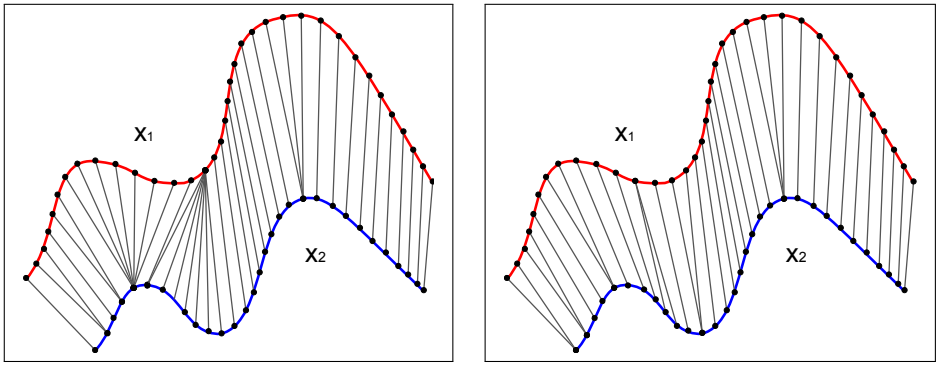

(a) DTW applied to sequences with decelerations in time.

(b) Derivative DTW applied to sequences with decelerations in time.

Figure 2-6: Synchronization of two trajectories with respectively 100 and 10 samples.

In this algorithm, the distance measurement $\mathbf{distance}(\mathbf{x}_1, \mathbf{x}_2$ is not one of the non elastic metrics described in the Section 2.3.1, but rather the square of the difference of the estimated derivatives, where the central derivative technique described in 2-26 is used for simplicity and generality and is expressed by:

$$\dot{\mathbf{x}}_1[i] = \frac{(\mathbf{x}_1[i] - \mathbf{x}_1[i-1]) + ((\mathbf{x}_1[i+1] - \mathbf{x}_1[i-1])/2)}{2}. \tag{2-26}$$

This expression represents the average of the slope of the line through every point and their left neighbors, and the slope of the line through their left neighbors and their right neighbors. This three-point estimation is a more accurate approximation and less to outliers than the corresponding two-point estimation. This approach is summarized in Algorithm 4.

Data: $x_1[n], x_2[m]$
Result: MD-DDTW Similarity Distance
initialization;
x1=mean(x$_1$[1...n1]) $\mathbf{x}2 = mean(\mathbf{x}_2[1...n2])$ $\mathbf{x}1 =$
$\mathbf{x}1/StandardDeviation(\mathbf{x}_1[1...n1])$ $\mathbf{x}2 =$
$\mathbf{x}2/StandardDeviation(\mathbf{x}_2[1...n2])$ **for**k=*1* **to** n**do**
  for l=*1* **to** m **do**
    distance=distance+$(|\dot{\mathbf{x}}_1[k] - \dot{\mathbf{x}}_2[l]|)^2$;
  end
  MDDDTW[i,j]= distance + min(MDDDTW [i-1,j], MDDDTW [i,j-1], MDDDTW [i-1, j-1]);
end

Algorithm 4: MD-DDTW Algorithm.

In general, MD-DTW and MD-DTW have the same complexity (O(mn)) and take approximately the same time, however when real data are analyzed, MD-DDTW is very noise sensitive and its accuracy depends on the method implemented to calculate the derivatives [7].

2.3.3. Simulation Analysis (MD-DTW, MD-DDTW)

In this section, a robustness survey of techniques described in 2.3.2 and 2.3.2 was performed ([22]) using Matlab. Algorithms based on DTW were chosen due to the accuracy of the experimental results compared to other techniques [59, 104]. The variation of different parameters, such as the number of samples, the existence of outliers and noise in the measurements, has been taken into account. The objective is to point out practical issues while implementing the different DTW algorithms.

Number of Samples

A circular path with different number of samples (different sampling rate) was selected for simplicity in the data visualization (Figure 2.7(a)). The position data could be considered as time series where the dimension of the vector is equal to three. In every case, samples have a regular space and the frequency is high enough to have all the information in order to satisfy the Shannon condition:

$$fi_2 = \frac{fi_1}{2}. \tag{2-27}$$

With these two trajectories, both multidimensional synchronization techniques based on DTW were implemented. Figures 2.7(b) and 2.7(c) show an example of the synchronization between each point made by both techniques. The process with different variations in the number of samples was repeated and the *DTW* distance of the optimal path, found by both algorithms, was calculated. The results of the simulation are shown in Table **2-2**.

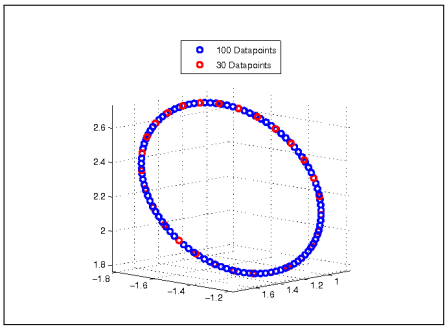

(a) Circular path with different numbers of samples.

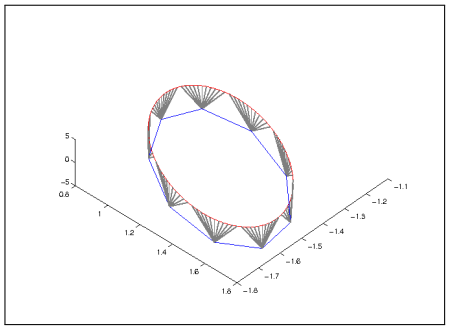

(b) Synchronization obtained with MD-DTW.

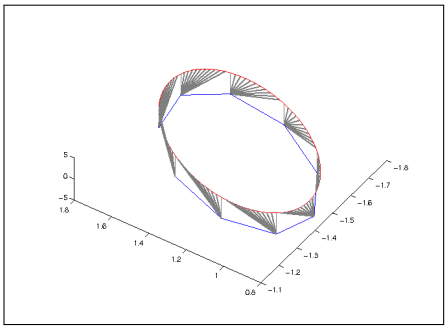

(c) Synchronization obtained with MD-DDTW.

Figure 2-7: Synchronization of two trajectories with respectively 100 and 10 samples.

Number of samples from the path 1	Number of samples from the path 2	d (MD-DTW)	d (MD-DDTW)
100	30	2.68	7.57
100	50	1.58	3.20
100	70	1.12	1.36
100	90	0.87	0.85

Table 2-2: Cumulative distance: variation of the number of samples.

The results show that the cumulative distance of MD-DTW remains constant within a wider range than MD-DDTW technique. In other words, these results point out that a better performance is obtained with MD-DTW technique while varying the number of samples. The reduction of the number of samples is equivalent to a loss representative information in the data resulting in a distortion of the derivative used signals in MD-DDTW. This phenomenon leads to a very different cumulative distance for MD-DTW compared to MD-DDTW. In contrast when the number of samples increases, the performance of both algorithms is similar.

Outliers

In this section, artificial outliers have been added to the trajectory (see Figure **2-8**) in order to study the sensitivity of the different techniques with respect to this factor.

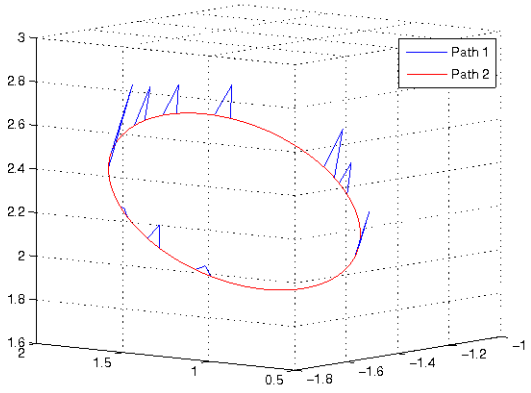

Figure 2-8: Artificial Outliers in the trajectory.

The analysis has been carried out according two criteria: a variation of the number of the outliers present (% respect to the samples number of the trajectory) in the path and a variation of the maximum amplitude of the outliers. Finally, we compare the results obtained with both techniques. The results are summarized in the Table **2-3** for two sets of data with the same number of samples.
Without filtering, the sudden changes in the trajectory generate very high variations of the derivative causing errors while performing the synchronization with MD-DDTW. In contrast, MD-DTW shows a better performance evidenced in lower distances for every case.

Noise

The last study concerns the effect of noise on the different algorithms. Different white noise levels have been applied to one trajectory (see Figure **2-9**).
With the addition of noise, MD-DTW and MD-DDTW distances are computed y compared in Table **2-4**.

% of outliers	Amplitude of added outliers	d (MD-DTW)	d (MD-DDTW)
5	0.05	0.23	0.48
	0.1	0.36	0.71
	0.3	1.04	2.09
10	0.05	0.45	0.87
	0.1	0.76	1.53
	0.3	2.69	5.38
15	0.05	0.54	1.00
	0.1	1.19	2.1
	0.3	3.03	5.45

Table 2-3: Cumulative distance: Outliers.

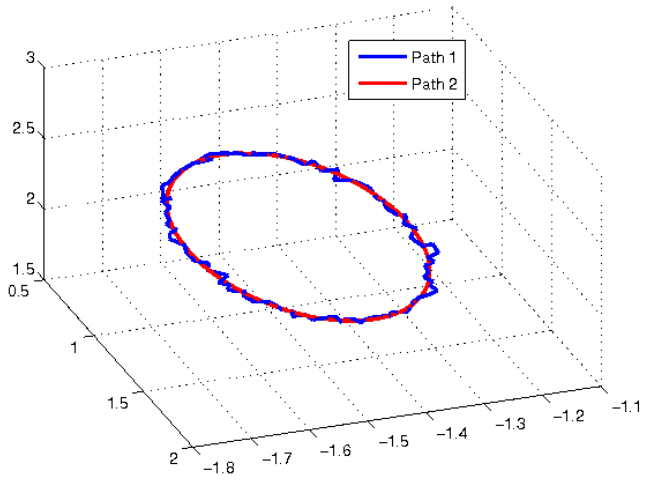

Figure 2-9: Artificial noise applied on one trajectory.

Like previously the results show that MD-DTW algorithm works better, calculating lower values of distance compared to MD-DDTW. Although MD-DDTW works better when local accelerations and decelerations are present (Figure **2-6**), outliers and noise (sudden amplitude changes) generate high values of derivatives, which increases the similarity distances obtained with this algorithm.

SNR (Signal to Noise Ratio)	d (MD-DTW)	d (MD-DDTW)
50	1.50	1.48
48	1.64	1.75
45	2.24	2.45
43	2.74	3.16
40	3.39	4.00
38	4.45	5.08
35	6.04	7.29

Table 2-4: Cumulative distance: Noise.

2.3.4. Experimental Results

To conduct the experiments of this section, we acquired the 3D position (x, y, z) of a simple gesture performed by five people. The right arm of the participants were dressed with a four degrees of freedom exoskeleton (Detailed information Section 3.5.2 and [90]), then they were asked to elevate their arm to simulate a gesture similar to the one made to stop/halt someone. The trajectory performed by one of them is shown in the Figure **2-10** and similar trajectories can be plotted for the other people.

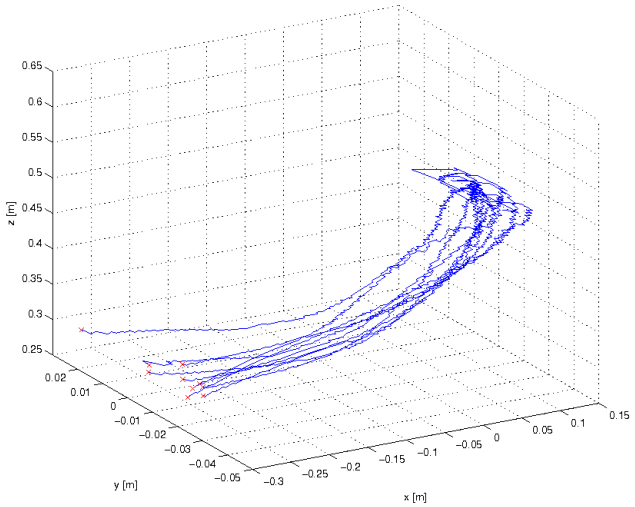

Figure 2-10: Trajectory Performed.

Based on the results presented in Section 2.3.3, MD-DTW has a better performance compared to MD-DDTW. However, as part of this work, an experimental study was performed in which the influence of the numerical approximation of the derivative was analyzed using a lowpass filter and MD-DDTW technique and comparing the results with a new approach that propose the use of a derivative filter and MD-DTW technique.

At this point, the low-pass filter and MD-DDTW technique to synchronize each trajectory was used. The Table **2-5** shows the distance $MD-DDTW$ obtained between each similar pair of paths for the gesture with this method.

MD-DDTW d_1	Person 2	Person 3	Person 4	Person 5
Person 1	0.48	0.41	0.51	0.43
Person 2	-	0.43	0.52	0.4
Person 3	-	-	0.48	0.45
Person 4	-	-	-	0.48

Table 2-5: Experimental results.

Finally, another alternative for the synchronization was used, a derivative filter was applied directly and the corresponding points were found with MD-DTW technique. The difference between these two alternatives can be highlighted on Figure **2-11**.

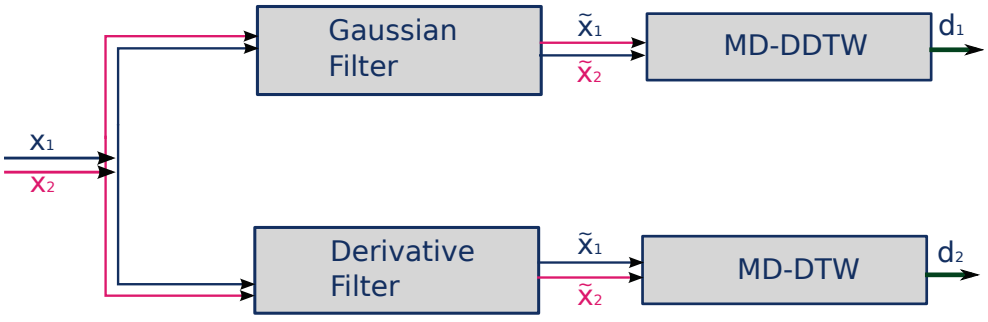

Figure 2-11: Derivative Filter.

The filter used in the MD-DDTW algorithm is a Gaussian filter because it is effective removing high frequency noise amplification, computationally efficient and it has an intuitive relationship between size of σ and the degree of smoothing [120, 130]. The one-dimensional gaussian filter has an impulse response given by:

$$g(x) = \frac{1}{\sqrt{2\pi}\sigma} e^{\frac{-x^2}{2\sigma^2}}, \tag{2-28}$$

where x is the distance from the origin in the horizontal axis and σ is the standard deviation of the Gaussian distribution. Thus, the derivative filter implemented is given by 2-29.

$$h(x) = \frac{dg(x)}{dx} = \frac{-x}{\sigma^2\sqrt{2\pi\sigma}} e^{\frac{-x^2}{2\sigma^2}}. \tag{2-29}$$

The results obtained with this alternative are summarized in the Table **2-6**.

MD-DDTW d_2	Person 2	Person 3	Person 4	Person 5
Person 1	0.35	0.38	0.4	0.37
Person 2	-	0.33	0.41	0.36
Person 3	-	-	0.36	0.35
Person 4	-	-	-	0.37

Table 2-6: Derivative Filter.

The last values show that the method using the derivative filter gives a distance values lower for similar trajectories. These results suggest that a more effective classification of the trajectories could be obtained. Since regular MD-DDTW method uses a numerical scheme to approximate the derivative it turns out that the computed distance depends somehow on the numerical scheme. By applying the second strategy, we use an analytical expression of the derivative to improve the accuracy of the results.

2.4. Conclusion

In this chapter different metrics (non-elastic and elastic) used to find similarities between time series, based on the 3D position of trajectories were explained. In particular, a simulation analysis was carried out based on DTW and its variations. This approach was chosen due to its accurate results, simplicity and computational efficiency. Section 2.3.3 shows the performance of each method, related to different parameters as the number of samples, the amount of outliers and noise that could be included in the acquired signal.

In section 2.3.4, the benefits of a modified version of MD-DDTW are shown. This proposed method includes a derivative filter instead of the use of a low pass filter and a numerical differentiation of the trajectories. The results show a more accurate behavior due to the analytical nature of the derivative filter implemented.

3 Dynamic Arc Length Warping (DALW)

In this chapter, a new analysis in gesture classification is proposed using a space-time independent parametrization. This approach includes an arc-length parametrization allowing for time independence and a geometric invariant like curvature that varies according to local geometry and not sensor location. Experimental results exposed in this work are focusing on the classification of hand gestures.

3.1. Arc Length Parametrization

A space trajectory $\mathbf{P}$ defined in 4D space by (t, x, y, z) can be seen as a vector $\mathbf{r}(t) = [x(t), y(t), z(t)]$ in 3D space where time $t \in [a, b]$ is now a dependent parametric variable. The problem with this classical time parametrization approach is that gestures are not necessarily time dependent as for example a circular gesture is basically independent of the rotation speed. Another way to parameterize space which is independent from time and coordinate system is to use the notion of cumulative arc-length. Cumulative arc-length is based on the total length S of the trajectory in 3D space between the beginning and the end of the gesture $[t_a, t_b]$ and is defined by :

$$S = \int_{t_a}^{t_b} ||\dot{\mathbf{r}}(t)|| dt, \tag{3-1}$$

where $||\dot{\mathbf{r}}(t)||$ is the speed of the curve and is defined as the euclidean norm of the first derivative of the trajectory with respect to time:

$$||\dot{\mathbf{r}}(t)|| = \sqrt{(\dot{x}(t))^2 + (\dot{y}(t))^2 + (\dot{z}(t))^2}. \tag{3-2}$$

Considering the assumption that $\dot{r}(t) \neq 0$, the arc length function is differentiable at t:

$$\frac{ds}{dt} = ||\dot{r}||. \tag{3-3}$$

One can re-parametrize $\mathbf{P}$ by using a normalized parameter s called the cumulative arc-length s defined by :

$$s = \frac{1}{S} \int_{t_a}^{t_b} ||\dot{\mathbf{r}}(t)|| dt, \tag{3-4}$$

where $s \in [0, 1]$. Figure **3-1** shows an arc-length parameterized spline curve, obtained using Equation 3-4.

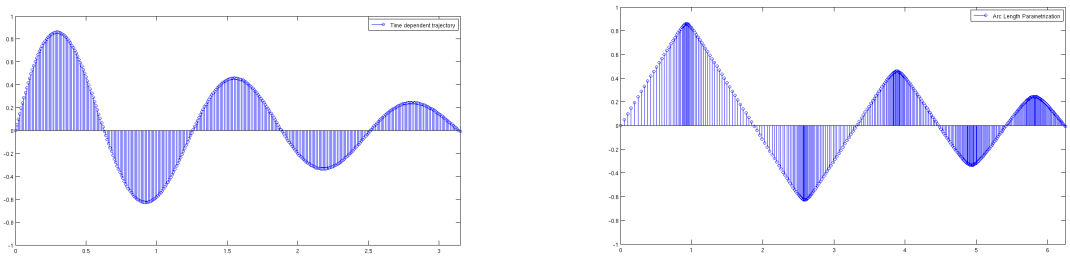

(a) Time Sequence (b) Arc Length Sequence

Figure 3-1: Arc Length Parametrization

The parametrization of the path with time means that motion description is not time invariant, and paths that follow identical trajectories at different speeds will be considered different. The new parametrization is quite useful because it avoids this problem and, in addition, cumulative arc length arises naturally from the shape of the curve and does not depend on a particular coordinate system.

3.2. Curvature

For a given point, the curvature vector $\ddot{\mathbf{r}}(s)$ of a curve is defined as the magnitude of the rate of change of the unit tangent vector $\mathbf{T}$ with respect to the cumulated arc-length s (Figure **3-2**). We define curvature as the length of the curvature vector. We will denote the curvature scalar quantity by the letter κ as follows:

$$\kappa(s) = ||\ddot{\mathbf{r}}(s)||. \tag{3-5}$$

In other words, the curvature of the trajectory at a given point is a measure of how quickly the curve changes in the direction at that point. Interestingly, when the parametrization with respect to the cumulative arc-length is used, the trajectory is sampled with unequal intervals in space. For this reason, one cannot apply the classical techniques of numerical differentiation to compute the curvature.

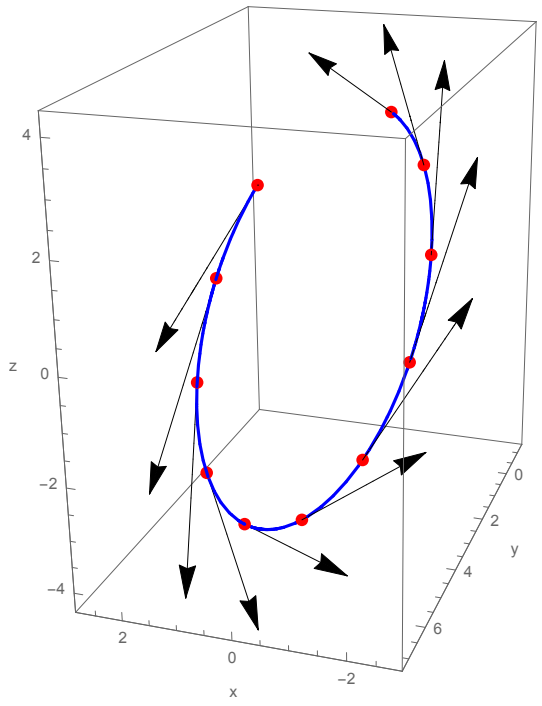

Figure 3-2: Unit tangent vector in different points of a curve.

In order to handle this problem, the data were fitted using polynomial functions. In this way, a second-order Lagrange polynomial interpolation scheme is used to fit each set of three adjacent points. We chose this interpolation technique for those reasons:

1. **Simplicity:** The Lagrange interpolating polynomial can be determined without having to solve a system of simultaneous equations;

2. **Roundoff:** Evaluation of the Lagrange polynomial is less sensitive to roundoff than another polynomial interpolation technique [110];

3. **Unequally Spaced Values:** The most important advantage of Lagrange interpolation is that the method does not need evenly spaced sampled values.

The second order polynomial can be differentiated analytically twice using the following. First, we fit a Lagrange interpolating polynomial to each set of three adjacent points:

$$f_n(s) = L_{i-1}(s)p_n(s_{i-1}) + L_i(s)p_n(s_i) + L_{i+1}(s)p_n(s_{i+1}), \tag{3-6}$$

$$f_n(s) = \frac{(s-s_i)(s-s_{i+1})}{(s_{i-1}-s_i)(s_{i-1}-s_{i+1})}p_n(s_{i-1}) + \frac{(s-s_{i-1})(s-s_{i+1})}{(s_i-s_{i-1})(s_i-s_{i+1})}p_n(s_i) + \frac{(s-s_{i-1})(s-s_i)}{(s_{i+1}-s_{i-1})(s_{i+1}-s_i)}p_n(s_{i+1}), \tag{3-7}$$

where the function f_n is the Lagrange polynomial for coordinate x, y, and z respectively, L_i is the Lagrange basis function, and p_n are the points to interpolate for each axis. In order to calculate the curvature values of each trajectory, one can differentiate twice the Lagrange polynomial as in :

$$f'_n(s) = \frac{(s-s_i)+(s-s_{i+1})}{(s_{i-1}-s_i)(s_{i-1}-s_{i+1})}p_n(s_{i-1}) + \frac{(s-s_{i-1})+(s-s_{i+1})}{(s_i-s_{i-1})(s_i-s_{i+1})}p_n(s_i) + \frac{(s-s_{i-1})+(s-s_i)}{(s_{i+1}-s_{i-1})(s_{i+1}-s_i)}p_n(s_{i+1}), \tag{3-8}$$

$$f'_n(s) = \frac{2s-s_i-s_{i+1}}{(s_{i-1}-s_i)(s_{i-1}-s_{i+1})}p_n(s_{i-1}) + \frac{2s-s_{i-1}-s_{i+1}}{(s_i-s_{i-1})(s_i-s_{i+1})}p_n(s_i) + \frac{2s-s_{i-1}-s_i}{(s_{i+1}-s_{i-1})(s_{i+1}-s_i)}p_n(s_{i+1}), \tag{3-9}$$

$$f''_n(s) = \frac{2p_n(s_{i-1})}{(s_{i-1}-s_i)(s_{i-1}-s_{i+1})} + \frac{2p_n(s_i)}{(s_i-s_{i-1})(s_i-s_{i+1})} + \frac{2p_n(s_{i+1})}{(s_{i+1}-s_{i-1})(s_{i+1}-s_i)}, \tag{3-10}$$

where s_{i-1}, s_i, s_{i+1} is the cumulative arc-length of three consecutive points.

3.3. Dynamic Arc Length Warping

Using the formulation derived in the previous section, one can calculate the numerical derivatives of two trajectories $\mathbf{r}_1(s)$ and $\mathbf{r}_2(s')$, where s and s' are the cumulative arc lengths for $\mathbf{r}_1$ and $\mathbf{r}_2$, in order to obtain their corresponding curvatures. In this case, the objective of **DALW** (Dynamic Arc Length Warping) is to compare the two curvature sequences $\boldsymbol{\kappa_1} = \{\kappa_1(s_1), \kappa_1(s_2), \kappa_1(s_3), ..., \kappa_1(s_l)\}$ of length $l \in \mathbb{N}$ and $\boldsymbol{\kappa_2} = \{\kappa_2(s'_1), \kappa_2(s'_2), \kappa_2(s'_3), ..., \kappa_2(s'_m)\}$ of length $m \in \mathbb{N}$.

To compare two different curvature signatures $\boldsymbol{\kappa_1}$ and $\boldsymbol{\kappa_2}$, a local comparison matrix $\mathbf{F}$ is defined. The matrix elements measures the distance between the curvature values $\kappa_1(s_i)$ and $\kappa_2(s'_j)$ according to a chosen norm. In the following, we will use the Euclidean norm for convenience. This *local similarity metric* is defined between any pair of elements $\kappa_1(s_i)$ and $\kappa_2(s'_j)$, using the following expression:

$$F(i,j) = (\kappa_1(s_i) - \kappa_2(s'_j))^2 \geq 0. \tag{3-11}$$

Typically $F(i,j)$ is small (low cost) if $\kappa_1(s_i)$ and $\kappa_2(s'_j)$ are similar to each other and otherwise $F(i,j)$ is large (high cost). Evaluating the local cost measure between two sequences $\boldsymbol{\kappa}_1$ and $\boldsymbol{\kappa}_2$ leads to a cost matrix by $\mathbf{F}$. Then main goal of this algorithm is to find an alignment between $\boldsymbol{\kappa}_1$ and $\boldsymbol{\kappa}_2$ which minimize the overall cost function.

A warping path of a curvature signature $\boldsymbol{\kappa}_n$ is denoted by ϕ_n, where $k = 1, 2, ..., W$ and $\max(l,m) \leq W < l+m-1$. Consequently, the curvature array defined for this warping path is defined by:

$$\kappa'_n(s_j) = \kappa_n(s_{\phi_n}), \tag{3-12}$$

where s_j value corresponds to the previous signature value at s_k. Using this notation, the warping functions $\phi_1(k)$ and $\phi_2(k)$ re-map the cumulative arc-length index of κ_1 and κ_2, respectively. Given ϕ, one can compute the total distance between the warped arc-length series as:

$$d = \sum_{k=1}^{W} \frac{1}{\alpha_\phi} \Big(\kappa_1(s) - \kappa_2(s')\Big)^2 M_\phi, \tag{3-13}$$

where α_ϕ is a per-step weighting coefficient and M_ϕ is the corresponding normalization constant, which ensures that the distances are comparable along different paths. The value of M_ϕ depends on the application and in most cases it is the length of the path, but it can also be omitted [111].

The optimal warping corresponds to the warping $\phi_1(k^*)$ and $\phi_2(k^*)$ that minimize the distance:

$$DALW(\kappa_1, \kappa_2) = d(k^*). \tag{3-14}$$

This result is equivalent to the distance or similarity measure between paths found with DALW. This optimization problem can be efficiently solved by using a dynamic programming technique [9].

In order to ensure reasonable optimal paths, constraints are usually imposed on the warping function $\phi_n(k)$:

1. **Boundary Condition:** This condition restricts the beginning and the ending points of the path.
   Beginning point : $\phi_1(1) = \phi_2(1) = 1$
   Ending point : $\phi_1(W) = N$; $\phi_2(W) = M$.

2. **Monotonicity Condition:** The order of the measurements collected on each variable has a crucial importance to the meaning of arc length. Accordingly, imposing a reasonable monotonicity-constraint to maintain the respective order in the arc length while performing DALW is necessary:
   $\phi_1(k+1) \geq \phi_1(k)$ and $\phi_2(k+1) \geq \phi_2(k)$.

3. **Step size Condition:** This criterion limits the warping path from long jumps (shifts in arc length axis) while aligning sequences. We use the basic step size condition formulated as:
   $|\phi_1(k+1) - \phi_1(k)| \leq 1$ and $|\phi_2(k+1) - \phi_2(k)| \leq 1$.

The new algorithm consists of using the proposed arc length dynamic warping to match two curvature signals first, then, with the information of the alignment between each pair of points, one can reconstruct the matching between both original 3D trajectories.

3.4. Simulation Analysis

In this section, two artificial series were analyzed. The objective is to visualize that the proposed technique not only is efficient and produce quantitative results but also provide qualitative results compared to other techniques such as Multi-Dimensional Dynamic Time Warping MD-DTW [21]. In Figure **3-3**, two simple trajectories are shown, which can represent any physical quantity (position, orientation, force, etc), and one of them is scaled and is at a different location in space. The number of samples of both trajectories is also different.

Figure **3-4** shows the characteristic curvatures for each trajectory. Taking into account the curvature values parametrized in function of the arc length, dynamic warping is performed and a preliminary alignment between both curvature signals is obtained. From this point on, using the matching curvature points, the alignment between both 3D trajectories is reconstructed (Figure 3.5(a)).

Figure **3-5** shows that **DALW** algorithm generates better results with a more natural alignment between both 3D trajectories. Furthermore, the Euclidean distance has been computed between each pair of matching points with both techniques (DALW and MD-DTW) in order to obtain a quantitative comparison.

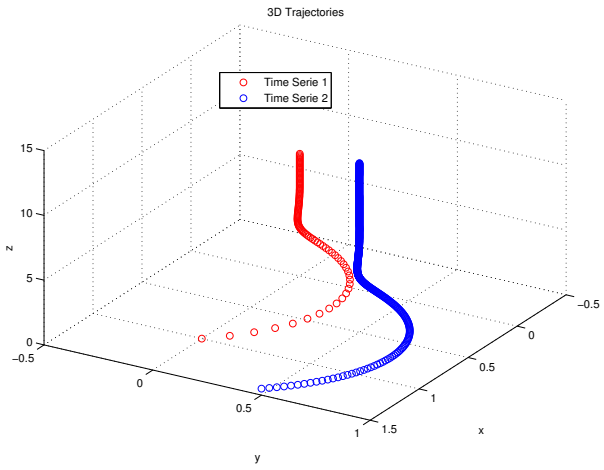

Figure 3-3: Artificial Series.

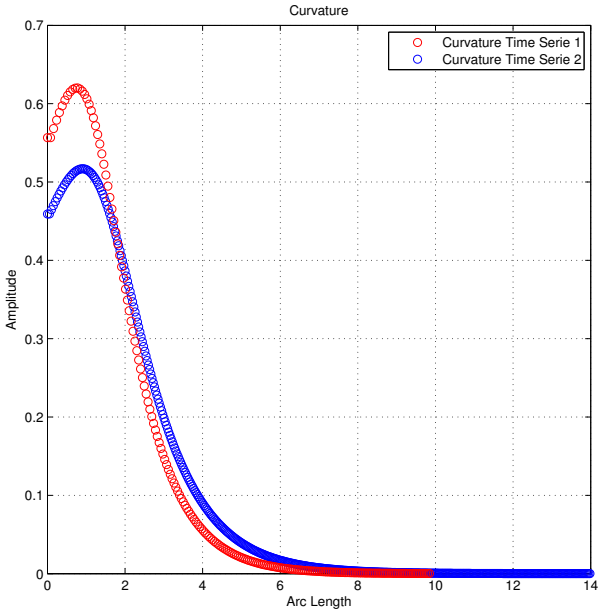

Figure 3-4: Curvature calculated for both signals.

The comparison results are shown in Figure **3-6**. This distance gives us a better idea on the performance of each technique. In this case, DALW generates a smaller value of distance for similar trajectories obtaining a more precise alignment. In many ways this makes sense because the curvature is invariant to the spatial location of the trajectories relative to the sensor coordinate system.

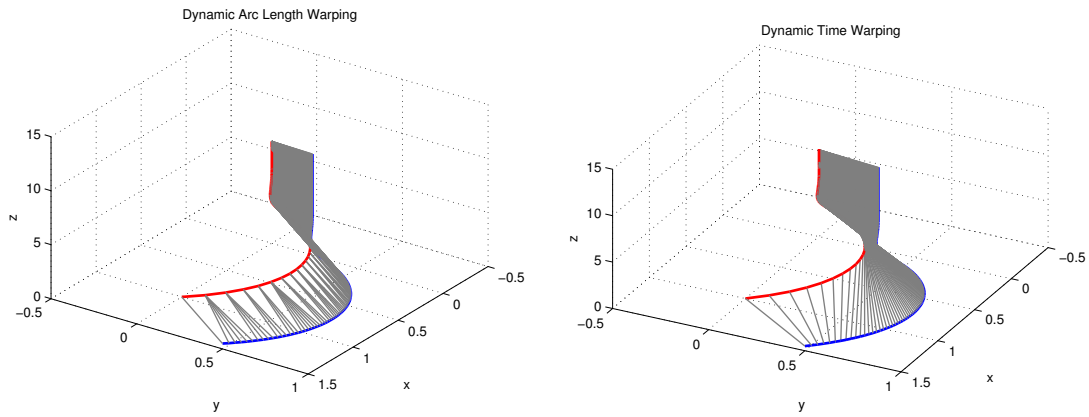

(a) Dynamic Arc Length Warping (*DALW*). (b) Multi Dimensional- Dynamic Time Warping (*MD-DTW*).

Figure 3-5: Comparison: Arc Length Warping and Time Warping.

DALW	MD-DTW
60.25	61.86

Figure 3-6: DALW and MD-DTW distances for trajectories shown in Figure **3-5**

3.5. Experimental Position Data Analysis

In the previous section, the proposed technique has been tested with 3D artificial trajectories obtaining not only efficient quantitative results but also qualitative results compared to other techniques such as Multi-Dimensional Dynamic Time Warping MD-DTW [21]. The aim of this section is to perform a validation of this algorithm using real generic human hand gestures and real surgical gestures based on position data.

3.5.1. Filtering Trajectories

A low-pass filter without phase shift and without magnitude distortion is applied to the 3D measurements to reduce the noise. This low-pass filter is easily implemented using a non-causal zero-phase digital filter by processing the input data with an IIR low-pass Butterworth filter in both the forward and reverse direction using a 'filtfilt' procedure from Matlab.

The cut-off frequency ω_c of the low-pass filter is chosen to avoid any distortion of magnitude on the filtered signals within the bandwidth of the gestures. It has been determined experimentally by analyzing the Fast Fourier Transform (FFT) of each component of the gesture. Using this analysis, one can then calculate the frequency for which the magnitude values is

less than 15 % of the maximum (see Figure **3-7**). By obtaining the maximum value of these frequencies one can make sure that important information is not missing in any coordinate. It is noteworthy that, in practice for a real-time application robust filtering techniques could be used [73, 74].

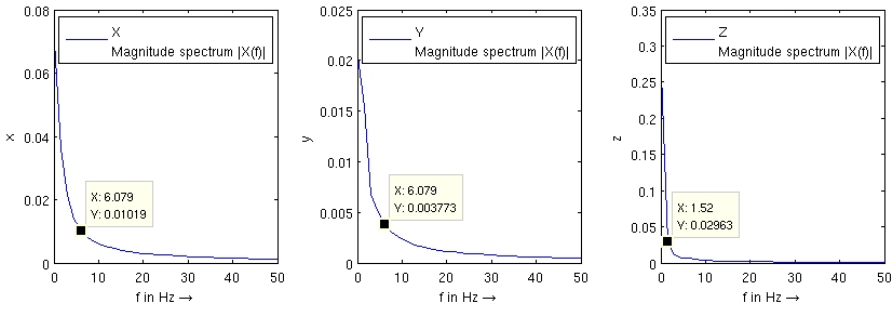

Figure 3-7: Example: Fourier transform of each coordinate.

3.5.2. Gesture Comparison Using an Exoskeleton

To test this new approach, simple gestures were studied. The position measurements of each gesture were recorded using an exoskeleton of the upper extremity [90]. It has four degrees of freedom achieved using four links and four actuated revolute joints:

- The shoulder abduction/adduction;
- The shoulder flexion/ extension;
- The shoulder internal/ external rotation;
- The elbow flexion/ extension.

Figure **3-8** shows the exoskeleton used and its kinematic model. The exoskeleton's links are essentially made of aluminum and plastic components and steel is present in motors and joints areas. The user's arm is fixed to the exoskeleton using an external arm and wrist holders using internal pneumatic holders (Figure **3-9**). A safe workspace for the user is guaranteed by limiting the motion range using mechanical stoppers in joints. Range values are shown in Table **3-1**.

Different people can use this exoskeleton due to its adaptability. DC motors are used in order to adjust the shoulder height and width and the upper arm length. In the same way, mechanical gliders are used to modify the forearm length, and the arm holder and wrist holder positions.

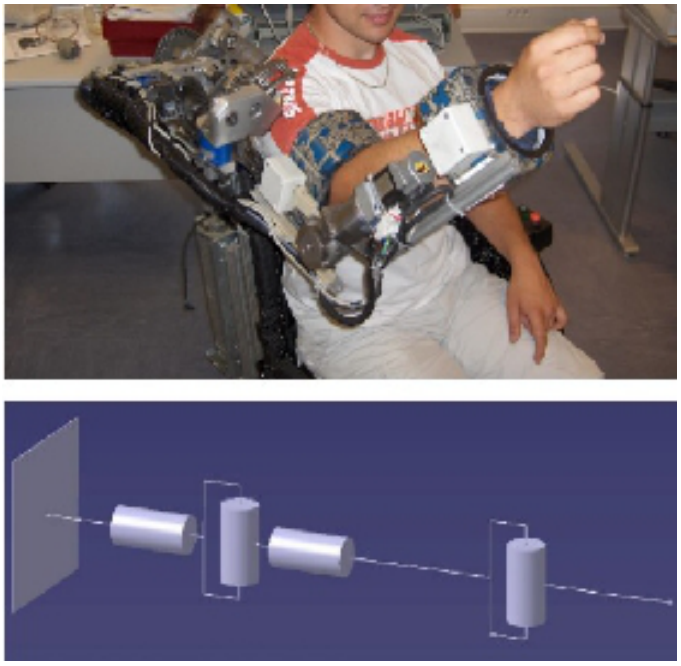

Figure 3-8: The upper extremity exoskeleton with its 4 four active degrees of freedom.

Table 3-1: Joints characteristics

	Shoulder abduction/ adduction	**Shoulder flexion/ extension**	**Shoulder external/ internal rotation**	**Elbow extension/ flexion**
Arm's Range (°)	- 180 → 0	-140 → 90	- 110 → 80	0 → 145
Exoskeleton's Range	- 90 → 0	-90 → 0	- 80 → 15	0 → 135

For these experiments, a total of 10 subjects were involved. They were asked to do two kind of gestures (10 times each) with their right arm (all subjects are right handed). The first one was a communication gesture as the subject wanted to say stop to someone running towards him/her. The second one was a simple gesture where the subject had to place his/her hand as there was a wall in front of him/her. These gestures were chosen because they were quite similar from a kinematic viewpoint. Figure **3-10** shows one example of position values for each gesture. This figure represents the trajectories of a subject's wrist.

To avoid any disturbances for the subjects during the experiment, a gravity compensation technique was used to give the illusion the exoskeleton had no weight [89]. Using this exoskeleton, we were able to record precisely the displacement of the subject's right arm and

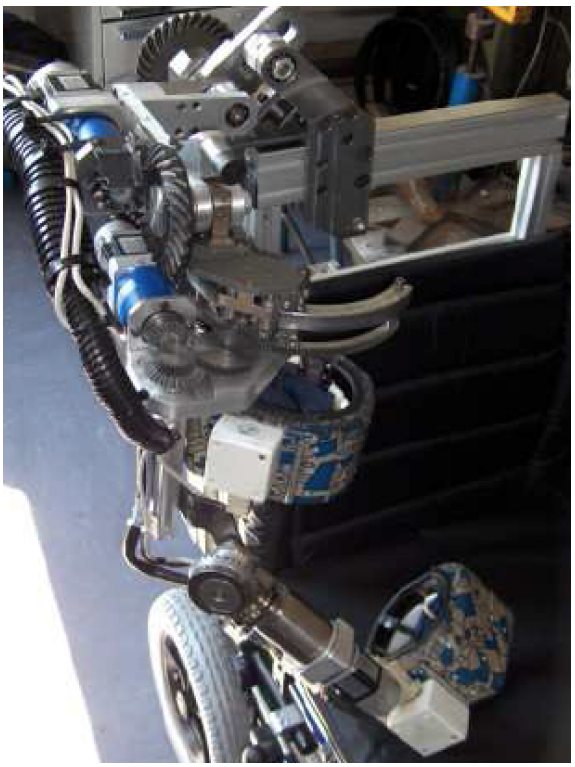

Figure 3-9: The upper extremity exoskeleton.

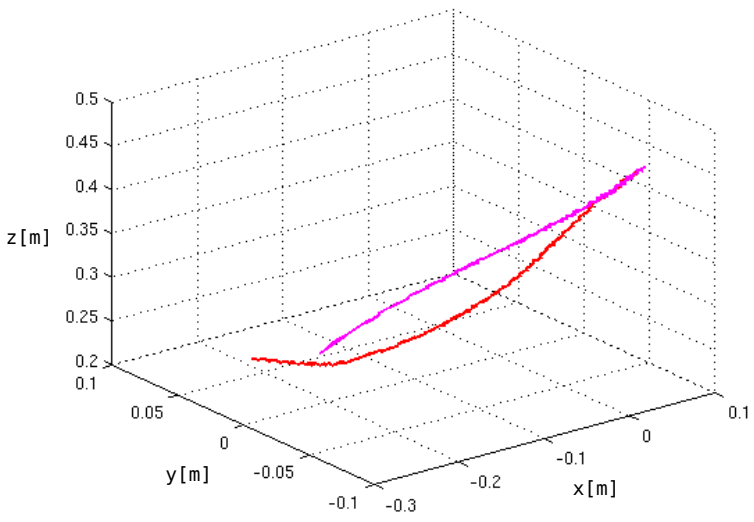

Figure 3-10: An example of position values for both gestures.

to eventually decompose the gestures in different anatomic planes for further studies on the different human joints. After the acquisition process of the position values, a filtering stage

was used based on Section 3.5.1. The different trajectories were aligned according to four different analysis (Table **3-2**).

Table 3-2: Different Experiments.

Nature of Gestures	**Carried out by**
Similar	Same person
	Different people
Different	Same person
	Different people

The **DALW** and **DTW** distance are computed with position data according to these four criteria. The results of DALW and DTW distance values and their deviations for each experiment with the position data can be seen in Figure **3-11**. The results show the similarity measurements between each pair of trajectories based in the proposed analysis in Table **3-2**. Figure **3-11** shows the distances obtained with both algorithms (DALW and DTW). One can distinguish similar and different gestures regardless of whether these trajectories were performed by one person or by different people.

In particular, the deviations obtained with the DALW algorithm are smaller than those obtained with the DTW algorithm in most cases. This result shows it is possible to achieve an accurate way to differentiate the various gestures suggested by this experimental setup. Figure 4 shows also that since the trajectories of each gesture are closely bounded to the people who execute them, it is possible to get small distances for the experiment involving different gestures carried out by the same person compared to the experiment involving similar gestures carried out by different people.

3.5.3. Gesture Comparison Using an Instrumented Laparoscopic Device

In this section, surgical gestures were evaluated on a laparoscopic training system. An instrument prototype, shown in Figure **3-12**, with a Yaw-Roll actuated tip was used to record several trajectories.

The handle and shaft orientations are decoupled with a free ball joint to improve the ergonomic performance. This configuration allows to explore the whole intra-abdominal workspace and to avoid excessive wrist flexion or deviation. The robotic instrument configuration used was the Standard Fixed Handle Configuration where the joints were locked in their central

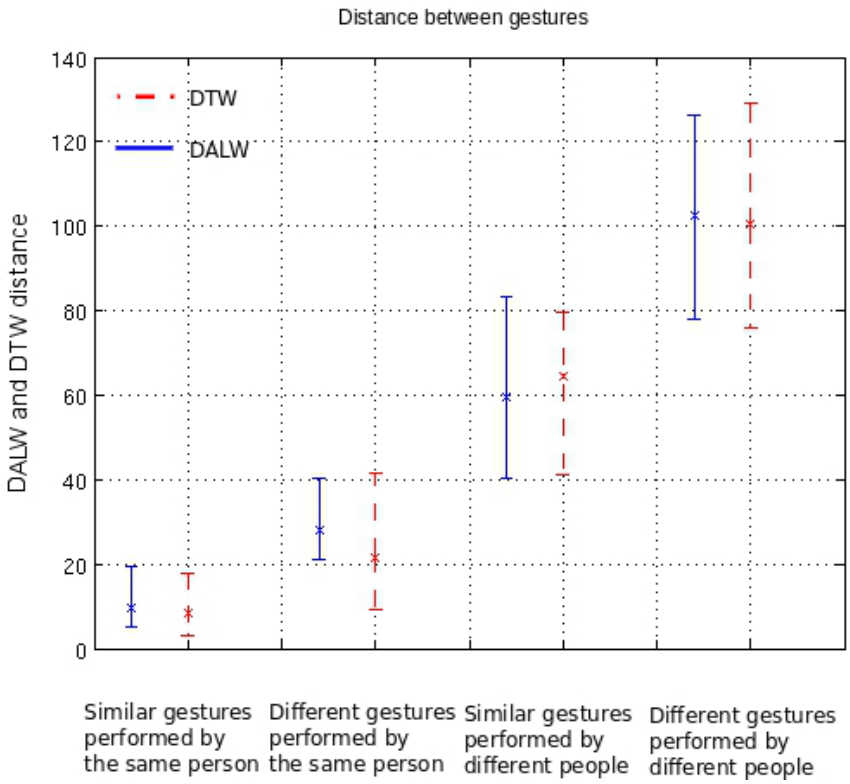

Figure 3-11: DALW and DTW distance computed with position data from exoskeleton.

position [53].

This training system allows to set up a representative configuration of a real surgery where the instrument motions remained confined in a small region of the intra-abdominal workspace. Five people with no experience participated in the experiments and five repetitions were completed in this configuration for a pick-and-place task. Each experiment took one of the five specific positions in the virtual abdomen to cover the whole workspace (Figure **3-13**) with 4 repetitions for each trajectory. The **DALW** and **DTW** distances are computed based on the previous configuration. The results of DALW and DTW distance values and their deviations for each classification can be seen on Figure **3-14**.

Results obtained with surgical gestures are quite different compared with the generic gestures (Section 3.5.2), obtained with the exoskeleton. In this case, the trajectories analyzed for each task are pretty different no matter who perform them. This means that the distances obtained for the experiments performed with different gestures by the same person are higher than for the experiments performed with the same gesture by different people, in contrast with the results shown in Figure **3-11** when using a exoskeleton.

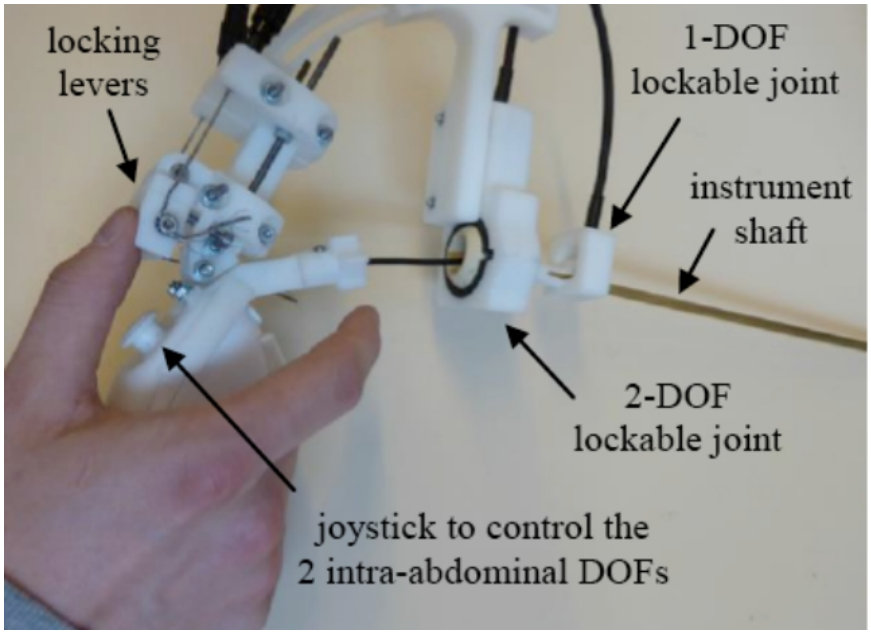

Figure 3-12: Laparoscopic Device.

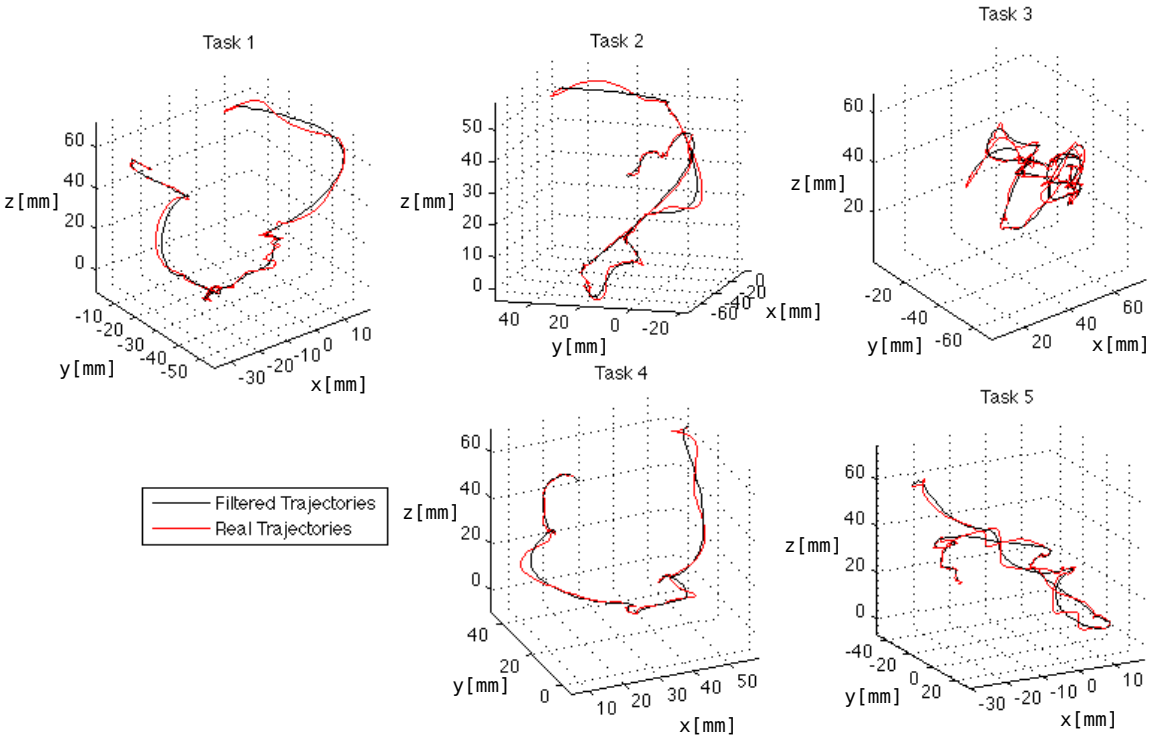

Figure 3-13: Position on different surgical gestures using laparoscopic device.

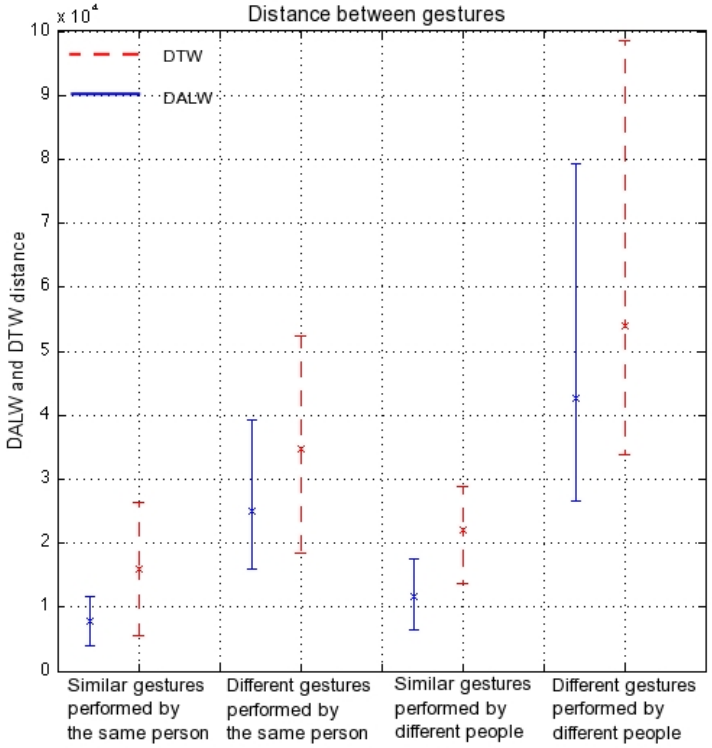

Figure 3-14: DALW and DTW distances computed with position data from laparoscopic device.

The experimental results show the distance computed with the DALW algorithm leads to an easier classification of the experiments involving different gestures than different people. Also, in Figure **3-14**, it is possible to observe that DALW distances have a lower deviation than DTW distances, allowing to distinguish more easily the different groups of experiments.

3.5.4. Gesture Comparison Using an Obstetrical Forceps

In this section, an analysis of several data sets, acquired by an instrumented obstetrical forceps coupled with the BirthSIM simulator, is presented (Figure **3-17**). With this device, a medical practitioner can make a transvaginal assessment diagnosis. The BirthSIM simulator consists of anthropomorphic models of the maternal pelvis and the fetal head. The forceps, on the other hand, allows to measure displacements inside the pelvis. Parts of the system and its functioning are described in Figure **3-15**.

In general, the system is composed by three important parts:

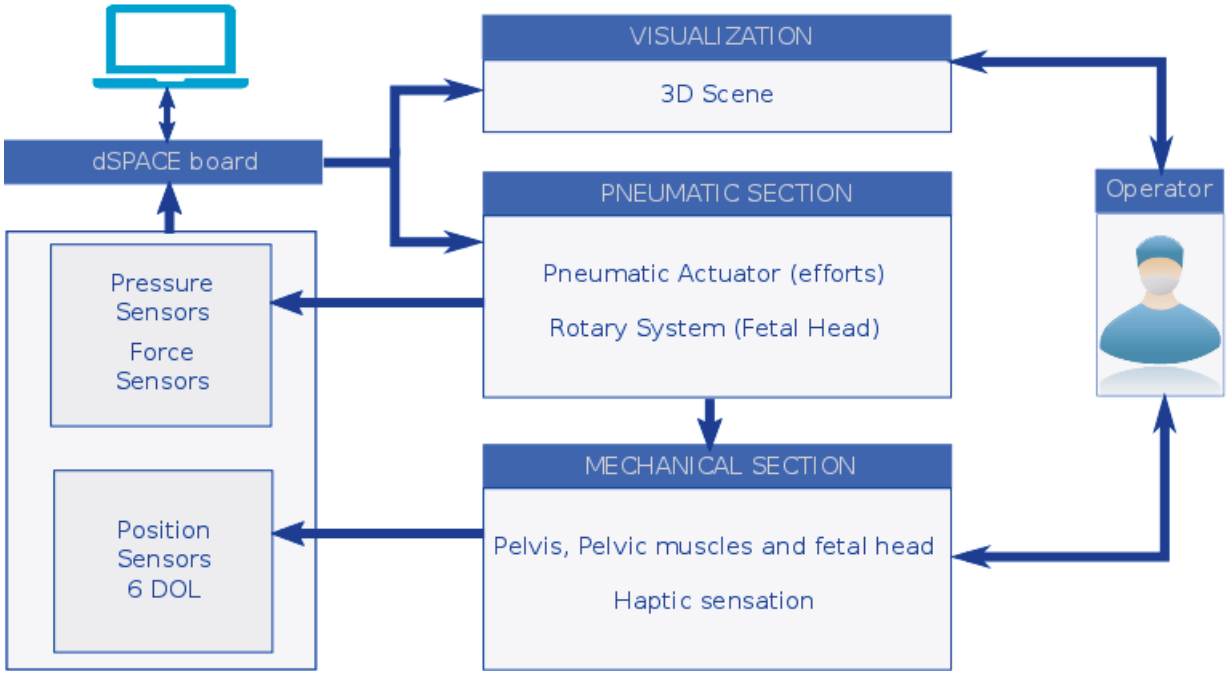

Figure 3-15: Functioning and parts of the BirthSIM simulator.

- **A mechanical segment:** It establishes the anthropomorphism of the simulator. BirthSIM includes the main anatomical parts such as: the ischial spines, coccyx, sacrum and pubis (Figure **3-16**). The fetal head, on the other hand, was rebuilt from MRI images provided by the hospital in order to reproduce the anatomy and, additionally, an skull was built by rapid prototyping to improve the haptic sensation. The fetal head has been installed at the end of a pneumatic cylinder representing the fetal back in order to reproduce the movements of the head. The flexion/extension movements of the head are reproduced by a pivot mounted between the head and the cylinder. This pivot connection provides range of motion of 75° in extension and 45° flexion. Lateral flexion is ensured using another pivot with an amplitude of 40°.

- **An electro-pneumatic actuator:** The electro-pneumatic part consists of a pneumatic cylinder with an instrumented servo valve. The objective of this cylinder is to locate the fetal head automatically by a certain level of presentation and to reproduce the different types of effort (resistive efforts of the pelvic muscles, involuntary and voluntary efforts (FEA and FEV) produced by the pregnant woman). The servo valve used is manufactured by FESTO with reference MPYE-5-M5-010B and the actuator used is a double acting cylinder with a single rod.

- **Visualization:** This section is available for the instructor and for the user (if necessary) in order to check several parameters (level of presentation of the fetal head, forceps position on the fetal head and involuntary and voluntary effort of the pregnant woman).

Figure 3-16: The maternal pelvis provided by BirthSIM.

Specifically, users can see, on a screen, the position of their obstetric instruments in real time relative to the fetal head and maternal pelvis .

The system is instrumented with electromagnetic sensors, with 6 Degrees of Freedom, that can track masked objects. In order to avoid interference in the device, the forceps includes nonmagnetic material [88].

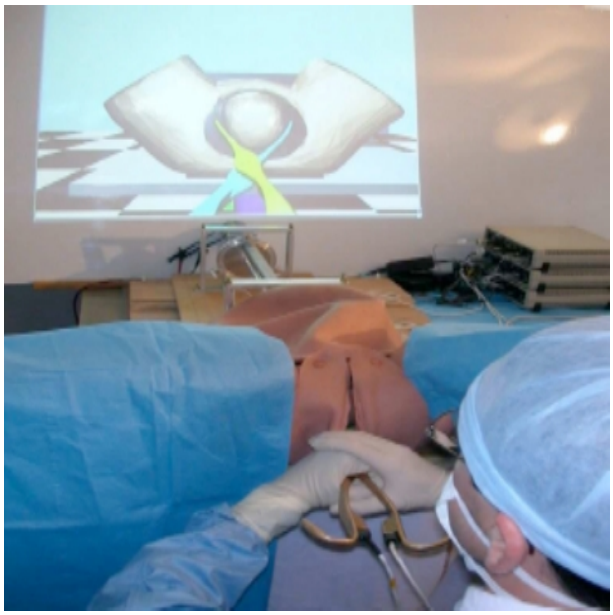

Figure 3-17: Obstetrical Forceps.

The numerical values of position errors in this system are summarized in Table **3-3**.

Table 3-3: Tolerance for position measurements

Axes	Tolerance - Position [mm]	Tolerance - Orientation [deg]
X	0.119	0.0685
Y	0.2234	0.0437
Z	0.2234	0.0451

In the experiments, six obstetric students were asked to perform 30 forceps blade placements providing for each trainee 60 trajectories: 30 left blade trajectories and 30 right blade trajectories. The forceps placements are carried out in two different sessions of 15 forceps blade placements (Figure **3-18**). In each trajectory, the fetal head is positioned according to the ACOG (American College of Obstetrics and Gynecology) classification [26] on an outlet OA+4 presentation (Occiput Anterior location and station +4cm from the ischial spines plan).

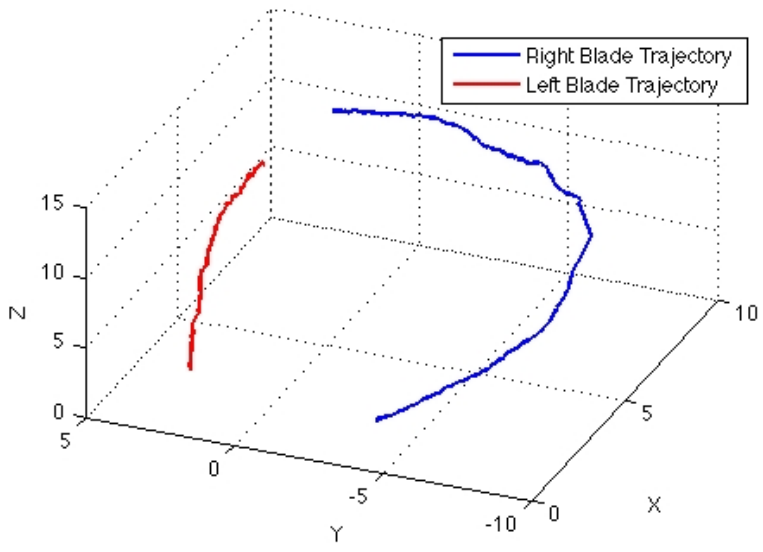

Figure 3-18: Left and right blade trajectories.

After the acquisition process, a low-pass filter is tuned and implemented based on the approach described in Section 3.5.1. Subsequently, DTW and DALW distances are calculated for each pair of paths according to the experiments described in Table **3-2**. The results of DALW and DTW distances for each experiment can be seen on Figure **3-19**.

Results are similar to those obtained with laparoscopic data (Section 3.5.3). Distance values for the experiment performed by the same person with different gestures are higher than for

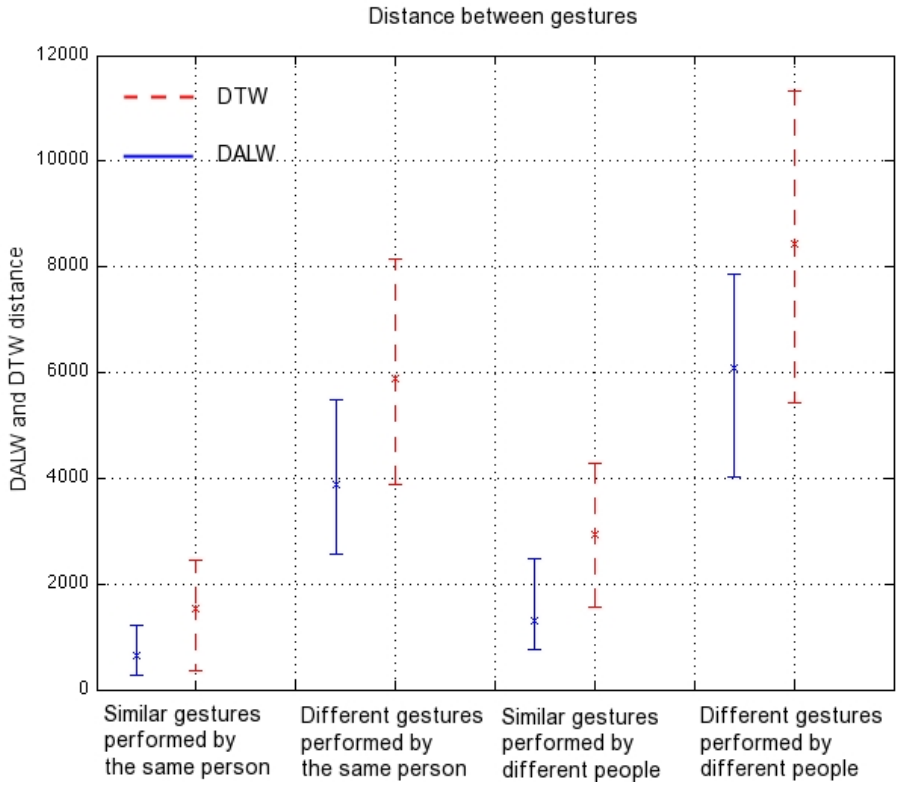

Figure 3-19: DALW and DTW distances computed with position data from BirthSIM device.

the experiment performed by different people for the same gesture. This result is obtained because the gestures analyzed are quite different compared to the variation obtained between different people. For this reason, two groups are easy to classify: those that involve similar gestures and those that involve different gestures. One can also see that the deviation for the two algorithms is smaller than for the experiments performed with the laparoscopic device. This is mainly due to the amount of gestures available for the two analysis. Finally, as in the previous sections, DALW distance allows a better classification of the experiments compared with DTW distance.

3.6. Hand Gesture Analysis Using Quaternions

In tracking 3D objects, full localization can be achieved not only with position information but also with their orientation information. Specifically, quaternions have been widely used to represent these kind of data. In [20], normalized quaternions are used to obtain a kinematic model that describes the relative orientation between the reference frames of a link-mounted sensor and the link on a robot manipulator. In addition, this mathematical tool have been used to model the hand-orientation errors in the control of manipulators

[139]. The importance of this formulation lies in their simplicity to analyse stability of the orientation error dynamics. These advantages haven been so considerable that, some authors have used this representation to design controllers in the task-space tracking field for robot manipulators [135, 24].

Particularly, for the evaluation of medical gestures, the orientation of the tip of the instrument is essential to determine how tissues are manipulated in a surgical procedure. In [87], obstetrical gestures orientation are expressed in the quaternion unit space in order to compute and compare the quaternions curvature. The quantitative results present a method to objectively assess gestures.

In this section, we use a quaternion representation of the angles to classify a gesture. Based on the results obtained in Section 3.5, Dynamic Arc-Length Warping (DALW) was implemented, in order to perform a comparison between different hand gestures.

3.6.1. Orientation Data and Quaternions

Multi-dimensional temporal series are data sets with multiple measurements made simultaneously that varies over time. They are typically a vector of feature values for each time occurrence. In this section, we carry out an analysis of orientation data of the wrist produced by an exoskeleton measuring exactly the orientation information in real-time.

Most of works on gesture recognition are focused only on the analysis of position values. Orientations, on the other hand, have not been widely evaluated due mostly to their representation dependency. In the following paragraphs, a quaternion representation will be described and its advantages in this field will be exposed by comparing with the results using euler angles.

Orientation of an object in three-dimensional space can be parametrized using quaternions. This element is conformed by a 4-tuple obtained from the sum:

$$\mathbb{Q} = q_0 + q, \tag{3-15}$$

where q_0 is called the scalar part and q is called the vector part of the quaternion. Defined in this way, a general expression for these elements is given by [65]:

$$\mathbb{Q} = a + i \cdot b + j \cdot c + k \cdot d, \tag{3-16}$$

where $a, b, c, d \in \mathbb{R}$ are scalars and i, j, k are different imaginary units.

A rotation can be described based on the rotation axis L, its unit vector $l = [l_x, l_y, l_z]^T$ and the rotation angle ϕ with the unit quaternion as described by:

$$\mathbf{Q} = \cos\frac{\phi}{2} + i.l_x \sin\frac{\phi}{2} + j.l_y \sin\frac{\phi}{2} + k.l_z \sin\frac{\phi}{2}. \tag{3-17}$$

Figure **3-20** shows a quaternion where α, β and γ represent the orientations of a unit vector $\mathbf{n}$ that lies in the axis of rotation.

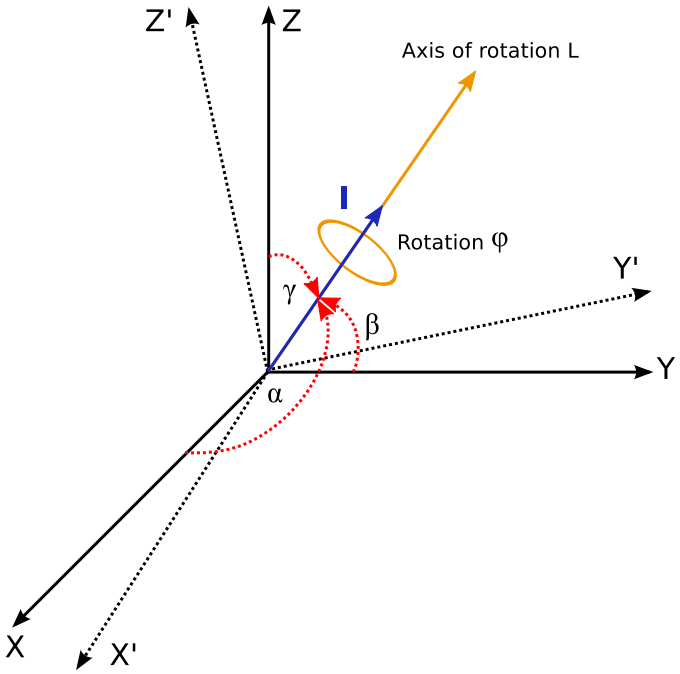

Figure 3-20: Quaternion Representation

The main advantage of quaternion is that its representation is independent of a central coordinate system which avoids singular situations such as the so called *gimbal lock* for Euler angles. A quaternion is also more compact and faster than the traditional matrix representations. One can calculate a quaternion based on orientation measurements using the following expression [46]:

$$\mathbf{Q} = \begin{bmatrix} \cos(\alpha/2)\cos(\beta/2)\cos(\gamma/2) + \sin(\alpha/2)\sin(\beta/2)\sin(\gamma/2) \\ \sin(\alpha/2)\cos(\beta/2)\cos(\gamma/2) - \cos(\alpha/2)\sin(\beta/2)\sin(\gamma/2) \\ \cos(\alpha/2)\sin(\beta/2)\cos(\gamma/2) + \sin(\alpha/2)\cos(\beta/2)\sin(\gamma/2) \\ \cos(\alpha/2)\cos(\beta/2)\sin(\gamma/2) - \sin(\alpha/2)\sin(\beta/2)\sin(\gamma/2) \end{bmatrix}, \tag{3-18}$$

where α, β and γ are the angles around the axes x, y and z.

3.6.2. Experimental Results

Algorithm described in section 3.3 was implemented. In particular, DALW distances were computed for orientation data using the euclidean norm as a local distance between each pair of points. The DALW distances using quaternions, in turn, have a modification: instead using Euclidean norm, distances between two succesive quaternions (Q_1 and Q_2) were computed as follows:

$$d(\mathbf{Q}_1, \mathbf{Q}_2) = 1 - \langle \mathbf{Q}_1, \mathbf{Q}_2 \rangle^2, \tag{3-19}$$

where $\langle \mathbf{Q}_1, \mathbf{Q}_2 \rangle$ denotes the inner product between the two quaternions and each quaternion ($\mathbf{Q}_1$ and $\mathbf{Q}_2$) is a unit quaternion that satisfies:

$$a^2 + b^2 + c^2 + d^2 = 1. \tag{3-20}$$

To test our method, simple gestures were studied. The orientation measurement for each gesture were recorded using an exoskeleton device described in [89]. Figure **3-8** shows the exoskeleton used and its kinematic model. This device has four degrees of freedom: three for the shoulder (internal-external rotation, abduction-adduction, flexion- extension) and one for the elbow (flexion-extension).

A total of 12 subjects were involved in this study. They were asked to do two kinds of gesture (10 times each) with their right arm (all subjects are right handed). The first one was a communication gesture as the subject wanted to say stop to someone running towards him. The second one was a simple gesture where the subject had to place their hand on a wall in front of them. Figure **3-21** represents an example of the average values of orientation trajectories of a subject's wrist.

The DALW distance is computed with orientation data and with the corresponding quaternion according to these four criteria. The results of DALW distance values and the standard deviations for each experiment can be seen in Figure **3-22**.

As one can see in Figure **3-22**, the DALW distance values obtained with quaternion differentiate clearly the different sets of experiments allowing a classification of the gestures. Clearly, the distance measured is higher for the experiment which involves different gestures performed by different people and lower for the experiment which compares similar gestures performed by the same person. Likewise, this similarity measure allows to differentiate the experiments involving different gestures performed by the same person or by different people. Also, it is clear that the DALW algorithm with quaternion leads to smaller standard deviations compared to the DALW algorithm with the angular orientation data allowing obtain data sets more clustered that facilitate the classification stage. The results obtained

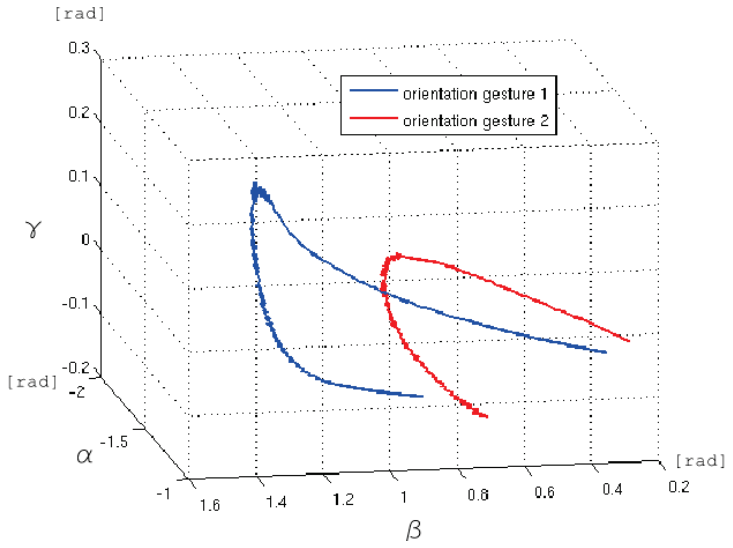

Figure 3-21: An example of orientation of the wrist.

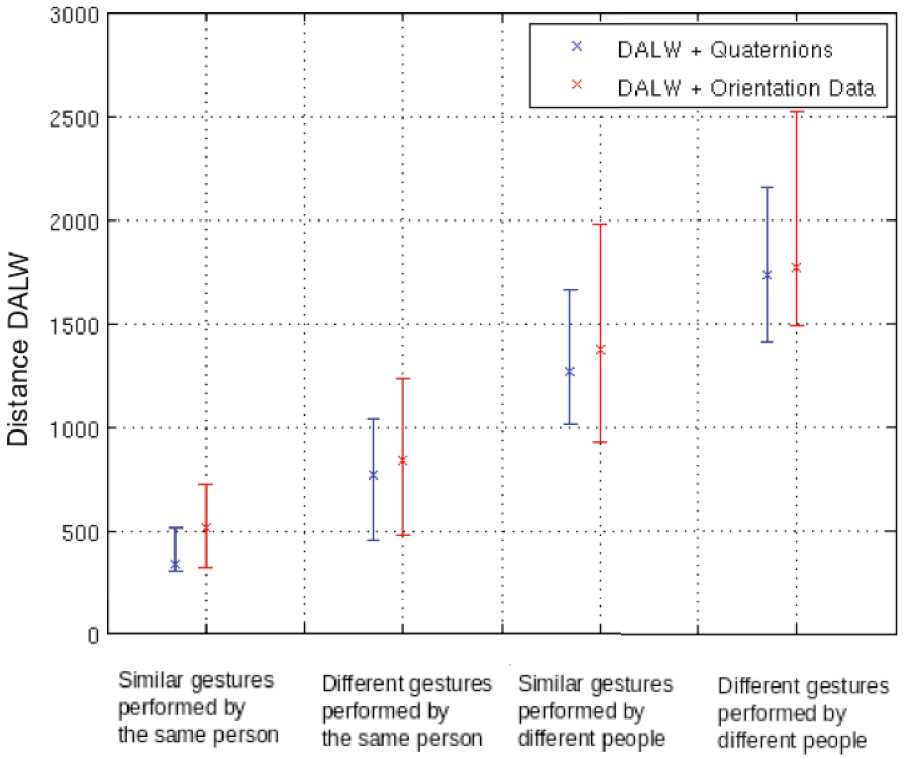

Figure 3-22: DALW Distance found with quaternions and orientation data.

in this work allow to take into account the quaternion information from angular orientation data and the Dynamic Arc-Length Warping algorithm as an appropriate tool for the hand human gesture recognition.

3.7. Conclusion

In sections 3.1, 3.2 and 3.3, a method based on a cumulative arc-length parametrization was proposed in order to distinguish different generic gestures. The study included several gestures that were performed repeatedly by different subjects; these data sets were acquired, also, with three different devices. The results suggest that different gestures can be distinguished on the basis of position measurements alone. The main contributions include the possibility to compare similar trajectories performed at different speeds using cumulative arc-length warping and curvature to guaranty invariance to the location of the sensor coordinate system. Based on these results, this new algorithm is proposed as an efficient alternative to surgical gesture classification.

In Section 3.5, we have presented the proposed approach method (Dynamic Arc-Length Warping algorithm) using a quaternion representation of data to perform gesture classification. An experimental study was carried out for two different kinds of gestures to validate our approach. The results show also that the distances obtained with a quaternion representation lead to a standard deviation lower than those obtained with angular orientation data. Furthermore, the higher standard deviations while using the angular orientation data are greater for the comparison between different groups of experiments. The similarity measure obtained between the different sets of data allows to develop a relevant classification of human gestures. However, limitations for this last approach are focused on the acquisition system of data, only one of the devices exposed in this chapter has the possibility to acquire orientation data.

4 Medical Gestures Classification Using Equi-Affine Speed and Mechanical Ernergy Calculation

In this chapter, we are interested in finding the similarities and differences among different surgical gestures. So far, most of the works are developed to know what kind of variables (spatial or temporal) should be used to perform the classification. In all the cases, the variables involved should be related with both kinematic and dynamic aspects of trajectories generation. Some early studies have suggested that the CNS (Central Nervous System) associates representations for the movement based on geometrical and temporal attributes instead of motor execution or muscle activation [41, 114]. In particular, during drawing movements, humans tend to decrease the instantaneous tangential velocity of their hands at the same time the motion curvature increases and similarly, the velocity increases when the trajectory becomes straight [86, 2]. This relationship has been shown to be well adapted using a two-third power law, an empirical law that shows the correlation between local geometry and kinematics of human hand motion in planar drawing trajectories [68, 98].

However, if planar drawing movements follow this power law it does not imply that it is an explicit relationship for every human movement planned by the Central Nervous System (CNS). In any case, it has been generalized for some types of human movements and also for motion perception and prediction [30]. In [33], the two-third power law is applied to the smooth pursuit motion of eye, specifically controlled by distinct neural motor structures and a particular set of muscles. Whereas Vieilledent *et. al* have studied some curved locomotor trajectories with the hypothesis that, also during locomotion, movements obey this relationship [125]. Another important result in this field is related to the affine velocity of each trajectory. Pollick *et al.* show that if instead of computing the Euclidean speed, the affine velocity is calculated, then the unique function that involves the curvature and generates an affine invariant velocity is specifically the two-third power law [98]. It means that the hand writing trajectories implies motion at constant affine velocity. This fact shows that the power law and kinematic aspects of movement can be described by observing the affine space instead of the Euclidean one [50]. Specifically, in vision machine field, affine transformations are deals with rotation, translation, and posterior parallel projection of a planar object into the camera. Actually, affine concepts have been applied to the analysis of image motion and

to the perception of 3-D structure from motion in [38, 99, 11].

Furthermore, it was demonstrated that the two-third power law is not sufficient to explain general 3D drawing movements. Experimental results suggest that the movement at constant affine velocity is indeed the main principle and the two-third power law could be a special case. In this way, a new power law (one-sixth power law) has been proposed to facilitate the description of spatial drawing movements [79, 100]. Based in these results, it was demonstrated, that for the limited case of 3D scribbling movements, the one-sixth power law explains the data better than the two-third power law.

In this chapter, an analysis of the affine velocity on medical gestures is presented. Constant affine velocity is demonstrated for this kind of hand human gestures and the histogram behavior for each gesture, is presented. Additionally, some modifications of the power law's exponents across two different gestures are described. However, averaging over all subjects and gestures, the power law exponents are generally in accordance with constant spatial affine velocity. Finally, gesture classification is obtained on more complex trajectories, based on an affine velocity segmentation and a mechanical energy analysis.

4.1. Two-Third and One-Sixth Power Law

A 2D trajectory can be described as the movement performed by a point $p \in [0, 1]$ on the plane. Each value of p generates values in the curve $r(p) = [x(p), y(p)] \in R^2$. The velocity associated is represented by the tangent vector T. Based on the parametrization chosen, velocities can be different but still represent the same trajectory, such as the euclidean or the affine velocity (Figure **4-1**).

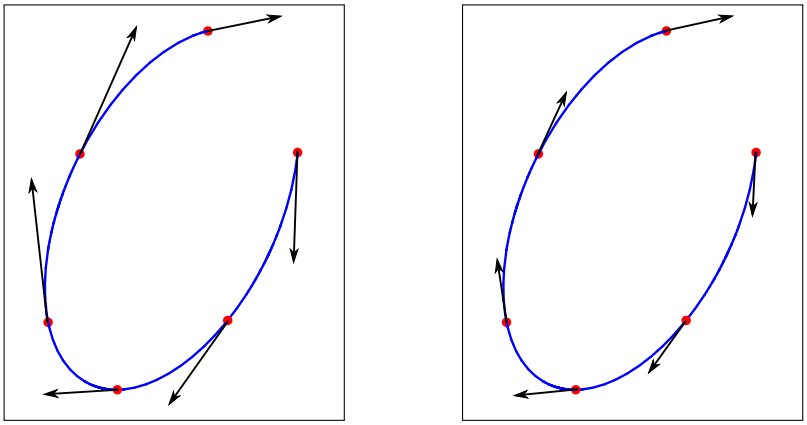

(a) (b)

Figure 4-1: Geometry of a 2D trajectory.

In particular, in figure **4-2** trajectories (a) and (b) show euclidean transformations and (a) and (c) describe affine transformations. While, in (a) and (b) the euclidean distance between p_1 and p_2 is preserved , in (a) and (c) the affine one is preserved. The two third power law will show that the time spent to arrive from p_1 and p_2 is the same for both curves if they are related by affine transformations. This particular law is going to be explained more in details in this section.

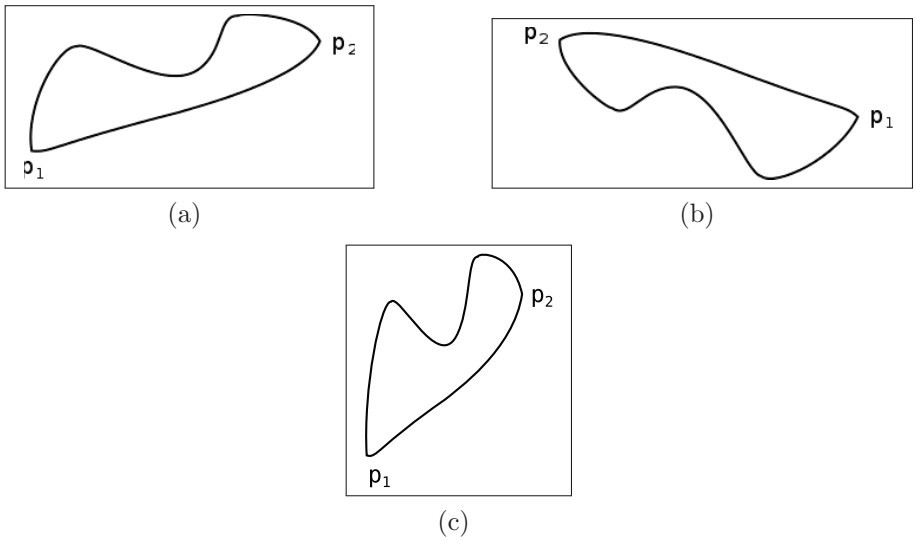

Figure 4-2: Curves related by Euclidean and Affine transformations.

The inverse relationship between modulus of the Euclidean velocity v and curvature κ during planar drawing hand trajectories is defined by the two-third power law (4-1):

$$v = \alpha\kappa^{-\frac{1}{3}}, \tag{4-1}$$

where v and κ are defined for a planar motion by:

$$v = \sqrt{\dot{x}^2 + \dot{y}^2} \quad \text{and} \quad \kappa = \frac{|\dot{x}\ddot{y} - \ddot{x}\dot{y}|}{(\dot{x}^2 + \dot{y}^2)^{\frac{3}{2}}}, \tag{4-2}$$

and where α is a gain factor. In this case, $\dot{x}, \dot{y}$ and $\ddot{x}, \ddot{y}$ are the first and second derivatives of x, y relative to time. Previous works have demonstrated that in drawing movements, the gain factor α is approximately constant for simple elliptical shapes, but is piecewise constant for more complex shapes [126, 127].

Meanwhile, the affine velocity v_a for planar motion is defined by:

$$v_a = |\dot{x}\ddot{y} - \dot{y}\ddot{x}|^{\frac{1}{3}}. \tag{4-3}$$

This equation describes the cube root of the signed area of the parallelogram created by the instantaneous first and second position derivative of the trajectory with respect to time. With some algebraic manipulations of (4-2) and (4-3), it is possible to express the Euclidean Velocity as :

$$v = v_a \kappa^{-1/3}. \tag{4-4}$$

If (4-4) is compared with (4-1), one can conclude that motion with constant affine velocity is equivalent to motion that obeys the two-third power law. If one performs the same transformation, one can obtain the equations that describe motion in drawing trajectories. Formally, for a trajectory v, κ, and the torsion τ are defined by:

$$v = \sqrt{\dot{x}^2 + \dot{y}^2 + \dot{z}^2}, \tag{4-5}$$

$$\kappa = \frac{\sqrt{(\ddot{z}\dot{y} - \ddot{y}\dot{z})^2 + (\ddot{x}\dot{z} - \ddot{z}\dot{x})^2 + (\ddot{y}\dot{x} - \ddot{x}\dot{y})^2}}{(\dot{x}^2 + \dot{y}^2 + \dot{z}^2)^{\frac{3}{2}}}, \tag{4-6}$$

$$\tau = \frac{|\frac{dr}{dt}, \frac{d^2r}{dt^2}, \frac{d^3r}{dt^3}|}{||\frac{dr}{dt} \times \frac{d^2r}{dt^2}||}, \tag{4-7}$$

where $||\bullet||$ and $\times$ denote vector magnitude and cross product, respectively. Spatial affine transformations preserve the volume (rather than area) enclosed by the shape. Then, the spatial affine velocity at any point is defined in terms of the volume of the parallelepiped defined by the first, second, and third-derivative at that point is defined by:

$$v_a = \left|\frac{dr}{dt}, \frac{d^2r}{dt^2}, \frac{d^3r}{dt^3}\right|^{\frac{1}{6}}, \tag{4-8}$$

where $|\bullet|$ denotes the scalar triple product. Using some algebraic manipulations of (4-5), (4-6) , (4-7), and (4-8), it is possible to prove that spatial motion at constant affine velocity entails the one-sixth power law as following:

$$v = v_a(\kappa^2|\tau|)^{-\frac{1}{6}} = v_a \kappa^{-1/3}|\tau|^{-1/6}. \tag{4-9}$$

4.2. Obstetrical Gestures

An analysis of several data sets, acquired by an instrumented obstetrical forceps coupled with the BirthSIM simulator, is presented in Section 3.5.4. In the experiments, six obstetrical residents were asked to perform 30 forceps blade placements providing for each trainee 60 trajectories: 30 left blade trajectories and 30 right blade trajectories. The forceps placements are carried out in two different sessions of 15 forceps blade placements (Figure. **3-18**). In

each trajectory, the fetal head is positioned according to the ACOG (American College of Obstetrics and Gynecology) classification on an outlet LOA+5 presentation (Left Occiput Anterior location and station +5cm from the ischial spines plan).

4.2.1. Linear Regression

The position data were interpolated using a cubic splines to calculate the different derivatives with smoother trajectories. Based on the splines computation, variables such as affine velocity v_a, curvature κ, and torsion τ were calculated using their analytical derivatives. In order to avoid singularities when the torsion is zero, a threshold was used in the different calculations (5 % on the value of absolute torsion).

Several simulations were performed in order to examine if the relationship between the velocity, curvature, and absolute value of torsion could represent the obstetrical gestures. Fig. **4-3** presents some examples of the correlation found between $x = k^{\frac{1}{3}}|\tau|^{-1/6}$ and the norm of the Euclidean velocity y using a least square fitting technique.

Linear least squares approach is used to fit the data with a model of the form:

$$y \simeq \theta_0 + \theta_1 x. \tag{4-10}$$

Where θ is the vector composed by the coefficients associated to the $y-$intercept and the slope of the straight line ($\theta_0 = b$ and $\theta_1 = m$) and (x, y) are values for $k^{\frac{1}{3}}|\tau|^{-1/6}$ and $|v|$ respectively. The residuals (defined as the differences between the observations and the model) are:

$$r_i = y_i - (\theta_0 + \theta_1 x_i), \quad i = 1, ..., m, \tag{4-11}$$

where m is the number of samples. In order to make the residuals as small as possible, sum of the squares of the residuals is minimized:

$$||r||^2 = \sum_{1}^{m} r_i^2 \tag{4-12}$$

In particular, the Moore-Penrose pseudoinverse is used to solve the linear least square problems, taking into account that this mathematical tool provides the minimization in this way:

$$\theta = w^+ y, \tag{4-13}$$

where $w = [1 \;\; x]$ and w^+ is the pseudoinverse of w:

$$w^+ = (w^T w)^{-1} w^T \tag{4-14}$$

These results show that there is a proportional relationship between both quantities (v and $k^{\frac{1}{3}}|\tau|^{-1/6}$), taking into account that θ_0 or the $y-$intercept is close to 0 (0.0582 in average). That means that obstetrical gestures, like scribbling movements, are also governed by the one-sixth law. In order to analyze the variance found in each linear regression, a histogram that describe the distance between the straight line and each sample was computed for each gesture. Figure **4-4** represents the histogram that describes the results for the gesture with an average variance. Due to the data variance has a similar behavior than a Gaussian one, then a Gaussian density function was fitted to the samples. In this way, blue line shows the functions fitted to these results and finally, red lines ilustrate the gaussian functions calculated for gestures with maximum and minimum variance.

Due to the data variance has a similar behavior than a Gaussian one, then a Gaussian density function was fitted to the results. Fig. **4-4** shows the results calculated for a sample data set acquired from the experiments. Despite the fact that the left gesture is easier than the right one (less complex and less rotation), the dispersion is higher than the right one. This is due to the fact that the left hand is the less skillful hand for the people involved in the experiments. However the maximum dispersion to the linear regression is similar for both gestures.

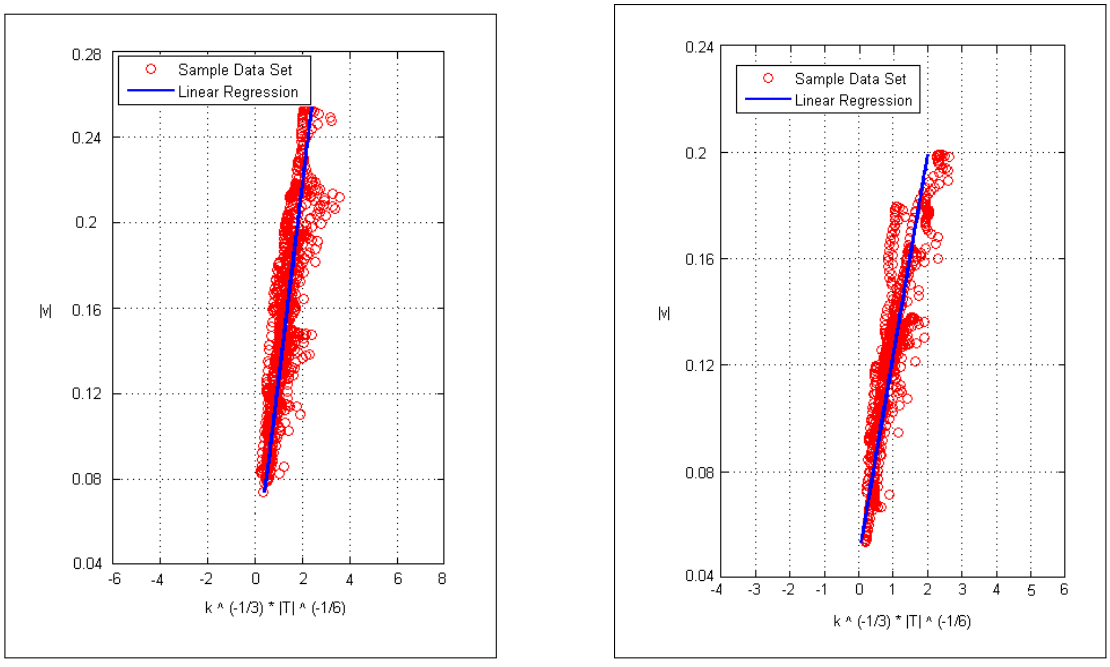

(a) Sample Data Set - Left Blade.

(b) Sample Data Set - Right Blade.

Figure 4-3: Linear regression obtained for a sample data set (Left and Right Hands)

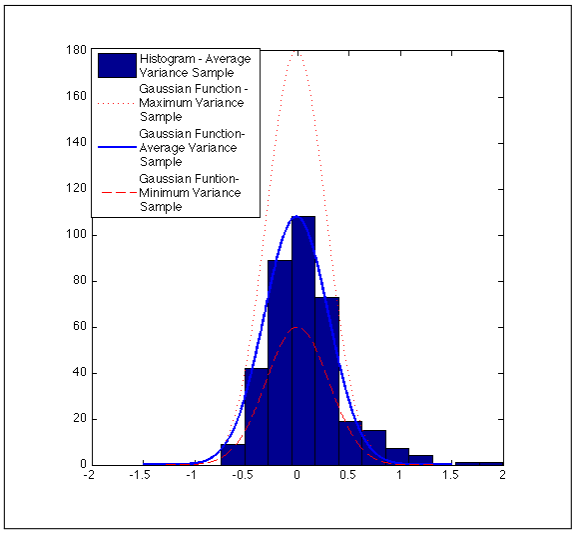

(a) Histogram Sample Data - Left Blade.

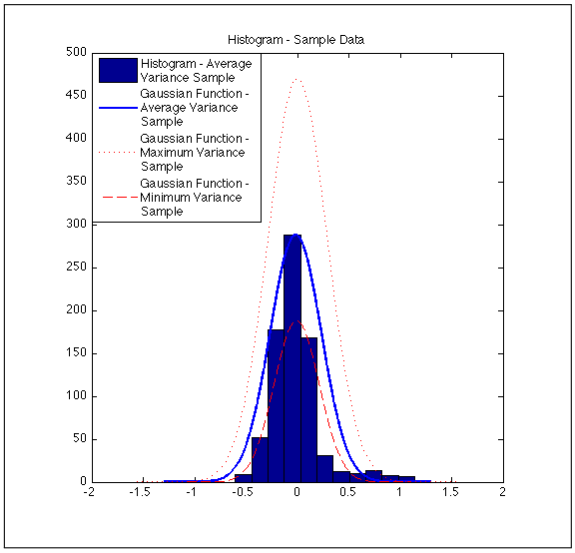

(b) Histogram Sample Data - Right Blade.

Figure 4-4: Histogram of a Sample Data (Left and Right Blade).

4.2.2. Power Law to Describe Obstetrical Gestures

In this case, the exponents of (4-9) were not taken as a fixed constant (4-15) and, in order to calculate the best exponents that fit the surgical data, a logarithmic linearization of this equation is used:

$$v = v_a \kappa^{\alpha} |\tau|^{\beta}, \tag{4-15}$$

$$\log(v) = \log(v_a \kappa^{\alpha} |\tau|^{\beta}) = \log(v_a) + \alpha \log(\kappa) + \beta \log(|\tau|). \tag{4-16}$$

This expression can be rewritten as $z = \gamma + \alpha x + \beta y$, where $z = \log(v)$, $x = \log(\kappa)$ and $y = \log(|\tau|)$. Based on this expression, in order to calculate α, γ and β, a multivariate linear regression was performed using a least square fitting technique. [49] (Figure **4-5** and Figure **4-6**).
Linear least squares approach is used to fit the data with a model of the form:

$$z \simeq \theta_0 + \theta_1 x + \theta_2 y \tag{4-17}$$

The residuals (defined as the differences between the observations and the model) are:

$$r_i = z_i - (\theta_0 + \theta_1 x_i + \theta_2 y_i), \quad i = 1, ..., m, \tag{4-18}$$

where m is the number of samples. In order to make the residuals as small as possible, sum of the squares of the residuals is minimized:

$$||r||^2 = \sum_{1}^{m} r_i^2 \tag{4-19}$$

In particular, the Moore-Penrose pseudoinverse is used to solve the linear least square problems, taking into account that this mathematical tool provides the minimization in this way:

$$\theta = w^+ z, \tag{4-20}$$

where $w = [1 \;\; x \;\; y]$ and w^+ is the pseudoinverse of w:

$$w^+ = (w^T w)^{-1} w^T \tag{4-21}$$

In Figure **4-7**, the average values for both exponents (α and β) are presented for each subject involved in this experiments. The results show that the exponent α has an average value of 0,2059 approximately $-\frac{1}{5}$ ranging from 0,1357 $\approx -\frac{1}{7}$ to 0,273 $\approx -\frac{1}{4}$. The exponent β, on the other hand, presents an average value of 0,0862 $\approx -\frac{1}{12}$ varying from values as 0,0603 $\approx -\frac{1}{16}$ to 0,1301 $\approx -\frac{1}{8}$. The deviation for each gesture shows that the left trajectories have a higher variance than the right ones for each exponent calculated.

Based on the values of the constant γ, the affine velocity was calculated taking into account the relationship $\gamma = \log(v_a)$. Figure **4-8** presents the values of affine velocity for each gesture performed for each person involved in this experiments. As for the previous results the dispersion for the gesture performed by the left hand is higher compared with the right one. Additionally, Figure **4-8** shows that the affine velocity of the right gestures, in every case, is lower than the values calculated for the left gestures. The results obtained are clustered in such a way that is possible distinguish between both gestures for each subject.

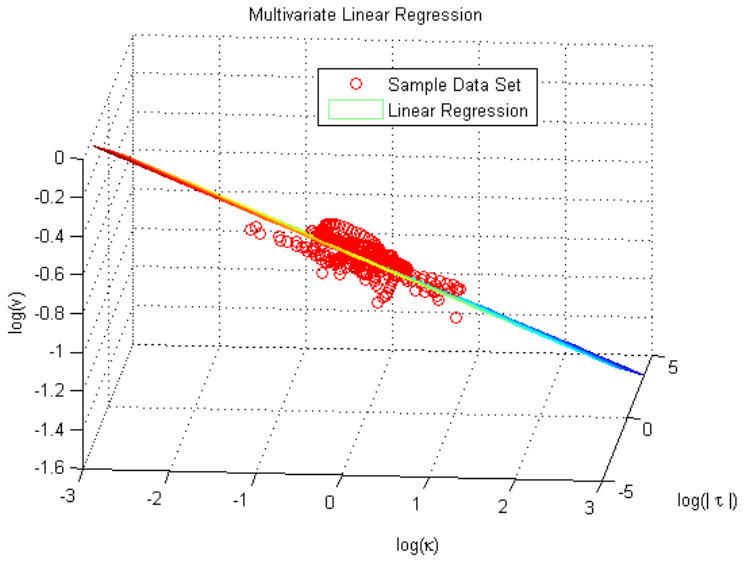

Figure 4-5: Multivariate Linear Regression - Left Blade.

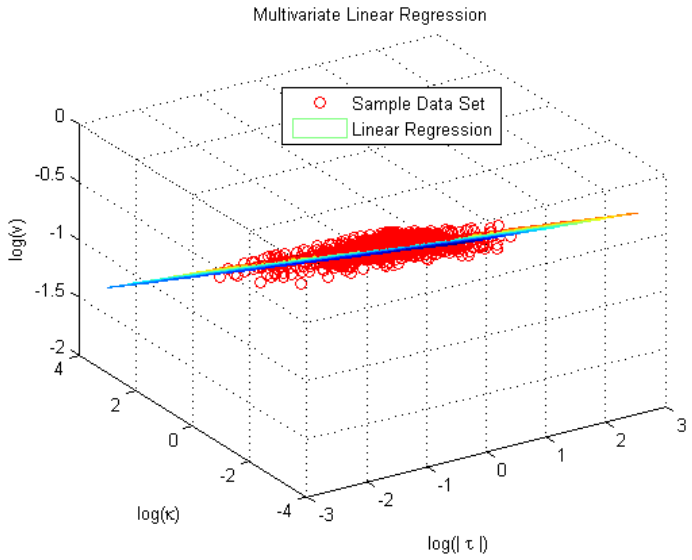

Figure 4-6: Multivariate Linear Regression - Right Blade.

4.3. Gestures in Surgical Training

4.3.1. Data Capture System

A data capture system was used to record all data from the motion tracking system and the force and torque sensors. The processing was accomplished using a computer with a quad-core processor and a 4 gigabytes RAM. Microsoft Windows Operating System was required for compatibility with the motive tracker ®. Force and torque data were acquired

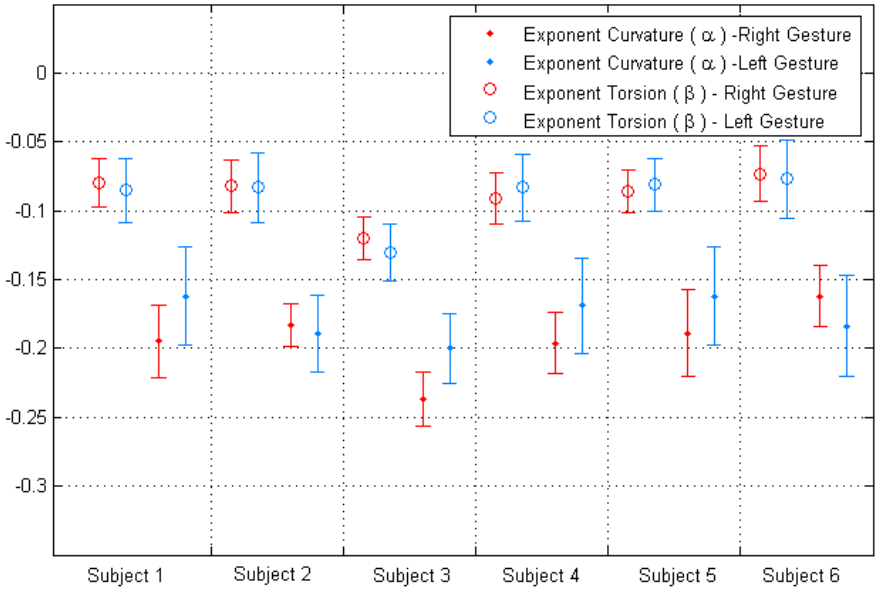

Figure 4-7: Free exponents calculation.

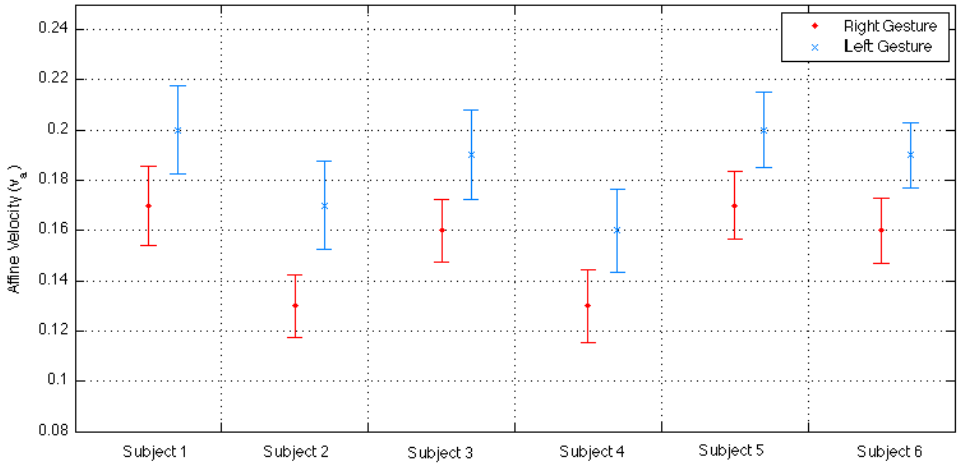

Figure 4-8: Affine velocity for each gesture.

and synchronized using a program developed in Labview ® with a frequency of 30 Hz. A schematic diagram of the system is depicted in Figure **4-9**.

Participants performed different tasks used in surgerical training in an Endo-trainer from 3D-Med (Figure **4-10**). This trainer simulates a laparoscopic surgery environment with an adjustable camera to simulate a laparoscope. A training board is placed inside the Endo-

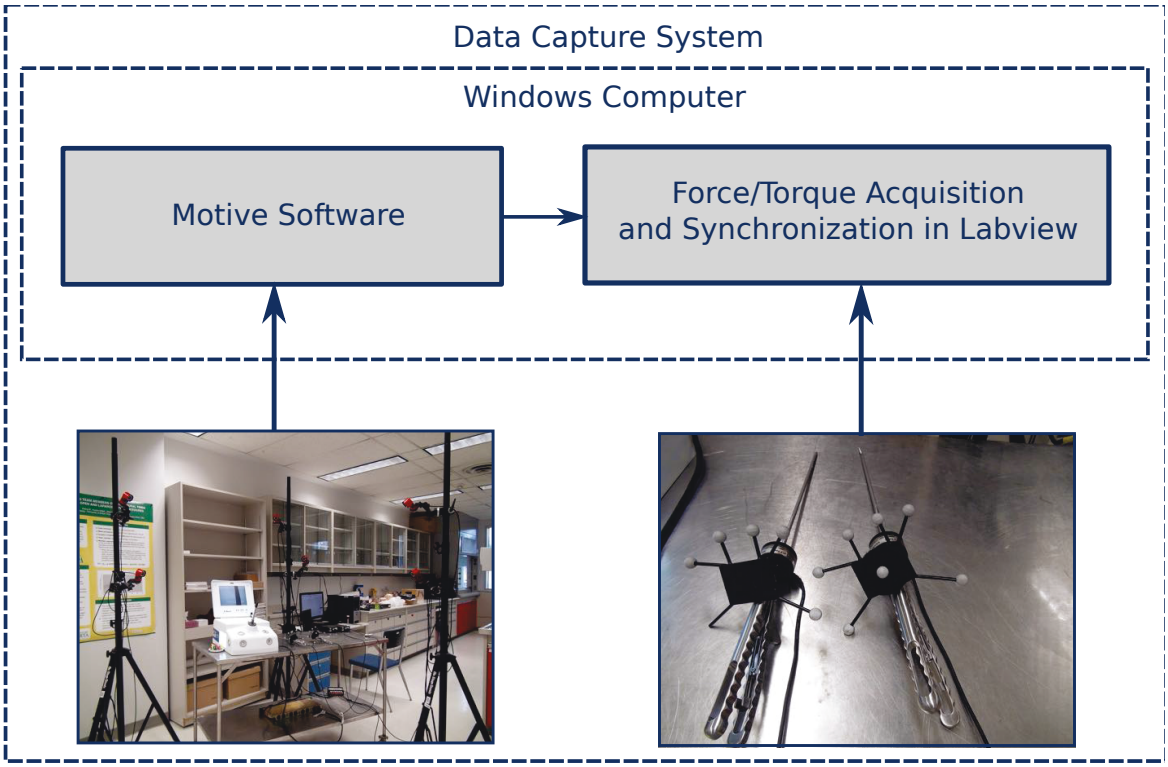

Figure 4-9: Data capture system

trainer to be manipulated by the participants using laparoscopic instruments.

Figure 4-10: Endo-trainer.

Motion Tracking

The position was obtained based on an arrangement of six cameras and the OptiTrack Motive Software ®. Each camera has 1.3 MP resolution at 120 FPS and the sampling rate was 30 samples per channel per second. Based on this configuration, the laparoscope was identified using reflective markers attached at the end of a calibration rod (Figura 4.11(a)).

(a) Markers Location

(b) Calibration Tool

Figure 4-11: Experiment tools.

The calibration is made using the tools provided by the software. In this particular case, markers at different distances are located in a particular tool (Figure 4.11(b)) in order to place them in different positions in the workspace. After this process is completed, an optimization algorithm, included in the software, calculate the suitable focal values for each camera (Figure **4-12**), each one with an excellent accuracy. It is also important to note that effective tracking filters are included in this process allowing a very accurate results.

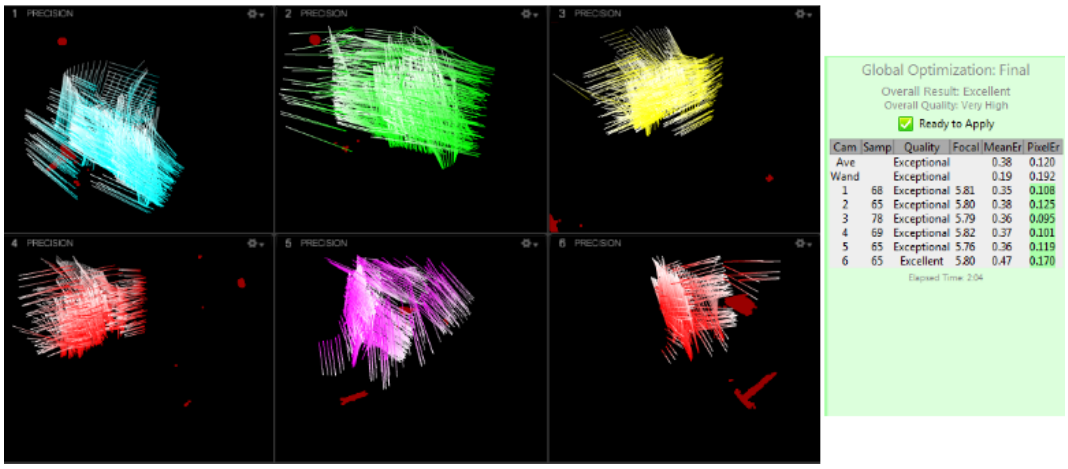

Figure 4-12: Calibration results

With this configuration, a rigid body identified by markers is created in order to represent the laparoscope (Figure **4-13**). The rigid body position (center of mass), and rigid body rotation (recorded in quaternions) are recorded into an array to make saving data easier.

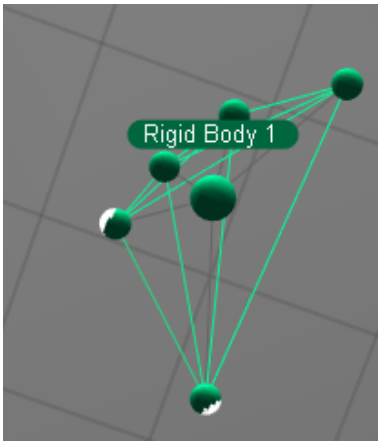

Figure 4-13: Rigid body.

In this way, the marker's position is recorded using this tracking system. In order to calculate the position of the instrument tip, a FARO Titanium Arm scanning device equipped with a FARO Laser Line (Figure 4.14(a)) was used in order to measure the distance between the markers and the instrument tip. This device has become in a very trusted source for 3D measurement with a maximum precision: ±0,041 mm, for our particular case. The digitized instrument is shown in Figure 4.14(b).

The distance between the center of mass of markers and the instrument tip was computed based on these results, the following transformation matrix was used to compute the final position values:

$$T = \begin{bmatrix} 1 & 0 & 0 & 367{,}62571 \\ 0 & 1 & 0 & 44{,}4895 \\ 0 & 0 & 1 & -15{,}73163 \\ 0 & 0 & 0 & 1 \end{bmatrix} \text{[mm]}. \tag{4-22}$$

Force and Torque Data

Each laparoscope was instrumented with a force and torque sensor (Figure **4-15**) located between the tool tip and the handle of the tool to capture the interaction between participant and the manipulated material. The Mini40 force and torque sensor from ATI Industrial [1] is composed by six strain gauges that react to the load of the instrument. This sensor was calibrated based in the values shown in Table **4-1** and the z-axis was aligned with the instrument shaft.

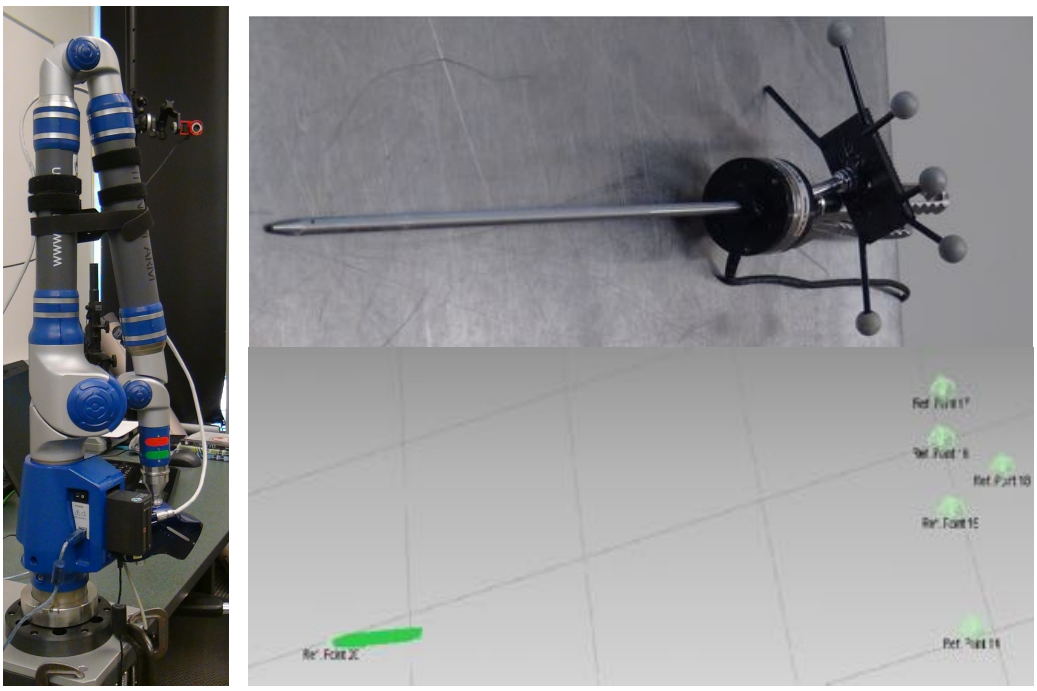

(a) 3D measure device.

(b) Digitized Instrument.

Figure 4-14: 3D Measurements

Table 4-1: Calibration Data.

Sensor	Max. Value	Min. Value	Tolerance	Axis
Force	35 N	-35N	± 0.3 N	X
	35 N	-35N	± 0.3 N	Y
	106 N	-106N	± 0.3 N	Z
Torque	1.5 N.m	-1.5 N.m	± 0.008 N.m	X
	1.5 N.m	-1.5 N.m	± 0.008 N.m	Y
	1.5 N.m	-1.5 N.m	± 0.008 N.m	Z

In the framework of this thesis, a Labview program was developed in the AMMI (Advanced Man-Machine) Laboratory of the University of Alberta in order to perform the data synchronization between force and torque and position and orientation data. For each position sample, a sample of force and torque was obtained. The sampling rate for data acquisition was 30 Hz. Additionally, the program shows the visualization of acquired data and the relevant information of the instruments used.

Figure 4-15: Force and torque sensor

4.3.2. Experimental Methodology

The tasks involved in these experiments were performed in a complete minimally invasive training system that did not require any video equipment. Two subjects with previous surgical experience and 6 subjects with no experience were involved in this experiment. Before performing the trajectories, participants completed a questionnaire that included information such as age, gender, dominant hand and current training status (no experience or some surgical skills) (Table **4-2**). Participants performed two different trajectories that involve depth perception skills. The aim was focused on avoiding collisions for different navigation paths using the dominant hand (Figure **4-16**). Particularly, Figure 4.16(b) shows the trajectories in black, the obstacles in gray and the initial and final point in green. For this task, participants were instructed for each trajectory, they had 5 trials before recording the final 10 experiments. Motion started and finished approximately in the same point. Figure **4-17** shows one example of position values for each gesture.

Table 4-2: Participants Information.

	Age	Gender	Dominant hand	Training Status
Subject 1	20	Male	Right	No experience
Subject 2	22	Male	Right	Surgical Skills
Subject 3	34	Female	Right	No experience
Subject 4	27	Female	Right	No experience
Subject 5	23	Male	Right	No experience
Subject 6	30	Male	Right	No experience
Subject 7	35	Female	Right	Surgical Skills
Subject 8	29	Female	Right	No experience

(a) Minimally invasive training system.

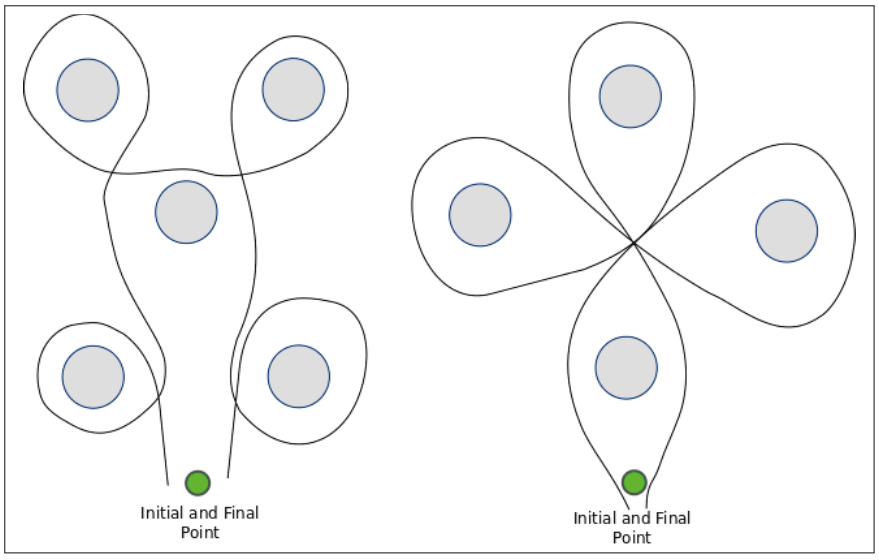

(b) Trajectories shape.

Figure 4-16: Navigation trajectories involved in the experiments.

4.3.3. Power Law to Describe Surgical Gestures

A filtering stage was implemented using a lowpass FIR filter with a cutoff frequency of 5 Hz and order 20. The position data, for 160 trajectories, were interpolated using cubic splines to calculate the analytical derivatives. Based on the splines computation, variables such as velocity modulus v, curvature κ, and torsion τ were computed. In order to avoid singularities when the torsion is zero, a threshold was used in the different calculations (5 % on the value of absolute torsion).

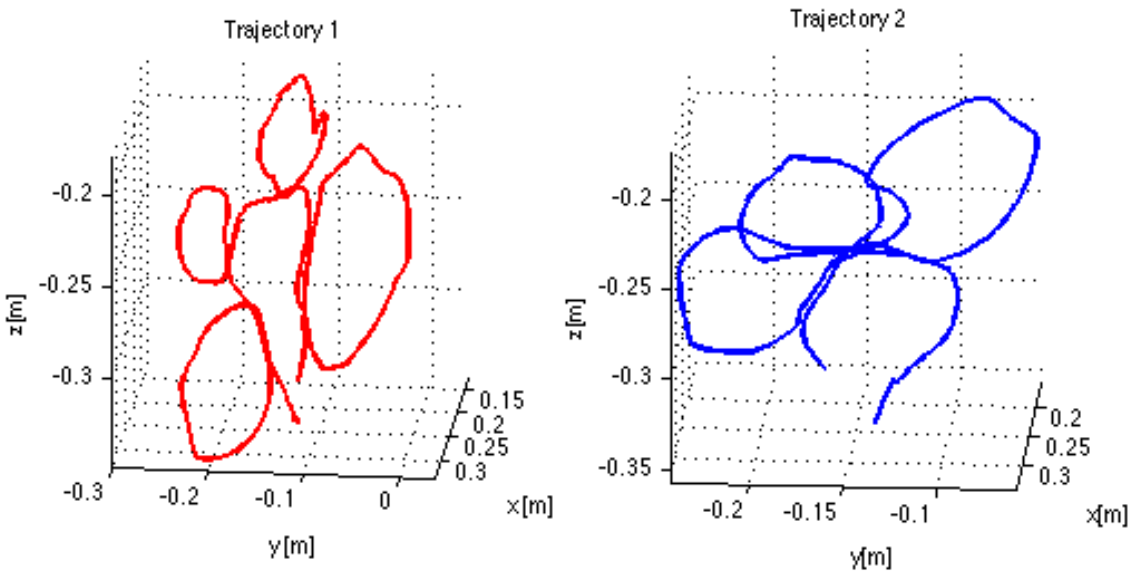

Figure 4-17: Real trajectories.

In order to determine the exponents for curvature α and torsion β but also for the affine velocity v_a, a similar analysis to the section 4.2.2 was performed. In this way, a multivariate linear regression was used and a least square fitting algorithm was implemented to solve this problem [49]. Regression results for both gestures, shown in Figure **4-18**, suggest that the movements, acquired in the experiments, follow the power law described in Equation 4-15.

In Figure **4-19**, the distributions for both exponents (α and β) are presented. The results show that both histograms can be fitted using normal distribution curves. The average values for the curvature exponents α and the torsion exponents β were $-0{,}2059 \approx -\frac{1}{5}$ and $-0{,}0990 \approx -\frac{1}{10}$, respectively.

Based on the values of the constant γ, the affine velocity was calculated taking into account the relationship $\gamma = \log(v_a)$. Figure **4-20** presents the variability of affine velocity values for both trajectories performed by each participant involved in the experiments.

The distribution of data values shows that the affine velocity for the first trajectory, in every case, is higher than the values calculated for the second one. This fact could be explained because the first trajectory has combinations of curvature-torsion values higher than the

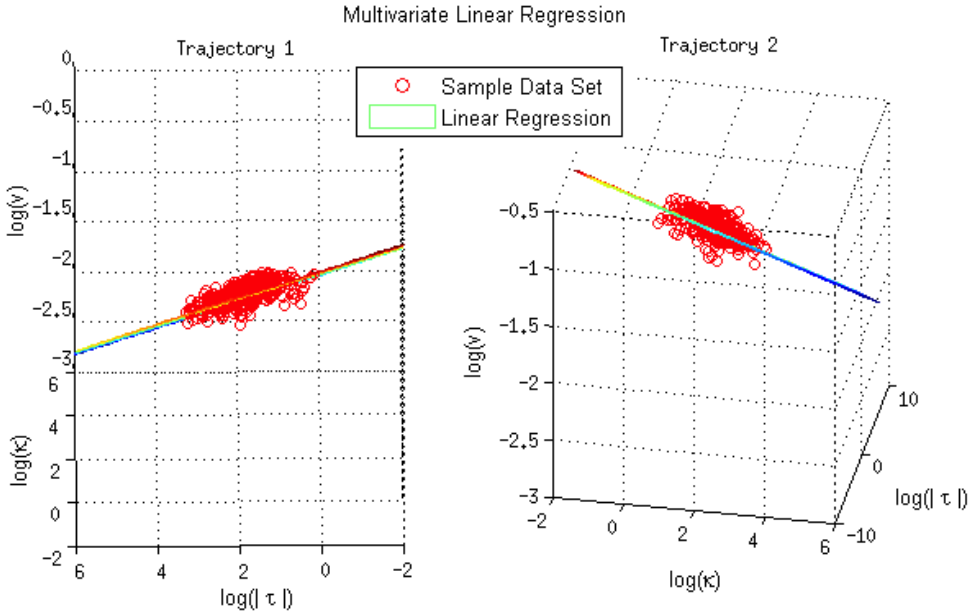

Figure 4-18: Multivariable linear regression for one trial of each trajectory.

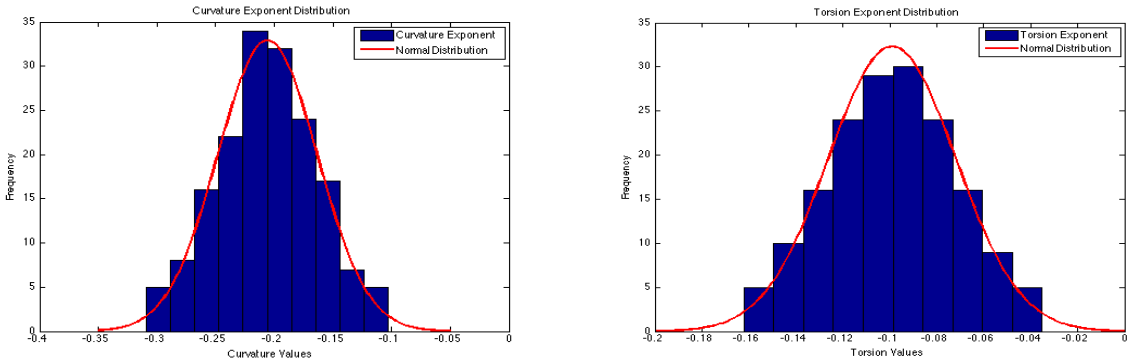

(a) Curvature Exponents Distribution (b) Torsion Exponents Distribution

Figure 4-19: Value Distribution for Curvature and Torsion Exponents.

second one. The results obtained are clustered in such a way that is possible to distinguish between both gestures for each subject. Additionally, based on Table **4-2**, results show a biggest difference for the affine velocities obtained from participants with previous surgical training (Dotted rectangle in Figure **4-20**). In contrast, participants with no experience at all have higher variance in their affine velocity calculations. This behaviour could be explained by the presence of collisions that could disturb the movements and expand the range of measurements.

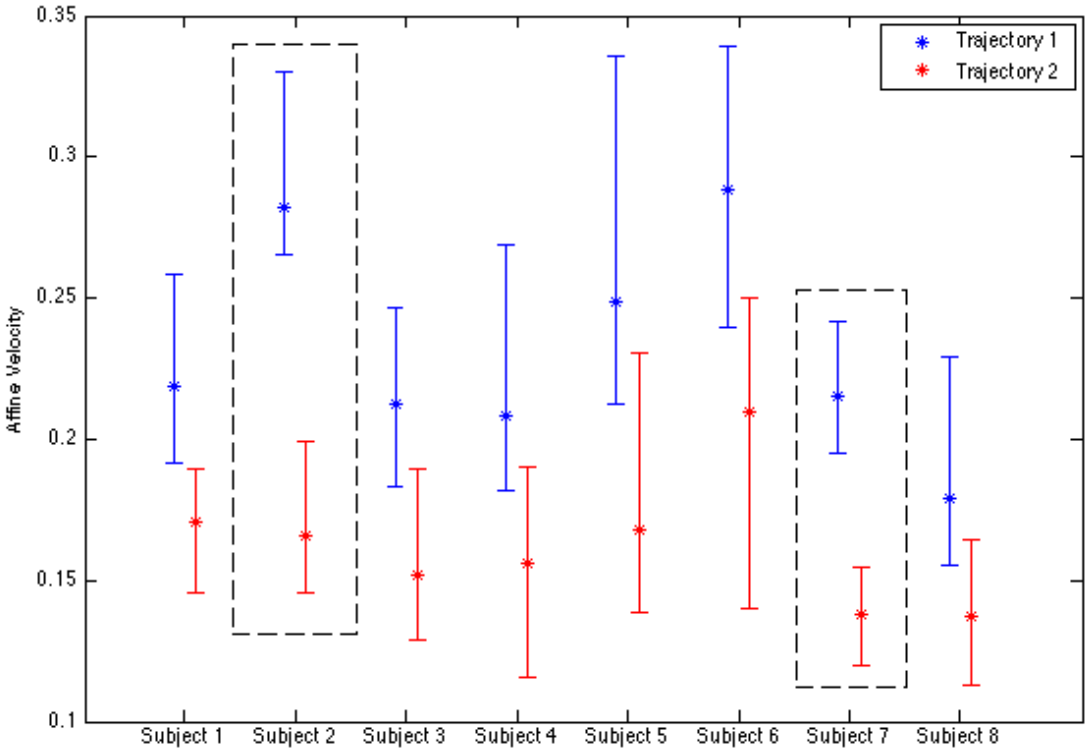

Figure 4-20: Affine Velocity for both gestures.

It suggests that navigation skills in surgical training have an important correlation with the mathematical statement that relates the torsion, the curvature, and the Euclidean velocity. This is an important contribution in the gesture recognition field, which allows us to find an adequate classification using a simple algorithm based on both, kinematic and geometric data.

Based on these results, affine velocities for basic navigation trajectories could be calculated based on the two-third power law. Now, the problem lies in finding affine constant velocities for more complex trajectories, which are present in the training process and in real operations. For this reason, the last part of this work is focused on the segmentation, analysis and classification of more complex trajectories.

4.4. Segmentation and Classification using Affine Velocity and Mechanical Energy Calculation

4.4.1. Methodology

In this section, tasks usually performed during the mini-invasive surgical training were included in the experiments. Specifically, trainees work using a task box where users had to learn to transfer rings back and forth on pegs to get used to use the laparoscope based on a visual input from the camera. In these experiments, two particular trajectories were taken into account (Figure **4-21**) and each participant had five attempts to practice the task before starting the recording of data. After this practice, ten trials using the dominant hand were recorded for each participant. The initial and final positions were the same (Green dot in Figure **4-21**).

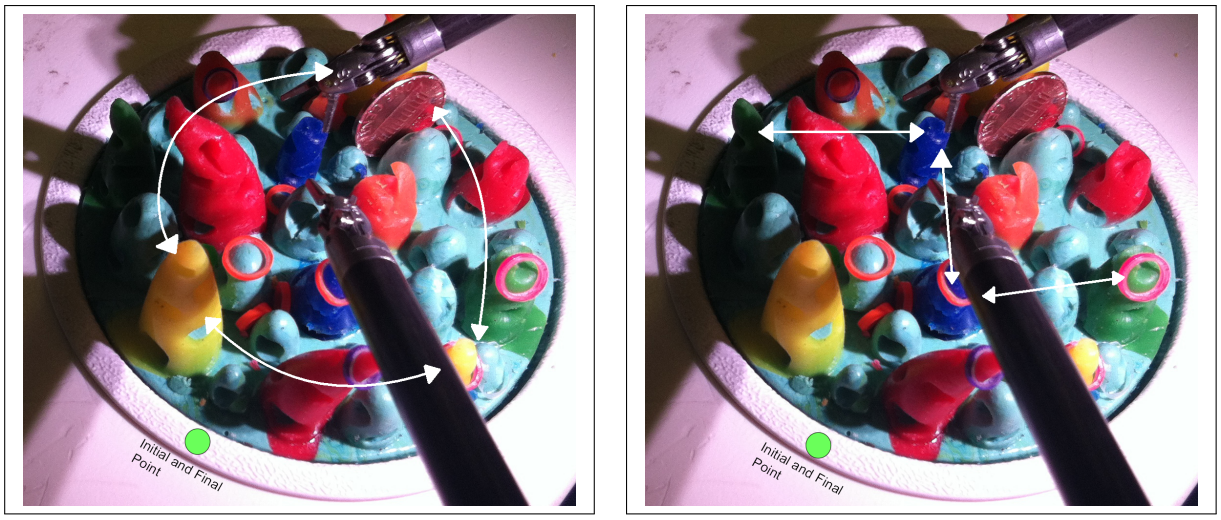

(a) Task 1 (b) Task 2

Figure 4-21: Ring Transference Trajectories.

Trajectories for both tasks performed by each participant are shown in figures **4-22** and **4-23**.

4.4.2. Data Processing

A filtering stage was implemented using a lowpass FIR filter with a cutoff frequency of 5 Hz and order 20. Based on the filtered trajectories, affine velocity was calculated based on the exponents computed in Section 4.3.

Affine velocity maximums are directly related with big and simultaneous changes in torsion and curvature. Based on this fact, trajectories that involve pick-and-drop tasks have two maximums in their affine velocity related to these particular movements. Then, taking into account previous information about the nature of the movement, this segmentation can be carried out by considering breaks after two consecutive maximums are found in the affine velocity signals. For these reasons, in order to segment the trajectory for each pick-and-drop task, first and final peak were computed at the beginning and the end of each trajectory. Starting from the initial one, next two peaks are found and the second one is taken as a reference point, the time distance between the initial peak and this reference is computed in order to include a window with this size that allows us to find the relevant peaks that we need for the segmentation (Algorithms 5 and 6).

Trajectories with no previous information about their nature will require a segmentation based on each maximum calculated in the affine velocity signals. Segmentation results for the affine velocity trajectories are shown in Figure **4-24** and **4-25**.

Affine velocity signals have an important component of noise due to the derivatives involved in the torsion and curvature computations. These trajectories are represented in these figures in blue; curves in black, on the other hand, are splines fitted to each signal in order to facilitate the analysis. Finally, red lines indicate the location of maximum points computed through the whole trajectory.

Indexes for each maximum peak were recorded and used to segment the original position trajectories. In Figures **4-26** and **4-27**, different segments were computed using this information. In particular, on first gesture figures, the basic tasks can be recognized almost in every trajectory being similar each other, in contrast, in second gesture figures, where trajectories have higuer variations, is quite difficult to recognize the nature of the basic task involved in the movement.

Function maxinf= maxdetection(x,tolerance)
Data: $minv = \infty, maxv = -\infty$
Data: $minindex = NaN, maxindex = NaN$, Flag= 1
for *i=1* **to** *length(x)* **do**
  actual=x(i);
  if $actual > maxv$;
  then maxv=actual, maxindex=i;
  if $actual < minv$;
  then minv=actual, minindex=i;
  if *Flag;*
  then **if** $actual < maxv - tolerance$;
  then maxinf=[maxinf; maxv maxindex];
  minv=actual;
  minindex=i;
  Flag=0;
  if $actual > minv + tolerance$ **then** maxv=actual;
  maxindex=i;
  Flag=1;
end

Algorithm 5: Maximum Peaks Detection.

```
maxinfo=maxdetection(x,tolerance);
WL=maxinfo(3,2)-maxinfo(1,2);
maxfinal=[maxfinal; maxinfo(1,1)];
indexfinal=[indexfinal; maxinfo(1,2)];
j=1 ;
while j >= 0;
do
    for i = (WL * j) + 1 to (WL * (j + 1)) + 1 do
        if (WL * (j + 1)) + 1 <=length(x);
        then  maxv=maxdetection(x(((WL+j)+1):(WL*(j+1))+1));
        j=j+1;
        maxfinal=[maxfinal; max(maxv(:,1))];
        indexfinal=[indexfinal; locate(max(maxv(:,1)))];
        else
            maxv=maxinfo(end,1);
            maxindex=maxinfo(end,2);
            j=-1;
            maxfinal=[maxfinal; maxv];
            indexfinal=[indexfinal; maxindex];
        end
    end
end
```

Algorithm 6: Relevant Peaks in Affine Velocity Signal.

4.4.3. Mechanical Energy Calculation

Based on the segmentation calculated in the previous section, a feature that characterize each segment should be computed in order to perform the classification. Some researches around the world had shown encouraging results using the total mechanical energy calculated for each movement.

In particular, mechanical energy involves force and torque and position and orientation data to compute the energy applied by each subject during the tasks. In the context of physics, this variable is referred to as work, but can be conceived as the energy used in the manipulation during an intervention. This measure could capture relevant information about the movement economy, errors,dropped objects, collisions, excessive force that could represent higher energy values.

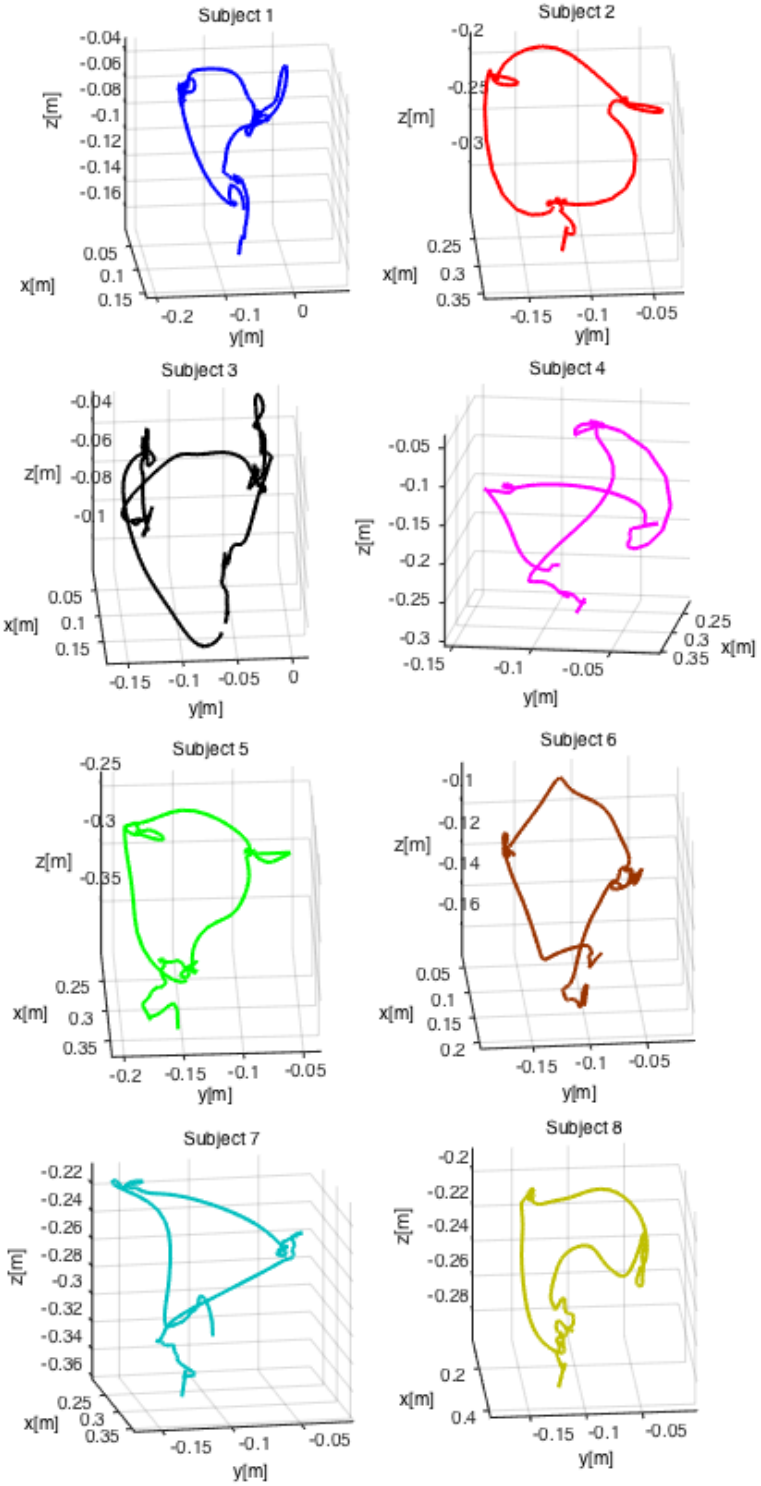

Figure 4-22: Trajectory 1.

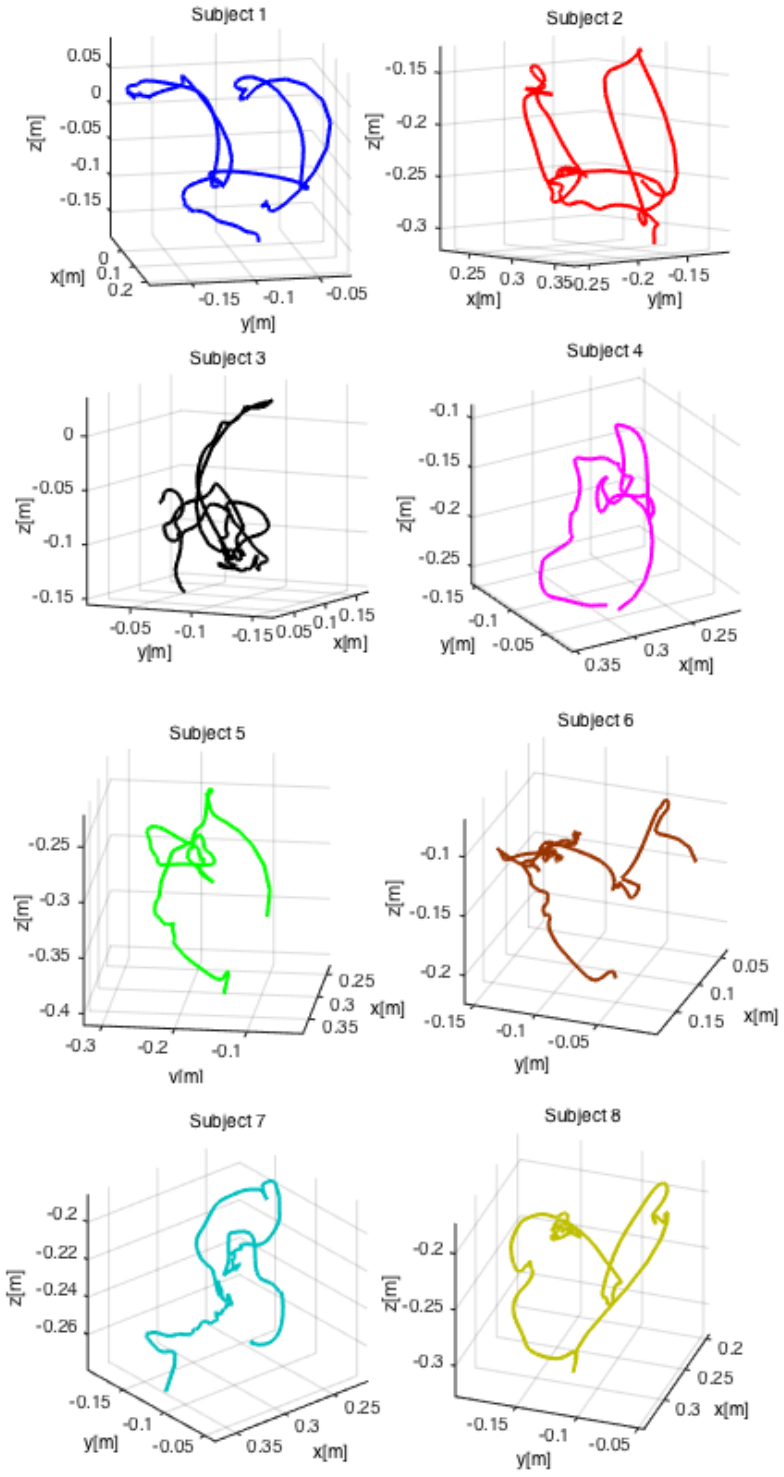

Figure 4-23: Trajectory 2.

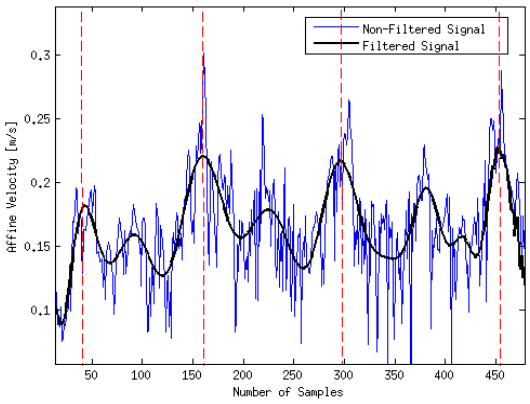

(a) Subject 1

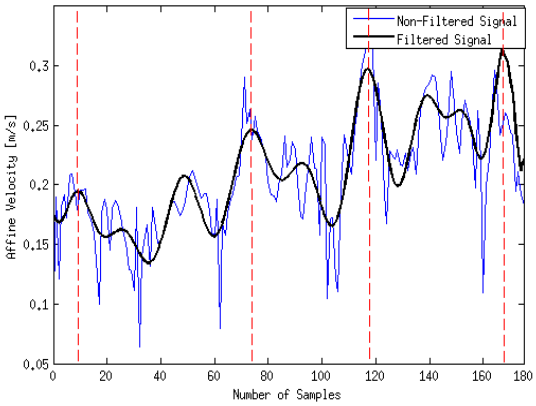

(b) Subject 2

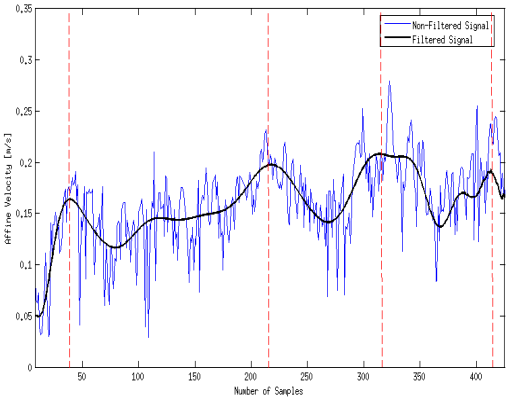

(c) Subject 3

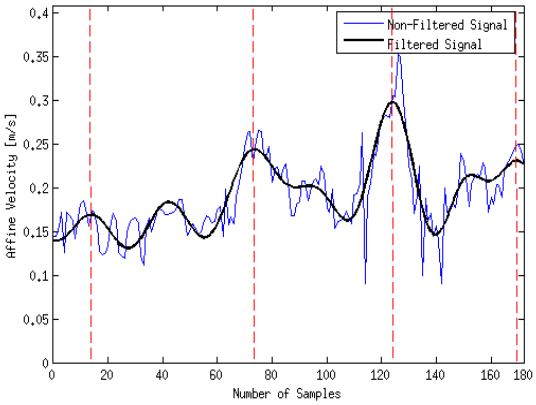

(d) Subject 4

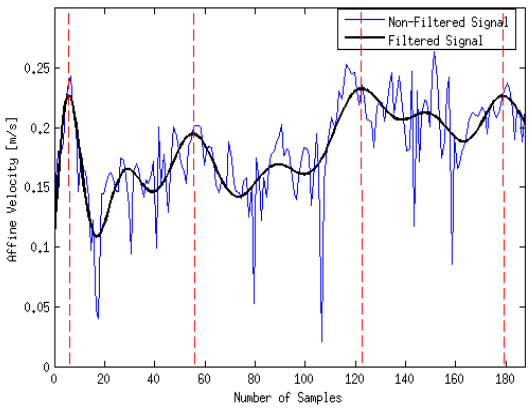

(e) Subject 5

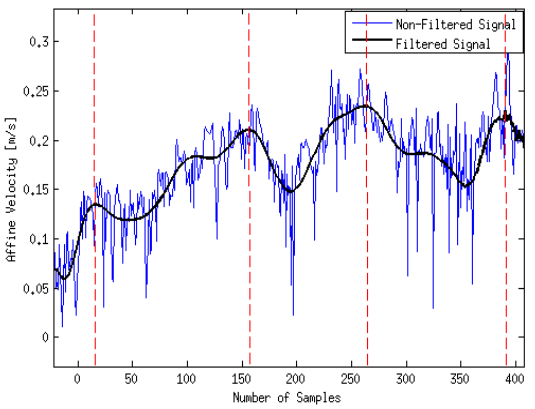

(f) Subject 6

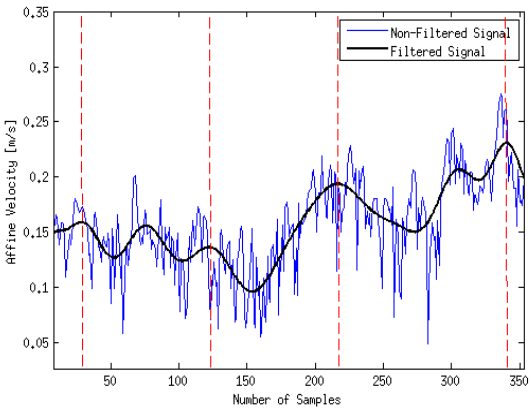

(g) Subject 7

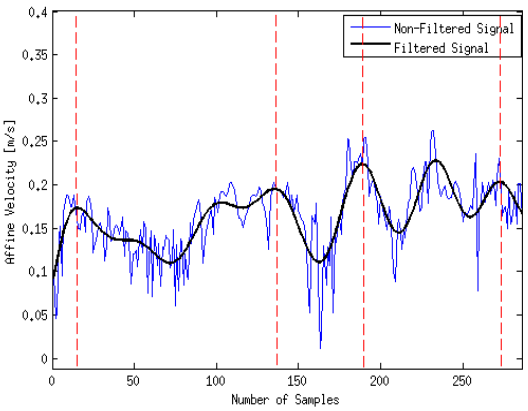

(h) Subject 8

Figure 4-24: Segmentation Affine Velocity- Trajectory 1.

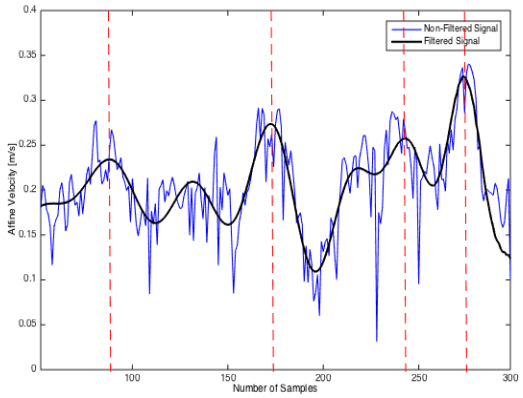

(a) Subject 1

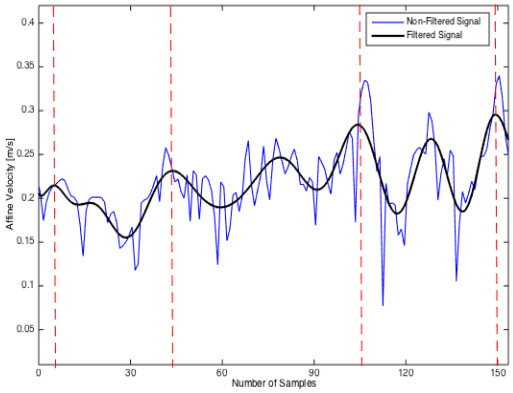

(b) Subject 2

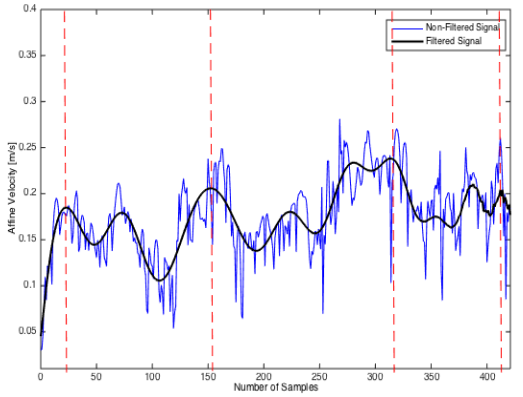

(c) Subject 3

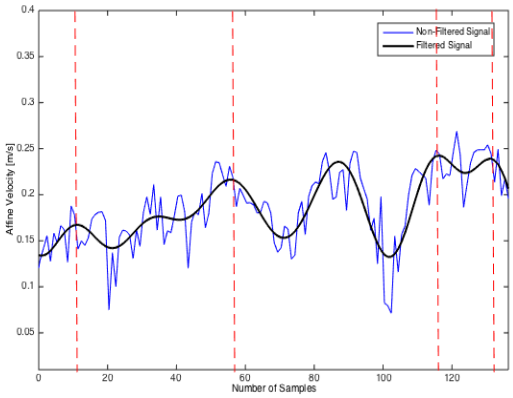

(d) Subject 4

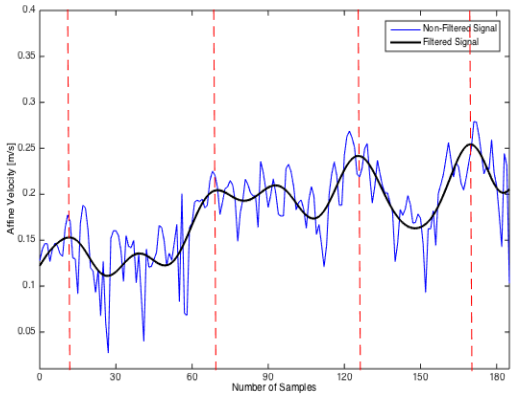

(e) Subject 5

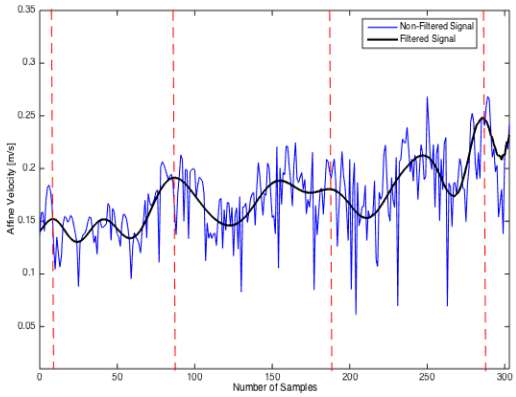

(f) Subject 6

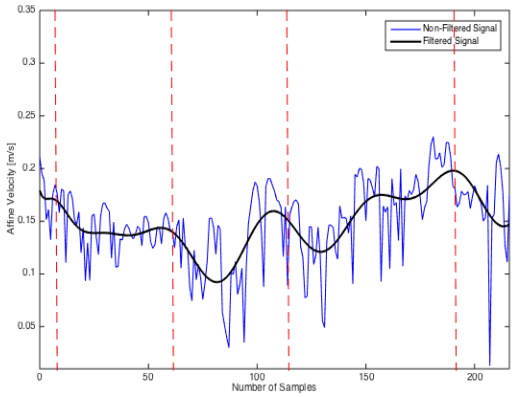

(g) Subject 7

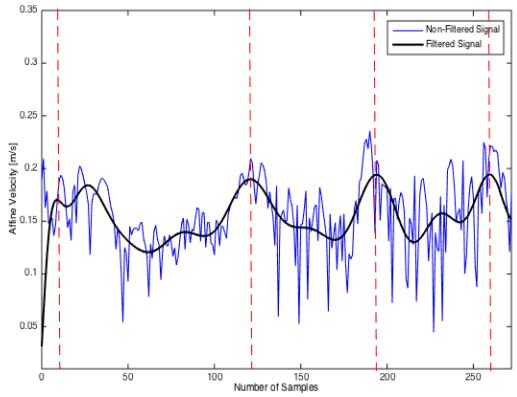

(h) Subject 8

Figure 4-25: Segmentation Affine Velocity- Trajectory 2.

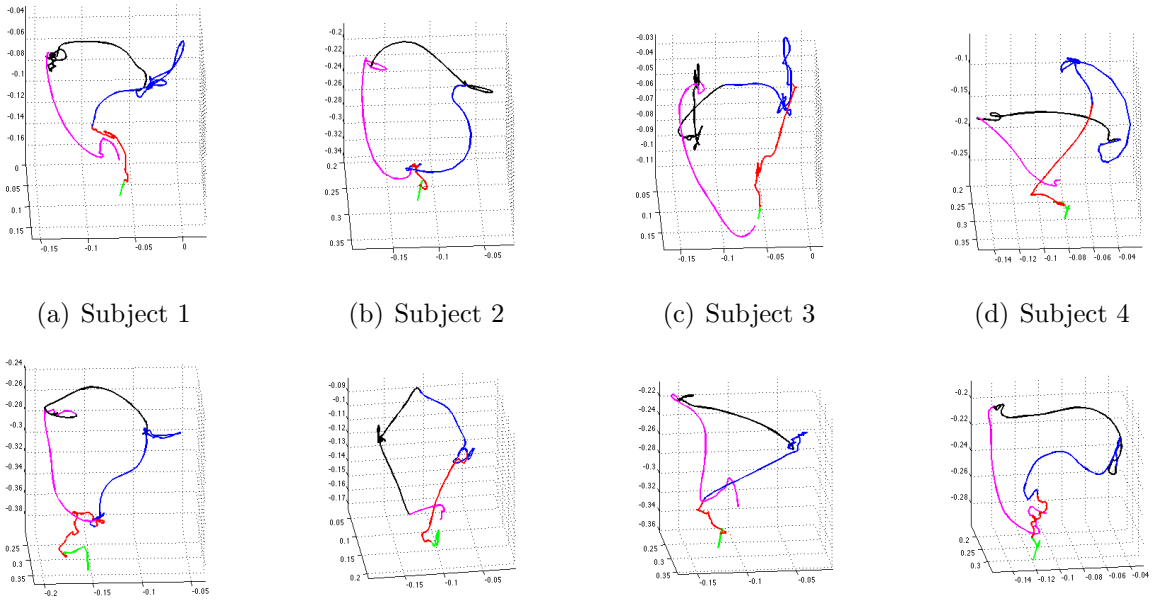

(a) Subject 1 (b) Subject 2 (c) Subject 3 (d) Subject 4

(e) Subject 5 (f) Subject 6 (g) Subject 7 (h) Subject 8

Figure 4-26: Segmentation Position - Trajectory 1.

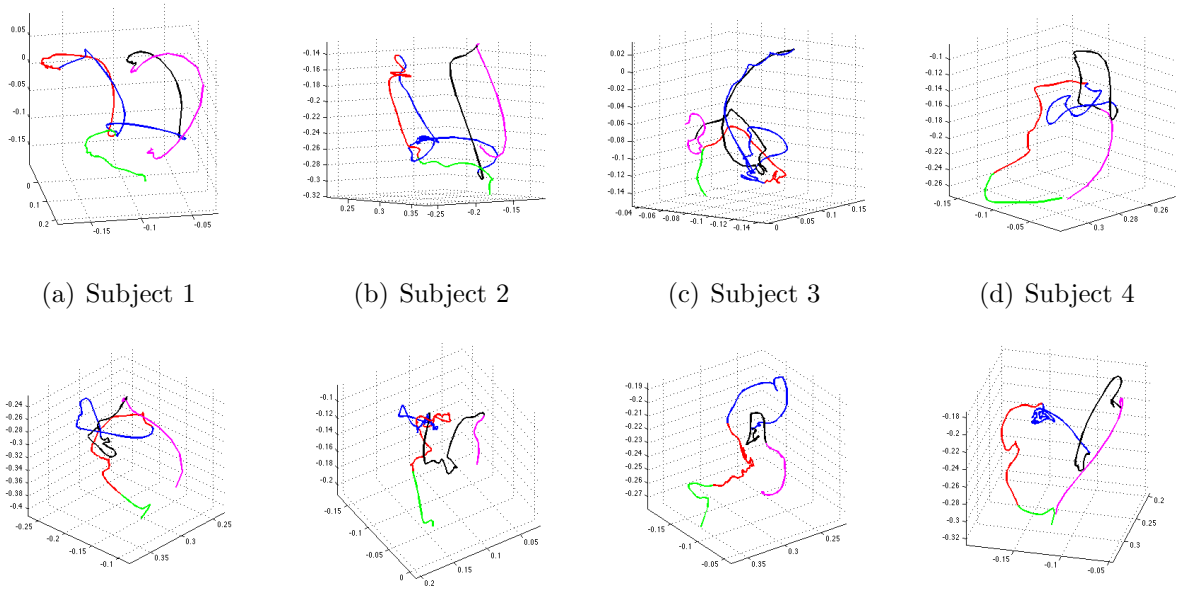

(a) Subject 1 (b) Subject 2 (c) Subject 3 (d) Subject 4

(e) Subject 5 (f) Subject 6 (g) Subject 7 (h) Subject 8

Figure 4-27: Segmentation Position - Trajectory 2.

Energy was computed from the force (F), torque (T), and tool tip position and orientation values (x and ω) based on the expression:

$$E = \int_0^t F.dx + \int_0^t T.d\omega \tag{4-23}$$

Resulting energy computations for each segment are shown in the following figures:

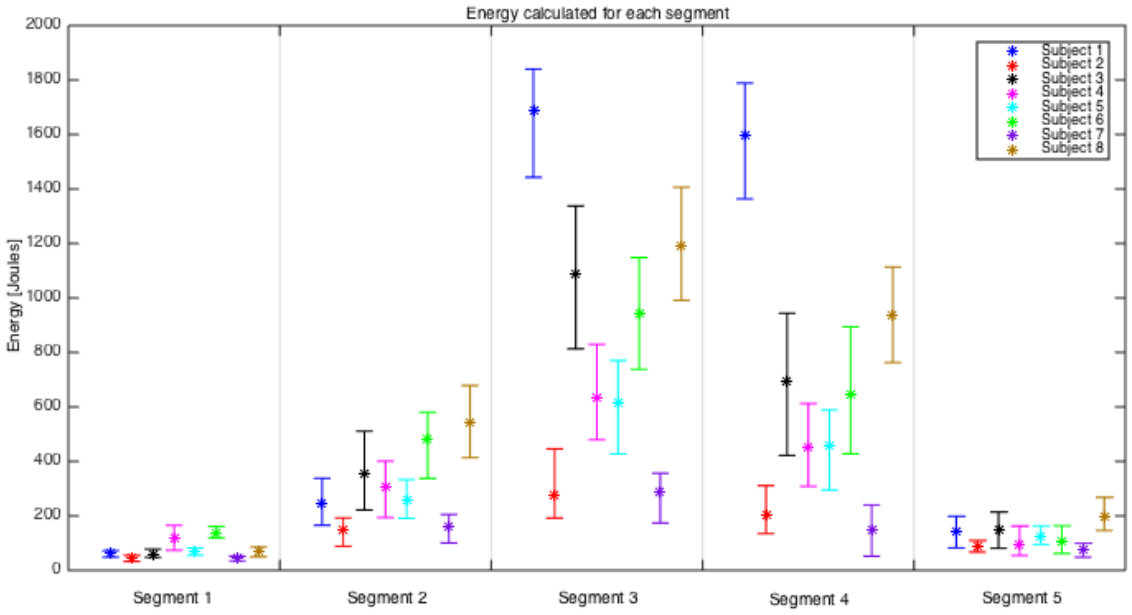

Figure 4-28: Energy calculated for the trajectory 1.

The results show that participants 2 and 7, subjects with some skills handling these instruments, have lower values of energy. Likewise, Figures **4-28** and **4-29** show low dispersion in the values of energy, being more clear in the intermediate segments where the variation in the path may be higher.

It is possible to notice that trajectory 1, in general, involves higher values of energy compared to trajectory 2. This behaviour is due to bigger changes in orientation and torsion are present in this movement. Similarly, subjects with higher values of energy in the first movement are reflected also in the second one, being more precise in the intermediate segments. These increased energy values may reflect collisions, dropped elements and any kind of interruption in movement. It can be noted that, although second gesture have higher variations among the movements for each participant, it correspond to the movement associated to the lowest energy. This behaviour can be explained because, despite the fact that this trajectory involved different possible paths to perform it, the movements are shorter and achieving the adequate orientation does not require big values of torsion or curvature.

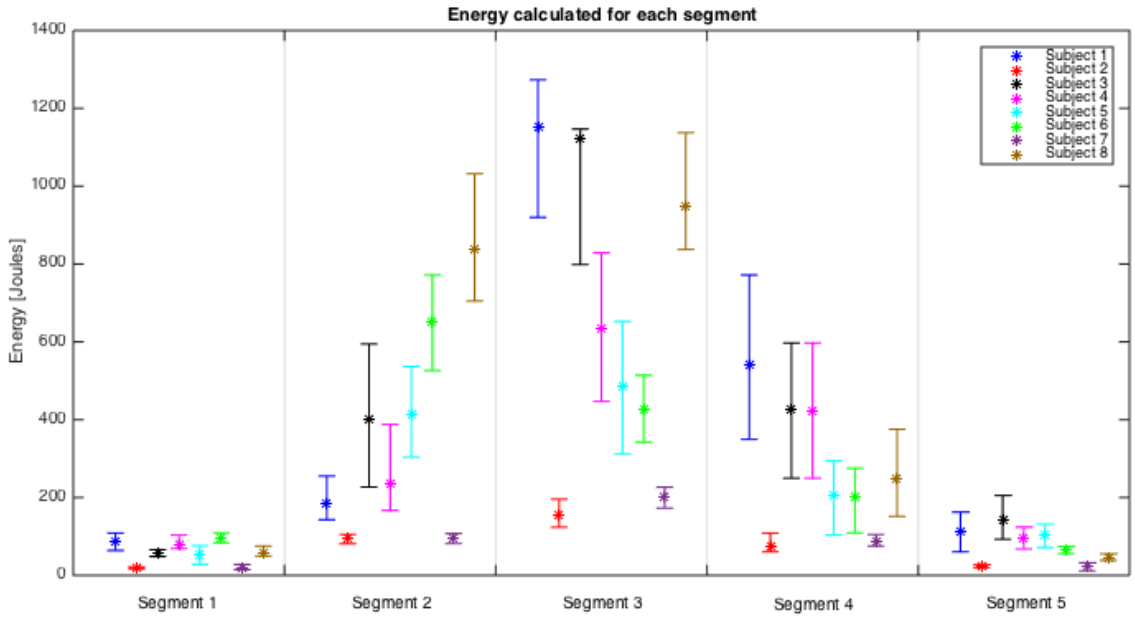

Figure 4-29: Mechanical energy calculated for the trajectory 2.

Based on the results, classification can be performed using just one intermediate segment, which represent the dynamic of a basic task, decreasing the problem complexity and the computation time. Although this method does not allows to distinguish between movements performed by different people, gesture recognition can be done based on gesture nature and surgical skills.

4.5. Conclusion

In this chapter, an experimental relationship between velocity, curvature, and torsion is used to calculate a new suitable feature to classify gestures: *The affine Velocity*. The experiments involved in this survey include two obstetrical gestures acquired using an instrumented forceps. The affine velocity calculations allow to classify between gestures for each subject involved in the experiments.

Likewise, this work describes experiments carried out based on two different navigation gestures. These movements involved depth perception skills, acquired using an arrangement of six cameras, the OptiTrack Motive Software and a complete minimally invasive training system. The affine velocity calculations allowed to classify gestures and distinguish the surgical skills for the participants involved in these experiments. The results obtained present a new alternative to analyze medical gestures by examining the affine space rather that the Euclidean one.

Finally, the last part of this work describes two trajectories performed during the training process in minimally invasive surgery. These trajectories have a more complex nature that avoid to obtain a constant affine velocity for whole trajectory. For these reason, a segmentation stage was implemented based on the maximum peaks computed in the affine velocity signals. For each segment, energy was calculated and compared between each participant involved in the experiments. Results suggest that segmentation could acquire the relevant information from the trajectory and in this way, improve computation time in the analysis stage. Mechanical energy, on the other hand, is a valuable feature that allows to distinguish movements performed by participants with previous surgical skills.

5 Conclusion

Objective evaluation of surgical skills has become an important challenge in medical training. Nowadays, methods developed in order to obtain an automated evaluation are not yet able to replace the expert-based assessment and its variability mainly because of the lack of adequate skill metrics. A critical stage in this process is related to the classification of gestures based on the nature of each movement and the level of skills of each participant. An adequate and accurate classification method is required to assess the trainees skills before they enter the operating room.

An algorithm based on a cumulative arc-length parametrization was proposed in order to perform an efficient classification, among different gestures. Specifically, this method involves an arc-length parametrization allowing for time independence and a geometric invariant like curvature that varies based on the local geometry. The main contributions include the possibility to compare similar trajectories performed at different speeds using cumulative arc-length warping and curvature to guaranty invariance to the location of the sensor coordinate system. In order to develop the implementation, it was necessary to take into account that using the parametrization with respect to the cumulative arc-length, trajectories are sampled with unequal intervals in space. Based on this premise, a second-order Lagrange polynomial interpolation scheme was used in order to compute the curvature values. An experimental study was conducted using tree different devices with the cooperation of different subjects and a low-pass filter without phase shift and magnitude distortion was applied to each 3D data set. In the first analysis, position measurements of each gesture were recorded using an exoskeleton of the upper extremity. In this particular case, a total of 10 subjects were involved and they were asked to do two kind of gestures (10 times each) quite similar from a kinematic viewpoint. Second experiment involves surgical gestures that were evaluated on a laparoscope training system (instrument prototype with a Yaw-Roll actuated tip). In this instance, five people with no experience participated for a pick-and-place task (five repetitions). Finally, an analysis of gestures acquired by an instrumented obstetrical forceps coupled with the BirthSIM simulator, was developed. In the experiments, six obstetric students were asked to perform 30 forceps blade placements providing for each trainee 60 trajectories: 30 left blade trajectories and 30 right blade trajectories. The results suggested that different gestures can be distinguished using position measurements.

Based on the approach suggested and the previous results, any trajectory (position, orientation, etc) can be analysed and compared in order to obtain an adequate classification. As complementary work, the algorithm proposed (Dynamic Arc-Length Warping) was tested on orientation data where a quaternion representation to perform orientation-based gesture classification. To validate our approach, orientation values for gestures acquired using the exoskeleton were analyzed. This is an important limitation because only this device had the possibility to acquire orientation data. The results show that the distances obtained with a quaternion representation lead to a standard deviation lower than those obtained with angular orientation data. Additionally, the higher standard deviations obtained while the angular orientation data were used, difficult to obtain an adequate comparison between the different groups of experiments. These results demonstrate that similarity measures obtained between the different sets of data allow to develop a classification scheme of human gestures based on orientation values.

While the first part of this work was developed based on the analysis of position or orientation values (kinematic data), the last part focus on the formulation of a new technique that takes into account both kinematic and dynamical data. In this way, an experimental relationship between velocity, curvature, and torsion is used to calculate a new suitable feature to classify gestures: The affine Velocity. The experiments first deal, with an analysis that include the two obstetrical gestures acquired using an instrumented forceps described previously. The results showed that affine velocity calculations allow to classify between gestures for each subject involved in the experiments suggesting a new alternative to medical gestures analysis using the affine space rather that the Euclidean one.

Based on these results, a system that is capable of recording a wide range of data from participants performing laparoscope tasks on a training box was proposed. The position and orientation of the instrument, were recorded using an arrangement of six cameras and the OptiTrack Motive Software ®. Based on this configuration, the laparoscope was identified using reflective markers attached at the end of a rod. In addition, force and torque sensors were located placed on a laparoscope in order to record the dynamics of the participants movements. All data were synchronized and digitally stored for off-line processing.

The first experiments performed, to test the method proposed, include two navigation gestures that involve depth perception skills. These movements were acquired using the system described previously and a complete minimally invasive training system. The results showed that affine velocity calculations allow to classify gestures and distinguish the surgical skills for the participants involved in these experiments.

The last analysis include tasks usually performed during the mini-invasive surgical training. Specifically, trainees used a task box learning to transfer rings back and forth on pegs based on a visual input from the camera. Specifically, two particular trajectories were taken into account and each participant had five attempts to practice the task before starting the recording of data. After this practice, ten trials using the dominant hand were recorded for each participant. Based on results obtained for navigation trajectories, a segmentation procedure was performed using affine velocity data. Finally, mechanical energy was calculated for each segment and used to distinguish gestures based on the surgical skills of each participant.

Ongoing research is focused on increasing the number of experts and the surgical gestures. Limitations in this work were focused on including the participation of professional people in medicine specialized in surgery that were available for the time required in the experiments involved for different gestures. In addition, preliminary results could indicate a correlation between hand dominance and affine speed. In this way, a comprehensive study to develop this theory should be performed. Finally, automatic analysis of gestures in real-time is a challenge that must be studied because it will allow improve performance and response times.

References

[1] *ATI. ATI industrial automation: Robotic end effectors and automation tooling.* http://www.ati-ia.com/. – Accessed: 2014-07-22

[2] Abend, W. ; Bizzi, E. ; Morasso, P.: Human arm trajectory formation. En: *Brain : a journal of neurology* 105 (1982), Juni, Nr. Pt 2, p. 331–348. – ISSN 0006–8950

[3] Aggarwal, Charu C.: On effective classification of strings with wavelets. En: *Proceedings of the eighth ACM SIGKDD international conference on Knowledge discovery and data mining* ACM, 2002, p. 163–172

[4] Agrawal, Rakesh ; Faloutsos, Christos ; Swami, Arun: Efficient similarity search in sequence databases. En: Lomet, DavidB. (Ed.): *Foundations of Data Organization and Algorithms* Vol. 730. Springer Berlin Heidelberg, 1993. – ISBN 978–3–540–57301–2, p. 69–84

[5] Allen, Isobel: *Doctors and their careers.* Vol. 675. Policy Studies Institute, 1988

[6] Bahlmann, C. ; Burkhardt, H.: Measuring HMM similarity with the Bayes probability of error and its application to online handwriting recognition. En: *Document Analysis and Recognition, 2001. Proceedings. Sixth International Conference on*, 2001, p. 406–411

[7] Benedikt, Lanthao ; Kajic, Vedran ; Cosker, Darren ; Rosin, Paul L. ; Marshall, A D.: Facial Dynamics in Biometric Identification. En: *BMVC*, 2008, p. 1–10

[8] Bergroth, Lasse ; Hakonen, Harri ; Raita, Timo: A survey of longest common subsequence algorithms. En: *String Processing and Information Retrieval, 2000. SPIRE 2000. Proceedings. Seventh International Symposium on* IEEE, 2000, p. 39–48

[9] Berndt, D. ; Clifford, J.: Using Dynamic Time Warping to Find Patterns in Time Series / New York University. 1994. – Informe de Investigación

[10] Bernecker, Thomas ; Houle, Michael E. ; Kriegel, Hans-Peter ; Kröger, Peer ; Renz, Matthias ; Schubert, Erich ; Zimek, Arthur: Quality of similarity rankings in time series. En: *Advances in Spatial and Temporal Databases.* Springer, 2011, p. 422–440

[11] Beusmans, JackM.H.: Computing the direction of heading from affine image flow. En: *Biological Cybernetics* 70 (1993), Nr. 2, p. 123–136. – ISSN 0340–1200

[12] Bharkad, Sangita D. ; Kokare, Manesh: Performance evaluation of distance metrics: application to fingerprint recognition. En: *International Journal of Pattern Recognition and Artificial Intelligence* 25 (2011), Nr. 06, p. 777–806

[13] Blum, Tobias ; Feussner, Hubertus ; Navab, Nassir: Modeling and segmentation of surgical workflow from laparoscopic video. En: *Medical Image Computing and Computer-Assisted Intervention–MICCAI 2010*. Springer, 2010, p. 400–407

[14] Boom-Saad, Zackary ; Langenecker, Scott A. ; Bieliauskas, Linas A. ; Graver, Christopher J. ; O'Neill, Jillian R. ; Caveney, Angela F. ; Greenfield, Lazar J. ; Minter, Rebecca M.: Surgeons outperform normative controls on neuropsychologic tests, but age-related decay of skills persists. En: *The American Journal of Surgery* 195 (2008), Nr. 2, p. 205–209

[15] Cha, Sung-Hyuk ; Tappert, Charles C. ; Srihari, Sargur N.: Optimizing Binary Feature Vector Similarity Measure using Genetic Algorithm and Handwritten Character Recognition. En: *ICDAR* Citeseer, 2003, p. 662–665

[16] Cha, Sung-Hyuk ; Yoon, Sungsoon ; Tappert, Charles C.: Enhancing binary feature vector similarity measures. (2005)

[17] Chmarra, Magdalena K. ; Grimbergen, Cornelis A. ; Jansen, Frank-Willem ; Dankelman, Jenny: How to objectively classify residents based on their psychomotor laparoscopic skills? En: *Minimally Invasive Therapy & Allied Technologies* 19 (2010), Nr. 1, p. 2–11

[18] Chmarra, Magdalena K. ; Klein, Stefan ; de Winter, Joost C. ; Jansen, Frank-Willem ; Dankelman, Jenny: Objective classification of residents based on their psychomotor laparoscopic skills. En: *Surgical endoscopy* 24 (2010), Nr. 5, p. 1031–1039

[19] Choi, Seung-Seok ; Cha, Sung-Hyuk ; Tappert, Charles C.: A Survey of Binary Similarity and Distance Measures. En: *Journal of Systemics, Cybernetics & Informatics* 8 (2010), Nr. 1

[20] Chou, Jack C. ; Kamel, M: Finding the position and orientation of a sensor on a robot manipulator using quaternions. En: *The international journal of robotics research* 10 (1991), Nr. 3, p. 240–254

[21] Cifuentes, Jenny A. ; Moreau, Richard ; Prieto, Flavio ; Pham, Minh T. ; Redarce, Tanneguy: Why and how to objectively evaluate medical gestures? En: *IRBM* 34 (2013), Nr. 1, p. 74–78

[22] Cifuentes, Jenny A. ; Pham, Minh T. ; Moreau, Richard ; Prieto, Flavio ; Boulanger, Pierre: Objective Assessment of Surgical Skills. En: *ASME 2012 11th Biennial Conference on Engineering Systems Design and Analysis* American Society of Mechanical Engineers, 2012, p. 253–259

[23] Clark, CI ; Snooks, S: Objectives of basic surgical training. En: *British journal of hospital medicine* 50 (1992), Nr. 8, p. 477–479

[24] Costic, BT ; Dawson, DM ; De Queiroz, MS ; Kapila, V: Quaternion-based adaptive attitude tracking controller without velocity measurements. En: *Journal of Guidance, Control, and Dynamics* 24 (2001), Nr. 6, p. 1214–1222

[25] Cotin, Stephane ; Stylopoulos, Nicholas ; Ottensmeyer, Mark ; Neumann, Paul ; Rattner, David ; Dawson, Steven: Metrics for laparoscopic skills trainers: the weakest link. En: *Medical Image Computing and Computer-Assisted Intervention - MICCAI 2002*. Springer, 2002, p. 35–43

[26] Cunningham, G. ; Gilstrap, L. ; Leveno, K. ; Bloom, S. ; Hauth, J. ; Wenstrom, K.: *Williams Obstetrics*. 22nd. McGraw-Hill Companies, 2005. – iSBN 0071413154.

[27] Darzi, Ara ; Datta, Vivek ; Mackay, Sean: The challenge of objective assessment of surgical skill. En: *The American Journal of Surgery* 181 (2001), Nr. 6, p. 484–486

[28] Darzi, Ara ; Smith, Simon ; Taffinder, Nick: Assessing operative skill: needs to become more objective. En: *BMJ: British Medical Journal* 318 (1999), Nr. 7188, p. 887

[29] Dath, D ; Regehr, G ; Birch, D ; Schlachta, C ; Poulin, E ; Mamazza, J ; Reznick, R ; MacRae, HM: Toward reliable operative assessment: the reliability and feasibility of videotaped assessment of laparoscopic technical skills. En: *Surgical Endoscopy and Other Interventional Techniques* 18 (2004), Nr. 12, p. 1800–1804

[30] Dayan, Eran ; Casile, Antonino ; Levit-Binnun, Nava ; Giese, Martin A. ; Hendler, Talma ; Flash, Tamar: Neural representations of kinematic laws of motion: evidence for action-perception coupling. En: *Proceedings of the National Academy of Sciences* 104 (2007), Nr. 51, p. 20582–20587

[31] Dermitzakis, Konstantinos ; Arieta, Alejandro H. ; Pfeifer, Rolf: Gesture recognition in upper-limb prosthetics: A viability study using dynamic time warping and gyroscopes. En: *Engineering in Medicine and Biology Society, EMBC, 2011 Annual International Conference of the IEEE*. IEEE, 2011, p. 4530–4533

[32] Derossis MD, Anna M. ; Fried MD, Gerald M. ; Abrahamowicz PhD, Michal ; Sigman MD, Harvey H. ; Barkun MD, Jeffrey S. ; Meakins MD, Jonathan L.: Development of a model for training and evaluation of laparoscopic skills. En: *The American journal of surgery* 175 (1998), Nr. 6, p. 482–487

[33] de'Sperati, Claudio ; Viviani, Paolo: The relationship between curvature and velocity in two-dimensional smooth pursuit eye movements. En: *The Journal of Neuroscience* 17 (1997), Nr. 10, p. 3932–3945

[34] Deza, Michel M. ; Deza, Elena: *Encyclopedia of distances*. Springer, 2009

[35] Ding, Hui ; Trajcevski, Goce ; Scheuermann, Peter ; Wang, Xiaoyue ; Keogh, Eamonn: Querying and mining of time series data: experimental comparison of representations and distance measures. En: *Proceedings of the VLDB Endowment* 1 (2008), Nr. 2, p. 1542–1552

[36] Dorner, Brigitte: *Chasing the colour glove: Visual hand tracking*, Simon Fraser University, Tesis de Grado, 1994

[37] Duarte, Ricardo J. ; Cury, Jose ; Oliveira, Luis Carlos N. ; Srougi, Miguel: Establishing the minimal number of virtual reality simulator training sessions necessary to develop basic laparoscopic skills competence: evaluation of the learning curve. En: *International braz j urol* 39 (2013), 10, p. 712 – 719. – ISSN 1677–5538

[38] Eagleson, Roy: Measurement of the 2D affine Lie group parameters for visual motion analysis. En: *Spatial vision* 6 (1992), Nr. 3, p. 183–198

[39] Eubanks, Thomas R. ; Clements, Ronald H. ; Pohl, Dieter ; Williams, Noel ; Schaad, Douglas C. ; Horgan, Santiago ; Pellegrini, Carlos: An objective scoring system for laparoscopic cholecystectomy. En: *Journal of the American College of Surgeons* 189 (1999), Nr. 6, p. 566–574

[40] Faloutsos, Christos ; Ranganathan, Mudumbai ; Manolopoulos, Yannis: *Fast subsequence matching in time-series databases*. ACM, 1994

[41] Flash, T. ; Gurevich, I.: Arm trajectory generation and stiffness control during motor adaptation to external loads. En: *Self-Organization, Computational Maps and Motor Contro* (1997), p. 423–482

[42] Fried, Gerald M. ; Feldman, Liane S.: Objective assessment of technical performance. En: *World journal of surgery* 32 (2008), Nr. 2, p. 156–160

[43] Gagner, Michel: Objective evaluation of a laparoscopic surgical skill program. En: *Archives of Surgery* 133 (1998), Nr. 8, p. 911–912

[44] Goshtasby, A. A.: *Image Registration: Principles, Tools and Methods*. Springer, 2012

[45] Gower, John C.: A general coefficient of similarity and some of its properties. En: *Biometrics* (1971), p. 857–871

[46] Gubaidullin, Gail G.: Euler Angles and Quaternions in Robotics. En: *Aktuelle Methoden der Laser-und Medizinphysik: Tagungsband der 2. Remagener Physiktage 2004, RheinAhrCampus Remagen, 29. September bis 1. Oktober 2004* (2005), p. 137

[47] Gumbs, Andrew A. ; Hogle, Nancy J. ; Fowler, Dennis L.: Evaluation of Resident Laparoscopic Performance Using Global Operative Assessment of Laparoscopic Skills. En: *Journal of the American College of Surgeons* 204 (2007), Nr. 2, p. 308 – 313. – ISSN 1072–7515

[48] Hance, Julian ; Aggarwal, Rajesh ; Moorthy, Krishna ; Munz, Yaron ; Undre, Shabnam ; Darzi, Ara: Assessment of psychomotor skills acquisition during laparoscopic cholecystectomy courses. En: *The American Journal of Surgery* 190 (2005), Nr. 3, p. 507 – 511. – ISSN 0002–9610

[49] Kap. Search and Optimization Methods In: Hand, D. J. ; Mannila, Hand ; Smyth, Padhraic: *Principles of Data Mining*. MIT Press, 2001, p. 253–260

[50] Handzel, Amir A. ; Flash, Tamar: Geometric methods in the study of human motor control. 6 (1999), Nr. 3, p. 309–321

[51] Hansen, MichaelEdberg ; Carstensen, JensMichael: Color-Based Image Retrieval from High-Similarity Image Databases. En: Bigun, Josef (Ed.) ; Gustavsson, Tomas (Ed.): *Image Analysis* Vol. 2749. Springer Berlin Heidelberg, 2003. – ISBN 978–3–540–40601–3, p. 1098–1105

[52] Hatzigiorgaki, Maria ; Skodras, Athanassios N.: Compressed domain image retrieval: a comparative study of similarity metrics. En: *Visual Communications and Image Processing 2003* International Society for Optics and Photonics, 2003, p. 439–448

[53] Herman, B. ; Zahraee, A.H. ; Szewczyk, J. ; Morel, G. ; Bourdin, C. ; Vercher, J.-L. ; Gayet, B.: Ergonomic and gesture performance of robotized instruments for laparoscopic surgery. En: *Intelligent Robots and Systems (IROS), 2011 IEEE RSJ International Conference on*, 2011. – ISSN 2153–0858, p. 1333–1338

[54] Hetland, Magnus L.: A survey of recent methods for efficient retrieval of similar time sequences. En: *Data mining in time series databases* 57 (2004)

[55] Hsu, Jeffrey ; Payandeh, Shahram: Toward tool gesture and motion recognition on a novel minimally invasive surgery robotic system. En: *Robotics and Automation,*

2006. ICRA 2006. Proceedings 2006 IEEE International Conference on IEEE, 2006, p. 631–636

[56] Huang, Anna: Similarity measures for text document clustering. En: *Proceedings of the sixth new zealand computer science research student conference (NZCSRSC2008), Christchurch, New Zealand*, 2008, p. 49–56

[57] Huang, Gan ; Zhang, Dingguo ; Zheng, Xidian ; Zhu, Xiangyang: An emg-based handwriting recognition through dynamic time warping. En: *Engineering in Medicine and Biology Society (EMBC), 2010 Annual International Conference of the IEEE* IEEE, 2010, p. 4902–4905

[58] Huang, Xuedong D. ; Ariki, Yasuo ; Jack, Mervyn A.: *Hidden Markov models for speech recognition*. Vol. 2004. Edinburgh university press Edinburgh, 1990

[59] Hunter, Garett: *Gesture Recognition using Hidden Markov Models, Dynamic Time Warping, and Geometric Template Matching*, University of Alberta, Tesis de Grado, 2013

[60] Jaffer, A ; Bednarz, B ; Challacombe, B ; Sriprasad, S: The assessment of surgical competency in the UK. En: *International Journal of Surgery* 7 (2009), Nr. 1, p. 12–15

[61] Keogh, Eamonn J. ; Pazzani, Michael J.: Derivative dynamic time warping. En: *the 1st SIAM Int. Conf. on Data Mining (SDM-2001), Chicago, IL, USA* SIAM, 2001

[62] Kokare, Manesh ; Chatterji, BN ; Biswas, PK: Comparison of similarity metrics for texture image retrieval. En: *TENCON 2003. Conference on Convergent Technologies for the Asia-Pacific Region* Vol. 2 IEEE, 2003, p. 571–575

[63] Kontaki, Maria ; Papadopoulos, Apostolos: Efficient Similarity Search in Streaming Time Sequences. En: *SSDBM*, 2004, p. 63–72

[64] Korn, Flip ; Jagadish, Hosagrahar V. ; Faloutsos, Christos: Efficiently supporting ad hoc queries in large datasets of time sequences. En: *ACM SIGMOD Record* 26 (1997), Nr. 2, p. 289–300

[65] Kuipers, Jack B.: *Quaternions and rotation sequences*. Vol. 66. Princeton university press Princeton, 1999

[66] Kumar, BVK ; Hassebrook, Laurence: Performance measures for correlation filters. En: *Applied optics* 29 (1990), Nr. 20, p. 2997–3006

[67] Kuno, Yoshinori ; Ishiyama, Tomoyuki ; Jo, K ; Shimada, Nobutaka ; Shirai, Yoshiaki: Vision-based human interface system: selectively recognizing intentional hand gestures. En: *Proceedings of the IASTED international conference on computer graphics and imaging*, 1998, p. 219–223

[68] Lacquaniti, Francesco ; Terzuolo, Carlo ; Viviani, Paolo: The law relating the kinematic and figural aspects of drawing movements. En: *Acta Psychologica* 54 (1983), Nr. 1-3, p. 115–130. – ISSN 0001–6918

[69] Lalys, Florent ; Bouget, David ; Riffaud, Laurent ; Jannin, Pierre: Automatic knowledge-based recognition of low-level tasks in ophthalmological procedures. En: *International journal of computer assisted radiology and surgery* 8 (2013), Nr. 1, p. 39–49

[70] LaViola, Joseph: A survey of hand posture and gesture recognition techniques and technology. En: *Brown University, Providence, RI* (1999)

[71] Lee, Sunil ; Yoo, Chang D.: Robust video fingerprinting for content-based video identification. En: *Circuits and Systems for Video Technology, IEEE Transactions on* 18 (2008), Nr. 7, p. 983–988

[72] Leong, Julian J. ; Nicolaou, Marios ; Atallah, Louis ; Mylonas, George P. ; Darzi, Ara W. ; Yang, Guang-Zhong: HMM assessment of quality of movement trajectory in laparoscopic surgery. En: *Computer Aided Surgery* 12 (2007), Nr. 6, p. 335–346

[73] Levant, A.: Robust exact differentiation via sliding mode technique. En: *Automatica* 34 (1998), Nr. 3, p. 379–384

[74] Levant, A.: Higher-order sliding modes, differentiation and output-feedback control. En: *International Journal of Control* 76 (2003), Nr. 9, p. 924–941

[75] Lines, Jason ; Bagnall, Anthony: Alternative quality measures for time series shapelets. En: *Intelligent Data Engineering and Automated Learning-IDEAL 2012*. Springer, 2012, p. 475–483

[76] Lines, Jason ; Davis, Luke M. ; Hills, Jon ; Bagnall, Anthony: A shapelet transform for time series classification. En: *Proceedings of the 18th ACM SIGKDD international conference on Knowledge discovery and data mining* ACM, 2012, p. 289–297

[77] MacKenzie, CL ; Ibbotson, JA ; Cao, CGL ; Lomax, AJ: Hierarchical decomposition of laparoscopic surgery: a human factors approach to investigating the operating room environment. En: *Minimally Invasive Therapy and Allied Technologies* 10 (2001), Nr. 3, p. 121–127

[78] Maguire, Peter: Assessing clinical competence. En: *BMJ: British Medical Journal* 298 (1989), Nr. 6665, p. 4

[79] Maoz, Uri ; Berthoz, Alain ; Flash, Tamar: Complex unconstrained three-dimensional hand movement and constant equi-affine speed. En: *Journal of neurophysiology* 101 (2009), Nr. 2, p. 1002–1015

[80] Martin, J. A. ; Regehr, G. ; Reznick, R. ; Macrae, H. ; Murnaghan, J. ; Hutchison, C. ; Brown, M.: Objective structured assessment of technical skill (OSATS) for surgical residents. En: *British Journal of Surgery* 84 (1997), Nr. 2, p. 273–278. – ISSN 1365–2168

[81] Martin, JÃ©rÃ´me ; Crowley, JamesL.: An appearance-based approach to gesture-recognition. En: Del Bimbo, Alberto (Ed.): *Image Analysis and Processing* Vol. 1311. Springer Berlin Heidelberg, 1997. – ISBN 978–3–540–63508–6, p. 340–347

[82] Megali, Giuseppe ; Sinigaglia, Stefano ; Tonet, Oliver ; Dario, Paolo: Modelling and evaluation of surgical performance using hidden Markov models. En: *Biomedical Engineering, IEEE Transactions on* 53 (2006), Nr. 10, p. 1911–1919

[83] Metwally, Ahmed ; Faloutsos, Christos: V-smart-join: A scalable mapreduce framework for all-pair similarity joins of multisets and vectors. En: *Proceedings of the VLDB Endowment* 5 (2012), Nr. 8, p. 704–715

[84] Modi, Chetan S. ; Morris, Guy ; Mukherjee, Ronan: Computer-Simulation Training for Knee and Shoulder Arthroscopic Surgery. En: *Arthroscopy: The Journal of Arthroscopic Related Surgery* 26 (2010), Nr. 6, p. 832 – 840. – ISSN 0749–8063

[85] Monahan, John F.: *Numerical methods of statistics*. Cambridge University Press, 2001

[86] Morasso, P.: Spatial control of arm movements. En: *Experimental Brain Research* 42 (1981), Nr. 2, p. 223–227. – ISSN 0014–4819

[87] Moreau, R. ; Ochoa, V. ; Pham, Minh T. ; Boulanger, P. ; Redarce, T. ; Dupuis, O.: Evaluation of obstetric gestures: An approach based on the curvature of quaternions. En: *Engineering in Medicine and Biology Society, 2008. EMBS 2008. 30th Annual International Conference of the IEEE*, 2008. – ISSN 1557–170X, p. 3430–3433

[88] Moreau, Richard ; Pham, Minh T. ; Silveira, Ruimark ; Redarce, Tanneguy ; Brun, Xavier ; Dupuis, Olivier: Design of a New Instrumented Forceps: Application to Safe Obstetrical Forceps Blade Placement. En: *IEEE Transactions on Biomedical Engineering* 54 (2007), Nr. 7, p. 1280–1290

[89] Moubarak, S. ; Pham, M.T. ; Moreau, R. ; Redarce, T.: Gravity compensation of an upper extremity exoskeleton. En: *In International Conference of the IEEE Engineering in Medicine and Biology Society (EMBC 2010)* Buenos Aires, Argentina, 2010, p. 4489–4493

[90] Moubarak, Salam ; Pham, Minh T. ; Pajdla, Thomas ; Redarce, Tanneguy: Design and modeling of an upper extremity exoskeleton. En: *World Congress on Medical Physics and Biomedical Engineering, September 7-12, 2009, Munich, Germany* Springer, 2009, p. 476–479

[91] Murphy, Todd E.: *Towards objective surgical skill evaluation with Hidden Markov Model-based motion recognition*, Citeseer, Tesis de Grado, 2005

[92] Nakatsu, Narao ; Kambayashi, Yahiko ; Yajima, Shuzo: A longest common subsequence algorithm suitable for similar text strings. En: *Acta Informatica* 18 (1982), Nr. 2, p. 171–179. – ISSN 0001–5903

[93] Nanopoulos, Alex ; Alcock, Rob ; Manolopoulos, Yannis: Feature-based classification of time-series data. En: *International Journal of Computer Research* 10 (2001), Nr. 3

[94] Pham, DT ; Oztemel, E: Control chart pattern recognition using neural networks. En: *Journal of Systems Engineering* 2 (1992), Nr. 4, p. 256–262

[95] Pham, DT ; Oztemel, E: Control chart pattern recognition using learning vector quantization networks. En: *THE INTERNATIONAL JOURNAL OF PRODUCTION RESEARCH* 32 (1994), Nr. 3, p. 721–729

[96] Pham, Minh T. ; Moreau, Richard ; Boulanger, Pierre: Three-dimensional gesture comparison using curvature analysis of position and orientation. En: *Engineering in Medicine and Biology Society (EMBC), 2010 Annual International Conference of the IEEE* IEEE, 2010, p. 6345–6348

[97] Pietroni, M: The assessment of competence in surgical trainees. En: *Annals of the Royal College of Surgeons of England* 75 (1993), Nr. 6 Suppl, p. 200–202

[98] Pollick, F. ; Sapiro., G.: Constant affine velocity predicts the 1/3 power law of planar motion perception and generation. En: *Vision Res* 37 (1997), Nr. 3, p. 347–353

[99] POLLICK, FRANK E.: The Perception of Motion and Structure in Structure-from-motion: Comparisons of Affine and Euclidean Formulations. En: *Vision Research* 37 (1997), Nr. 4, p. 447 – 466. – ISSN 0042–6989

[100] Pollick, Frank E. ; Maoz, Uri ; Handzel, Amir A. ; Giblin, Peter J. ; Sapiro, Guillermo ; Flash, Tamar: Three-dimensional arm movements at constant equi-affine speed. En: *Cortex* 45 (2009), Nr. 3, p. 325 – 339. – Special Issue on Cognitive Neuroscience of Drawing. – ISSN 0010–9452

[101] Pop, Petre G. ; Vaida, Mircea-F: Distances and numerical similarities in DNA repeats detection. En: *E-Health and Bioengineering Conference (EHB), 2013* IEEE, 2013, p. 1–4

[102] Popivanov, I. ; Miller, R.J.: Similarity search over time-series data using wavelets. En: *Data Engineering, 2002. Proceedings. 18th International Conference on*, 2002. – ISSN 1063–6382, p. 212–221

[103] Rafiei, Davood ; Mendelzon, Alberto: Efficient retrieval of similar time sequences using DFT. En: *arXiv preprint cs/9809033* (1998)

[104] Ratanamahatana, Chotirat A. ; Keogh, Eamonn: Making time-series classification more accurate using learned constraints SIAM, 2004

[105] Rehg, James M. ; Kanade, Takeo: Digit-Eyes: Vision-based human hand tracking / DTIC Document. 1993. – Informe de Investigación

[106] Reiley, Carol E. ; Lin, Henry C. ; Varadarajan, Balakrishnan ; Vagvolgyi, B ; Khudanpur, S ; Yuh, DD ; Hager, GD: Automatic recognition of surgical motions using statistical modeling for capturing variability. En: *Studies in health technology and informatics* 132 (2008), p. 396

[107] Rosen, Jacob ; Hannaford, Blake ; Richards, Christina G. ; Sinanan, Mika N.: Markov modeling of minimally invasive surgery based on tool/tissue interaction and force/torque signatures for evaluating surgical skills. En: *Biomedical Engineering, IEEE Transactions on* 48 (2001), Nr. 5, p. 579–591

[108] Rosen, Jacob ; Solazzo, Massimiliano ; Hannaford, Blake ; Sinanan, Mika: Objective laparoscopic skills assessments of surgical residents using Hidden Markov Models based on haptic information and tool/tissue interactions. En: *Studies in health technology and informatics* (2001), p. 417–423

[109] Rosser Jr, James C. ; Rosser, Ludie E. ; Savalgi, Raghu S.: Objective evaluation of a laparoscopic surgical skill program for residents and senior surgeons. En: *Archives of surgery* 133 (1998), Nr. 6, p. 657–661

[110] Ruckdeschel, Fred R.: *Basic Scientific Subroutines, Volume II*. ERIC, 1981

[111] Sakoe, H. ; Chiba, S.: Dynamic Programming Algorithm Optimization for Spoken Word Recognition. En: *IEEE Transactions on Acoustics, Speech, and Signal Processing* 27 (1978), Nr. 1, p. 43–49

[112] Schueneman, AL ; Pickleman, J ; Freeark, RJ: Age, gender, lateral dominance, and prediction of operative skill among general surgery residents. En: *Surgery* 98 (1985), Nr. 3, p. 506–515

[113] Schueneman, AL ; Pickleman, J ; Hesslein, R ; Freeark, RJ: Neuropsychologic predictors of operative skill among general surgery residents. En: *Surgery* 96 (1984), Nr. 2, p. 288–295

[114] Schwartz, Andrew B. ; Moran, Daniel W.: Arm trajectory and representation of movement processing in motor cortical activity. En: *European Journal of Neuroscience* 12 (2000), Nr. 6, p. 1851–1856

[115] Schwartz, R ; Donnelly, M ; Drake, D ; Sloan, D: Faculty sensitivity in detecting medical students' clinical competence. En: *Clin Invest Med* 16 (1993), Nr. Suppl B, p. B87

[116] Sielhorst, Tobias ; Blum, Tobias ; Navab, Nassir: Synchronizing 3d movements for quantitative comparison and simultaneous visualization of actions. En: *Proceedings of the 4th IEEE/ACM International Symposium on Mixed and Augmented Reality* IEEE Computer Society, 2005, p. 38–47

[117] Smith, C D. ; Farrell, Timothy M. ; McNatt, Stephen S. ; Metreveli, Ramaz E.: Assessing laparoscopic manipulative skills. En: *The American journal of surgery* 181 (2001), Nr. 6, p. 547–550

[118] Smith, CD ; Tung, P ; Stubbs, J ; Hananel, D: Assessing laparoscopic manipulative skill: Beyond the stopwatch. En: *Surgical Endoscopy* 12 (1998), p. 492

[119] Smith, John R. ; Chang, Shih-Fu: Automated binary texture feature sets for image retrieval. En: *Acoustics, Speech, and Signal Processing, 1996. ICASSP-96. Conference Proceedings., 1996 IEEE International Conference on* Vol. 4 IEEE, 1996, p. 2239–2242

[120] Smith, Steven W.: *Digital signal processing: a practical guide for engineers and scientists*. Newnes, 2003

[121] Smyth, Padhraic [u. a.]: Clustering sequences with hidden Markov models. En: *Advances in neural information processing systems* (1997), p. 648–654

[122] Speidel, Stefanie ; Delles, Michael ; Gutt, Carsten ; Dillmann, RÃ$\frac{1}{4}$diger: Tracking of Instruments in Minimally Invasive Surgery for Surgical Skill Analysis. En:

Yang, Guang-Zhong (Ed.) ; Jiang, TianZi (Ed.) ; Shen, Dinggang (Ed.) ; Gu, Lixu (Ed.) ; Yang, Jie (Ed.): *Medical Imaging and Augmented Reality* Vol. 4091. Springer Berlin Heidelberg, 2006. – ISBN 978–3–540–37220–2, p. 148–155

[123] Steele, RJC ; Walder, C ; Herbert, M: Psychomotor testing and the ability to perform an anastomosis in junior surgical trainees. En: *British Journal of surgery* 79 (1992), Nr. 10, p. 1065–1067

[124] Ten Holt, GA ; Reinders, MJT ; Hendriks, EA: Multi-dimensional dynamic time warping for gesture recognition. En: *Thirteenth annual conference of the Advanced School for Computing and Imaging* Vol. 119, 2007

[125] Vieilledent, Stéphane ; Kerlirzin, Yves ; Dalbera, Stéphane ; Berthoz, Alain: Relationship between velocity and curvature of a human locomotor trajectory. En: *Neuroscience letters* 305 (2001), Nr. 1, p. 65–69

[126] Viviani, P: Do units of motor action really exist. En: *Experimental Brain Research* 15 (1986), p. 201–215

[127] Viviani, Paolo ; Cenzato, Marco: Segmentation and coupling in complex movements. En: *Journal of experimental psychology: Human perception and performance* 11 (1985), Nr. 6, p. 828

[128] Vlachos, Michail ; Kollios, George ; Gunopulos, Dimitrios: Discovering similar multidimensional trajectories. En: *Data Engineering, 2002. Proceedings. 18th International Conference on* IEEE, 2002, p. 673–684

[129] Vogt, Florian ; Krüger, Sophie ; Niemann, Heinrich ; Schick, Christoph: A system for real-time endoscopic image enhancement. En: *Medical Image Computing and Computer-Assisted Intervention-MICCAI 2003*. Springer, 2003, p. 356–363

[130] Volk, Raimund ; Ville, Jean F.: Filters for contour measurement. En: *Wear* 264 (2008), Nr. 5, p. 469–473

[131] Wanzel, Kyle R. ; Ward, Myléne ; Reznick, Richard K.: Teaching the surgical craft: from selection to certification. En: *Current problems in surgery* 39 (2002), Nr. 6, p. 583–659

[132] Willett, Peter: Similarity-based virtual screening using 2D fingerprints. En: *Drug discovery today* 11 (2006), Nr. 23, p. 1046–1053

[133] Wu, Daniel ; Singh, Ambuj ; Agrawal, Divyakant ; El Abbadi, Amr ; Smith, Terence R.: Efficient retrieval for browsing large image databases. En: *Proceedings of the fifth international conference on Information and knowledge management* ACM, 1996, p. 11–18

[134] Wu, Yi-Leh ; Agrawal, Divyakant ; El Abbadi, Amr: A comparison of DFT and DWT based similarity search in time-series databases. En: *Proceedings of the ninth international conference on Information and knowledge management* ACM, 2000, p. 488–495

[135] Xian, B. ; de Queiroz, M.S. ; Dawson, D. ; Walker, I.: Task-space tracking control of robot manipulators via quaternion feedback. En: *Robotics and Automation, IEEE Transactions on* 20 (2004), Feb, Nr. 1, p. 160–167. – ISSN 1042–296X

[136] Xing, Zhengzheng ; Pei, Jian ; Keogh, Eamonn: A Brief Survey on Sequence Classification. En: *SIGKDD Explor. Newsl.* 12 (2010), November, Nr. 1, p. 40–48. – ISSN 1931–0145

[137] Yang, Kiyoung ; Shahabi, Cyrus: A PCA-based similarity measure for multivariate time series. En: *Proceedings of the 2nd ACM international workshop on Multimedia databases* ACM, 2004, p. 65–74

[138] Ye, Lexiang ; Keogh, Eamonn: Time series shapelets: a new primitive for data mining. En: *Proceedings of the 15th ACM SIGKDD international conference on Knowledge discovery and data mining* ACM, 2009, p. 947–956

[139] Yuan, J.S.: Closed-loop manipulator control using quaternion feedback. En: *Robotics and Automation, IEEE Journal of* 4 (1988), Aug, Nr. 4, p. 434–440. – ISSN 0882–4967

[140] Zhang, Yang ; Edgar, Thomas F.: A robust dynamic time warping algorithm for batch trajectory synchronization. En: *American Control Conference, 2008* IEEE, 2008, p. 2864–2869

INSA INSTITUT NATIONAL DES SCIENCES APPLIQUÉES LYON

FOLIO ADMINISTRATIF

THÈSE SOUTENUE DEVANT L'INSTITUT NATIONAL DES SCIENCES APPLIQUÉES DE LYON

NOM : CIFUENTES QUINTERO
(avec précision du nom de jeune fille, le cas échéant)

DATE de SOUTENANCE : 3 juillet 2015

Prénoms : Jenny Alexandra

TITRE : Development of a new technique for objective assessment of gestures in mini-invasive surgery.

NATURE : Doctorat

Numéro d'ordre : 2015ISAL0056

Ecole doctorale : EEA

Spécialité : Doctorat de Automatique Industrielle

RESUME : L'une des tâches les plus difficiles de l'enseignement en chirurgie, consiste à expliquer aux étudiants quelles sont les amplitudes des forces et des couples à appliquer pour guider les instruments au cours d'une opération. Ce problème devient plus important dans le domaine de la chirurgie mini-invasive (MIS) où la perception de profondeur est perdue et le champ visuel est réduit. Pour cette raison, l'évaluation de l'habileté chirurgicale associée est devenue un point capital dans le processus d'apprentissage en médecine. Aujourd'hui cette évaluation est faite de manière empirique en salle d'opérations par l'observation des chirurgiens, de sorte que des problèmes évidents de subjectivité apparaissent dans la formation des médecins, selon l'instructeur en charge de l'enseignement.

De nombreuses études et rapports de recherches dans le monde entier concernent le développement de techniques automatisées d'évaluation du geste et permettent de fournir un retour d'expérience objectif pendant le processus d'apprentissage. La première partie du travail présenté dans cette thèse introduit une nouvelle méthode de classification de gestes médicaux 3D reposant sur des modèles cinématiques et biomécaniques. Cette nouvelle approche analyse de manière qualitative mais aussi quantitative les mouvements associés aux tâches effectuées au cours de la formation médicale. La classification du geste est réalisée en utilisant un paramétrage reposant sur la longueur d'arc pour calculer la courbure pour chaque trajectoire. Les avantages de cette approche sont principalement motivés par l'indépendance du temps, d'un système de repérage absolu et la réduction du nombre de données à traiter. L'étude inclus l'analyse expérimentale de plusieurs gestes, obtenus avec plusieurs types de capteurs et réalisés par différents sujets.

La deuxième partie de ce travail se concentre dans une technique de classification reposant sur les données cinématiques et dynamiques. En premier lieu, une expression empirique, entre la géométrie du mouvement et les données cinématiques, est utilisée pour calculer une nouvelle variable appelée vitesse affine. Les expériences conduites dans ce travail de thèse montrent la nature constante de cette grandeur lorsque les gestes médicaux sont simples et identiques. De la même faon, les résultats expérimentaux montrent que l'utilisation de la vitesse affine conduit à une classification adéquate des gestes. Les paramètres associés au modèle de vitesse affine trouvé ont été pris en compte par la suite pour étudier des mouvements plus complexes et effectuer une segmentation des tâches de préhension et de dépôt. Finalement, une dernière technique de classification a été implémentée en utilisant un calcul de l'énergie utilisée au cours de chaque segment du geste. Cette méthode a été validée expérimentalement en utilisant six caméras et un laparoscope instrumenté. La position 3-D de l'extrémité de l'effecteur a été enregistrée, pour plusieurs participants, en utilisant le logiciel OptiTrack Motive et des marqueurs réfléchissants montés sur le laparoscope. Les mesures de force et de couple, d'autre part, ont été acquises à l'aide des capteurs fixés sur l'outil et situés entre la pointe et la poignée de l'outil afin de capturer l'interaction entre le participant et le matériau manipulé. Les résultats expérimentaux présentent une bonne corrélation entre les valeurs de l'énergie et les compétences chirurgicales des participants impliqués dans ces expériences.

MOTS-CLÉS : Analyse de Courbure; Classiffication des gestes; Dynamic Arc Length Warping; Énergie; Loi de Puissance Un-Sixième; Segmentation; Suivi du Mouvement de la Main; Vítesse Affine

Laboratoire (s) de recherche : Laboratoire Ampère

Directeur de thèse:

Hervé Tanneguy REDARCE Professeur
Laboratoire Ampère INSA de Lyon

Flavio Prieto, Professeur
Departamento de Ingeniería Eléctrica y Electrónica
Universidad Nacional de Colombia

Président de jury :

Composition du jury :

Jean Louis VERCHER, Directeur de Recherche CNRS
Institut des Sciences du Mouvement Etienne-Jules Marey
UMR 7287 CNRS & UNIVERSITE AIX-MARSEILLE

Jesús Francisco VARGAS BONILLA, Professeur
Departamento de Ingeniería Electrónica y Telecomunicaciones
Universidad de Antioquia
Email: jesus.vargas@udea.edu.co

Jan BACCA RODRIGUEZ, , Professeur
Departamento de Ingeniería Eléctrica y Electrónica
Universidad Nacional de Colombia

Pierre Boulanger, Professeur
University of Alberta
Department of Computing Science
Edmonton, Alberta, T6G 2E8, Canada

Flavio Prieto, Professeur
Departamento de Ingeniería Eléctrica y Electrónica,PhD
Universidad Nacional de Colombia

Hervé Tanneguy REDARCE Professeur
Laboratoire Ampère INSA de Lyon

Minh Tu PHAM Maître de Conférences
Laboratoire Ampère INSA de Lyon

Richard MOREAU Maître de Conférences
Laboratoire Ampère INSA de Lyon

Prof. Carlos Alberto PARRA RODRIGUEZ, Professeur
Departamento de Ingeniería Electrónica
Pontificia Universidad Javeriana